# Chemometric perspectives on plankton community responses to natural iron fertilization over and downstream of the Kerguelen plateau in the Southern Ocean

T. W. Trull[1, 2, 3*], D. M. Davies[1, 2], F. Dehairs[4], A.-J. Cavagna[4], M. Lasbleiz[5], E. C. Laurenceau-Cornec[1, 2, 3], F. d'Ovidio[6], F. Planchon[7], K. Leblanc[5], B. Quéguiner[5] and S. Blain[8,9]

1. CSIRO Marine and Atmospheric Research, Hobart, Tasmania, Australia
2. Antarctic Climate and Ecosystems Cooperative Research Centre, Hobart, Tasmania, Australia
3. Institute for Marine and Antarctic Studies, University of Tasmania, Hobart, Tasmania, Australia
4. Analytical, Environmental and Geo – Chemistry; Earth Sciences Research Group, Vrije Universiteit Brussel, Belgium
5. Aix-Marseille Université & Université de Toulon, Marseille, France
6. LOCEAN - IPSL. Université Pierre et Marie Curie, Paris, France
7. Laboratoire des Sciences de l'Environnement Marin (LEMAR), Université de Brest, IUEM, France
8. Sorbonne Universités, UPMC Univ Paris 06, UMR7621, Laboratoire d'Océanographie Microbienne, Observatoire Océanologique, 66650 Banyuls/mer, France
9. CNRS, Laboratoire d'Océanographie Microbienne, Observatoire Océanologique, 66650 Banyuls/mer, France

*Corresponding author: Tom.Trull@csiro.au

## Abstract

We examined phytoplankton community responses to natural iron fertilisation at 32 sites over and downstream from the Kerguelen plateau in the Southern Ocean during the austral spring bloom in October-November 2011. Community structure was estimated from chemical and isotopic measurements (particulate organic carbon POC, $^{13}$C-POC, particulate nitrogen PN, $^{15}$N-PN, and biogenic silica BSi) on size-fractionated samples from surface waters (300, 210, 50, 20, 5, and 1 μm fractions). Higher values of $^{13}$C-POC (vs. co-located $^{13}$C values for dissolved inorganic carbon, DIC) were taken as indicative of faster growth rates, and higher values of $^{15}$N-PN (vs. co-located $^{15}$N-$NO_3$ source values) as indicative of greater nitrate use (rather than ammonium use, i.e. higher *f* ratios).

Community responses varied in relation to both regional circulation and the advance of the bloom. Iron fertilised waters over the plateau developed dominance by very large diatoms (50-210 μm) with high BSi/POC ratios, high growth rates, and significant ammonium recycling (lower *f* ratios) as biomass built up. In contrast, downstream Polar Frontal waters with similar or higher iron supply were dominated by smaller diatoms (20-50 μm) and exhibited greater ammonium recycling. Stations in a deep water bathymetrically trapped recirculation south of the Polar Front with lower iron levels showed the large cell dominance observed on the plateau, but much less biomass. Comparison of these communities to surface water nitrate (and silicate) depletions as a proxy for export shows that the low biomass recirculation feature had exported similar amounts of nitrogen to the high biomass blooms over the plateau and north of the Polar Front. This suggests that early spring trophodynamic and export responses differed between regions with persistent low levels vs. punctual high levels of iron fertilisation.

## 1 Introduction

Natural iron fertilisation from islands, shelves, and plateaus in the Southern ocean produces local and downstream elevations of phytoplankton biomass, ~10-fold higher than in surrounding high nutrient low chlorophyll (HNLC) waters, e.g. (de Baar et al., 1995). In some of these systems, carbon export has been observed to be elevated ~2-3 fold, e.g over the Kerguelen Plateau (Blain et al., 2008;Savoye et al., 2008) and to the north of Crozet Island (Pollard et al., 2007). But these studies produced order of magnitude variations in estimates of the amount of carbon export per unit iron supply, as have deliberate iron fertilisation studies (Boyd et al., 2007). These variations appear to reflect both observational limitations and system complexity, including the possibility of variations in initial communities prior to fertilisation (as a result of north-south oceanographic variations or the extent of connection to coastal habitats).

General principles for expected phytoplankton responses to iron fertilisation have been elucidated, though they remain to be fully tested. These include increased growth rates for all size classes and elevated new production, i.e. increased nitrate use (e.g. (Armstrong, 1999;Maldonado et al., 2001)). A prevailing view of the overall community response is that it depends on the interaction of these changes with the response of zooplankton grazers, which are thought to be more able to keep up with small cell growth and thus to favour accumulation of larger phytoplankton (Assmy et al., 2013;Morel et al., 1991). This, in turn, may favour export via either direct sinking or aggregation (Smetacek, 1985;Smetack, 1998). Variations in diatom life cycles and strategies add seasonal complexity to this picture (Queguiner, 2013), and the translation of increases in new production into enhancements in export can be relatively weak, for example, as a result of strong N recycling (Mosseri et al., 2008).

The KEOPS2 expedition sought to examine these and other aspects of community responses to natural iron fertilisation over and downstream of the Kerguelen plateau, in austral spring, October-November 2011, as detailed in the multiple papers in this volume. In this paper, we examine a suite of chemical and isotopic indicators of phytoplankton community structure and function (chemometrics) and relate them to nitrate (and silicate) depletion in surface waters as a proxy for carbon export. The following paragraphs provide an overview of the approach and the structure of the paper.

First, we describe the complex regional circulation, and use it to cluster the stations into 5 groups (coastal, plateau, waters well downstream near the Polar Front, and waters in a recirculation close to the plateau - separated into a broad early survey and a later focused, quasi-Lagrangian time series). For these groups we briefly summarize the relative levels of iron fertilisation from dissolved and particulate standing stocks (Quéroué et al., 2014;van der Merwe et al., 2014) and Fe supply estimates (Bowie et al., 2014;d'Ovidio et al., 2014). We also assess the elapsed time since iron fertilisation and its persistence, from seasonal perspectives on vertical mixing (Bowie et al., 2014) and Lagrangian perspectives on water mass trajectories around the Kerguelen plateau (d'Ovidio et al., 2014). We also consider two other overarching perspectives on ecosystem responses: the elapsed time since the beginning of phytoplankton accumulation (from an animation of satellite ocean colour images; Supplementary Materials), and the level of biomass enrichment at the time of sampling. Our subsequent chemometric analysis is undertaken at the level of these 5 Groups, against this framework of relative intensities and timings of Fe fertilisation and biomass accumulation.

Next, we describe our chemometric approach. In brief, we relied on total particulate organic carbon (POC) as an indication of eutrophy, size distribution as a indicator of community structure, biogenic silica /particulate organic carbon (BSi/POC) ratios as a measure of diatom dominance, $^{13}C$ as a qualitative metric for growth rates, and $^{15}N$ as a

metric for ammonium recycling. To determine nitrate (and silicic acid) depletion by the biological pump, we explored both temperature and salinity based approaches to estimate initial winter surface water concentrations, and also evaluated the fraction of the observed depletion that still remained in the water column for potential future export using particulate nitrogen and biogenic silica stocks from CTD casts (Blain et al., 2014;Lasbleiz et al., 2014).

These chemometric approaches are not as direct as other methods (such as microscopy for community structure, incubation experiments for growth rates and *f*-ratios, and sediment trap collections for export), but offer some advantages in terms of quantitative connections to dissolved nutrient budgets and the ability to examine more sites. To address these shortcomings, we compared our $^{13}C$ growth rate and $^{15}N$ *f*-ratio estimates to shipboard incubation results from $^{13}C$ and $^{15}N$ tracer uptake experiments, (Cavagna et al., 2014), and discuss our more extensive results with respect to information on community composition from pigment and microscopic analyses (Lasbleiz et al., 2014), and carbon export from $^{234}Th$ depletions (Planchon et al., 2014) and sediment trap collections (Laurenceau et al., 2014). In summary, this provides an overview of the relative importance of Fe inputs and temporal evolution in the control of community structure and carbon export in springtime, for the phytoplankton bloom that forms over and downstream of the Kerguelen plateau.

## 2 Methods

### 2.1 Site description

The KEOPS2 campaign was carried out in October - November 2011 over and downstream of the Kerguelen plateau in the Southern Ocean, under conditions of complex circulation and rapidly changing phytoplankton biomass, as summarized in Figs. 1 and 2, and further showcased in the full annual satellite chlorophyll animation (Supplement).

The Kerguelen plateau is a northwest-southeast oriented seafloor feature which rises to ~500m below the surface over much of its extent. It also hosts several volcanic islands, in particular the large Kerguelen Island archipelago in the north and the smaller Heard Island at the southern edge of the central Kerguelen plateau. The plateau blocks the eastward flowing Antarctic Circumpolar Current (ACC). Much of the ACC flow goes to the south of the plateau and through the Fawn Trough (to the south of Heard Island), with a smaller portion associated with the Subantarctic Front flowing around the northern edge of Kerguelen island. A narrow jet of ACC water also flows across the plateau in the narrow, mid-depth (~1000m) channel just to the south of Kerguelen Island (Fig. 1). This feature corresponds with the northernmost presence of a subsurface temperature minimum formed by winter cooling (near 200m depth), and thus defines the northernmost branch of the Polar Front (Park et al., 2014a;Park et al., 2008). This jet was a particularly important feature of the area sampled during KEOPS2, because it separated the central plateau and downstream offshore stations to the south of the Polar Front (PF), from those to the north of the PF, where the coastal stations were also located. As discussed in section 2.2, the modes of supply of Fe to the waters north and south of this jet may also differ, with some downstream Polar Front stations potentially influenced by Fe inputs from coastal waters associated with Kerguelen Island or its shallow northern shelf (d'Ovidio et al., 2014).

From a dynamical perspective, the full ocean depth branch of the Polar Front lies to the south of Heard Island, where the ACC flow transits the Fawn Trough (Sokolov and Rintoul, 2009). As this flow passes to the east of the pleateau it follows the bathymetric contours to the north where it enters a bathymetrically-trapped recirculation region to the south of the Polar Front, before eventually exiting downstream (d'Ovidio et al., 2014;Park et al., 2014a). This recirculation feature and the flow along the PF jet are fixed in space by the bathymetry close to the plateau, but at their eastern edge over the abyssal plain (where the

146 strong ACC flows passing south and north of the plateau re-join) meandering is strong and
147 varies with time. For example, the animation of ocean colour (Supplement) suggests the PF
148 moved southward in this region over the course of the KEOPS2 observations.
149 As shown in Fig. 1, the initial sampling was carried out along a deep water transect
150 (stations TNS 1-10) run northwards from the central plateau (TNS-10) across the
151 recirculation feature and Polar Front and into Subantarctic waters (TNS-1). This was
152 followed by a west to east transect (stations TEW 1-8) running offshore from the Kerguelen
153 Island coast, across the middle of the recirculation, and reaching the southward meandering
154 Polar Front in the far east of the study region. This initial survey was followed by multiple
155 "time-series" visits to the recirculation feature, (designated as stations E1- E5, with two
156 stations at the E4 time step - to the western side, E4-W, and eastern side, E4-E, of this
157 recirculation). In addition several other features at the margins of the survey region were also
158 sampled, with rather complicated nomenclature based on locations, links to other programs,
159 durations, and purposes:
160 – Reference HNLC waters to the west of the plateau (stations R and R2)
161 – A central plateau station that had served as the bloom reference site in the previous
162 KEOPS campaign in late summer/autumn 2005 (station A3, sampled twice as A3-1
163 and A3-2).
164 – High biomass waters in the extreme northeast of the study region, near the
165 downstream location of the Polar Front (Stations F-L and F-S; L for long, S for short)
166 – Two stations carried out to compare geochemical tracer concentrations in waters over
167 the plateau (G1) with Kerguelen coastal waters (G2).
168 All of these stations (except TNS-4 and TNS-7) on the initial survey transect were sampled
169 for our size-fractionated chemometric analyses (with some stations also sampled both at night
170 and day).

The five colour-coded Groups mapped in Fig. 1 cluster the KEOPS2 stations based largely on the interactions of the circulation with the bathymetry (with some additional regard for temporal evolution and the timing and extent of iron supply and biomass accumulation, as discussed below). The properties of these Groups are summarized in Table 1. In brief, Groups 1 and 2 cluster stations from the recirculation feature. Group 1 consists of stations in this region occupied during the initial transects when biomass was low, and also includes the upstream HNLC reference site R2 (which was also sampled early in the voyage). Group 2 holds the stations subsequently occupied as a pseudo-Lagrangian time series within the recirculation. Group 3 holds the central plateau stations, including waters that flow northward to leave the plateau along the south side of the Polar Front jet. Group 4 holds the coastal stations, including TEW-3 at the plateau edge (which displayed a mix of coastal, plateau, and recirculation properties). Group 5 has the downstream stations near and north of the Polar Front. Two stations in this Group, at the northern Subantarctic end of the initial survey, TNS-1 and TNS-2, were included to keep the number of Groups low, but stand out as quite distinct in having lower biomass with greater proportions of non-diatom taxa (Lasbleiz et al., 2014), and are marked by distinct colouring in the figures. Additional discussion of stations near the boundaries of these Groups is provided below, and other clusterings are possible, especially for stations at the boundaries among the Groups (for further discussion see Lasbleiz et al., 2014). The majority of the analysis presented in this paper is based on comparisons across these Groups rather than individual stations (although variations within the Groups do occur and sometimes provide additional insights, and for this reason the figures display the individual stations in each group in chronological order (e.g. see Fig. 3).

## 2.2 Intensity and timing of Fe fertilisation

Iron sampling and analysis was carried out at a much-reduced subset of the stations discussed here, albeit with greater vertical resolution (Bowie et al., 2014;Quéroué et al., 2014;van der Merwe et al., 2014). Thus, comparisons to our results are only possible at the level of our station Groups, and only in a relative sense. The lowest Fe levels were observed at the HNLC reference station upstream to the west of the Kerguelen Plateau (slightly less than 0.1 nM at station R2). The recirculation region (Groups 1 and 2) had low to moderate dissolved Fe (0.06-0.38 nM at stations E2, E3 and E5). Slightly higher minimum concentrations were observed over the plateau (0.18- 0.21 nM at the Group 3 stations A3-1 and G1). Moderate enrichments were also observed in the Group 5 downstream waters near the Polar Front (~0.26 nM at station F-L). The highest dissolved Fe levels were in the Group 4 Kerguelen Island coastal waters (surface concentrations of 2.17 nM for TEW 1 and 1.26 nM for TEW 2).

Particulate Fe levels were not measured in coastal waters, but generally exceeded dissolved Fe levels in the Group 3 stations over the plateau (by factors of 13 - 20) and offshore in the Group 1 and 2 stations in the recirculation feature and the single Group 5 station in the downstream plume (by factors of 2 - 34). The bio-availability of this particulate Fe is unknown, but assuming a conservative fraction of 1% (for discussion see van der Merwe et al., 2014) leads to a 20% increase over the plateau of available iron and 4-34 % increase offshore.

Estimating Fe supply is more difficult. It appears possible that downstream waters north of the Polar Front (Group 5 stations F-S, F-L, TEW-7, and TEW-8, but not the Subantarctic influenced stations TNS-1 and TNS-2 ) receive more iron than the plateau (Group 3) especially in summer when stratification reduces vertical supply over the plateau, but advection continues to sweep iron-rich coastal waters from the northern Kerguelen shelf

along the northern side of the Polar Front jet (Bowie et al., 2014;d'Ovidio et al., 2014;Park et al., 2014a).

The nature of Fe fertilisation also varies among the regions, in terms of both its timing relative to our sampling, and its persistence. Recent and brief iron fertilisation appears likely to characterize the Polar Front (Group 3 region). Water parcel trajectories calculated from drifter trajectories and altimetry based geostrophic currents (d'Ovidio et al., 2014) suggest times of less than 0.5 to 1 month for the downstream Polar Front stations (Group 5 stations F-S, F-L, TEW-7, TEW-8), with rapid dispersal and thus low persistence. In comparison, it appears to take longer for northern Kerguelen shelf waters to reach the recirculation region (Group1and 2 stations), where the water is then retained for a relatively long time (30 to 60 days), but is also diluted by approximately equal volumes of waters derived from the south (d'Ovidio et al., 2014;Park et al., 2014a). These supply paths are also indicated by Ra isotope distributions (Sanial et al., 2014). Thus fertilisation of the recirculation feature appears to be less recent and intense than that of the Polar Frontal region, but probably more persistent. For the Kerguelen coastal stations (Group 4), where water columns were well mixed to the bottom, fertilisation is both recent and persistent. Fertilisation over the plateau is also relatively recent in a seasonal context, ~ 2 months from maximum winter mixing in August-September to sampling in Oct-Nov. Its persistence may be similar or somewhat larger than that of the recirculation region given estimates of water parcel residence times over the plateau of order 2-3 months (Park et al., 2008).

In summary, this evaluation of iron inputs yields rank orders as follows:

Intensity of Fe fertilisation (lowest to highest):

*recirculation feature* < *plateau* <≈ *Polar Front plume* << *coastal stations*

Elapsed time since Fe fertilisation and its persistence (most recent to oldest):

*Polar Front plume* < *recirculation feature* <≈ *plateau* < *coastal stations*

For easy reference these properties are summarized for the station Groups in Table 1.

### 2.3 Intensity and timing of phytoplankton biomass accumulation

The KEOPS2 sampling was carried out in spring, spanning the period when phytoplankton biomass was rapidly increasing both over and downstream of the plateau, forming rather complex patterns in satellite chlorophyll images (Fig. 2). Thus the time of sampling relative to the development of surface biomass enrichment varied strongly among the stations. The sequence of ocean colour images in Fig. 2. (see also the Supplement) suggests that this chlorophyll increase occurred first in coastal Kerguelen island waters (starting in mid-September very close to the island and extending northwards by mid October; but reaching only moderate Chl-a levels near 1 $\mu g\ L^{-1}$), followed by the downstream plume north of the Polar Front (near Group 5 stations F-S, F-L, TEW-7, TEW-8) where chlorophyll biomass jumped very rapidly from below 0.5 to above 2 $\mu g\ L^{-1}$ early in the first week of November.

At this time (as shown in the animation in the Supplement), the central plateau and the recirculation feature still had only minor biomass development, with concentrations near 0.5 $\mu g\ L^{-1}$. But, within a few days, by 9 November, all strongly Fe enriched regions (coastal, central plateau, and the downstream waters near the Polar Front) had Chl-a levels above 2.5 $\mu g\ L^{-1}$. Yet, the recirculation region still had low levels of ~0.5 $\mu g\ L^{-1}$for another week, and only reached levels of 1-1.5 $\mu g\ L^{-1}$ by end November. Only in early December, after the end of field sampling, did the recirculation feature reach levels of 2.5-3 $\mu g\ L^{-1}$. Interestingly, the downstream waters near the Polar Front maintained high levels throughout most of this period, but the central plateau bloom faded (as sampled by station A3-2) before being replaced by a second bloom somewhat further east, though still over the plateau. The

268 animation of these satellite chlorophyll images provides further detail of the structure and
269 sequence of biomass accumulation, both during and after the voyage (Supplement).
270 In summary, satellite biomass accumulation yields rank orders as follows:
271 Magnitude of biomass accumulation (lowest to highest, at end of voyage):
272 *recirculation feature < coastal stations < plateau <≈ Polar Front plume*
273 Elapsed time since initiation of biomass accumulation (most recent to oldest):
274 *recirculation feature < Polar Front plume <≈ plateau << coastal stations*
275 For easy reference these properties are summarized for the station Groups in Table 1.
276

277 **2.4 Samples**
278
279 This study is based primarily on chemical and isotopic compositions of dissolved
280 nutrients and size-fractionated particles sampled from surface waters using the ship's clean
281 seawater supply. Full details of the sample collection and analytical methods are provided in
282 Appendix A. In brief, particles were analysed for 6 size fractions collected by large volume
283 sequential filtration through a pre-screen (1000μm) and 6 filters (300, 210, 50, 20, 5 and 1
284 μm pore sizes). These samples were analysed for POC, PN, BSi, $^{13}$C-POC and $^{15}$N-PN
285 (although BSi could not be analysed on the 1μm fraction, as it was collected with a quartz
286 filter). Seawater samples collected from the same supply, and also from Niskin bottles on the
287 CTD system, were analysed for nitrate and dissolved inorganic carbon concentrations and
288 isotopic compositions (DIC, $^{13}$C-DIC, $NO_3^-$, $^{15}$N-$NO_3^-$, and $^{18}$O-$NO_3^-$). In addition,
289 approximately one litre samples were filtered for bulk POC and PN concentrations and these
290 are reported along with the total POC determined from the sum of the size fractions. Surface
291 water nitrate concentrations were continuously mapped using an ultra-violet nitrate sensor.
292 Speaking broadly for all stations, the largest size fractions (300-1000 μm) for the
293 suspended particles were dominated by zooplankton, primarily copepods. Intact faecal

pellets and phytoplankton aggregates did not contribute significantly to these fractions (presumably they were disaggregated by the pumping system, because both particle types were observed in sediment traps equipped with polyacrylamide gels (Laurenceau et al., 2014); although the presence of intact needles of *Thallasiothrix antarctica* and chains of *Fragilariopsis kerguelensis* diatoms suggests individual cells were largely undamaged). The smaller size-fractions were dominated by diatom frustules, with small centric diatoms abundant on the 5 μm filter, a mix of centric and pennate diatoms on the 20 and 50 μm filters, and large diatoms and chains of pennate diatoms and small copepods on the 210 μm filter. The particles on the 1 μm quartz filter were too small to examine in any detail using stereo microscopy. The light beige colour of these filters, in comparison to the greener shades of the intermediate sizes suggests important contributions from detritus and/or bacteria (and absorption of dissolved organic matter onto the 1 μm quartz filters may have also occurred, but was not assessed). These microscopic assessments of the materials present on the filters are rather limited, and may well have missed significant contributions from autotrophs and heterotrophs without frustules or carapaces, but other studies during KEOPS2 of bacterial abundances (Christaki et al., 2014), phytoplankton (Georges et al., 2014;Lasbleiz et al., 2014), diatom species (L. Armand, personal communication), and zooplankton (Carlotti et al., 2014) are consistent with our chemometric interpretation that detritus, bacteria, and phytoplankton contributed to the 1 μm fraction; phytoplankton and especially diatoms dominated the 5, 20, and 50 μm fractions; a mix of large diatoms and copepods were present in the 210 μm fraction and copepods, isopods, and occasionally krill were the primary contributions to the 300 μm fraction.

**2.5 Chemometric methods for community structure and function**

Evaluation of community structure and function is ideally done via detailed taxonomy and physiology, but the plethora of organisms makes this very difficult. Chemical methods offer an easier path with the added advantages of quantitative connections to dissolved chemical concentrations and budgets. Size fractionation adds value to this approach, firstly because it provides some separation of phytoplankton (which dominated the 1, 5, 20, and 50 μm fractions) from heterotrophs (210 and 300 μm fractions), and secondly because differing sizes of phytoplankton often occupy different biogeochemical niches (e.g. greater reliance on ammonium by small phytoplankton; less contribution to direct export owing to smaller sinking rates) and experience differing ecological couplings (e.g. tighter coupling to grazing control in smaller sizes, because smaller zooplankton have shorter life cycles).

Thus our primary chemometric tool is to simply examine variations in the distribution of POC across the size fractions as an indicator of community structure. (To remove the influence of our particular choice of filter sizes, we express the POC concentration variations as spectra, i.e. we divide the concentrations by the width of each filtration interval, yielding units of $\mu M\ \mu m^{-1}$). Secondarily we use high BSi/POC ratios as an indication of community dominance by diatoms. This is simplistic given the presence of silicoflagellates at some stations (Lasbleiz et al., 2014) and the occurrence of a wide range of BSi/POC ratios in diatoms (Ragueneau et al., 2006). We use low POC /PN ratios as an indication of contributions from heterotrophic biomass (below the values of ~6-7 that characterise most phytoplankton (Anderson and Sarmiento, 1994;Redfield et al., 1963).

### 2.5.1 Isotopic chemometric principles – $^{13}C$

The isotopic chemometric tools are not as common and require greater explanation. Variations in $^{13}C$-POC and $^{15}N$-PN values derive from both primary photosynthetic production and the overlay of secondary heterotrophic imprints, especially in the smallest

size fraction (1-5 µm) in which bacterial processing was important, and the two largest size fractions (210-300 and 300-1000 µm) which contained significant contributions from zooplankton. For the middle size fractions (5-20, 20-50 and 50-210 µm), biomass was dominated by phytoplankton and thus these fractions can be used to examine the impacts of iron fertilisation and other controls on primary production. This is our focus for the use of these tools. In particular we interpret $^{13}C$ enrichment as potentially indicative of higher growth rates and $^{15}N$ enrichment as indicative of higher *f* ratios (i.e. greater use of nitrate in comparison to reduced forms of nitrogen). In the following paragraphs we introduce quantitative expressions for these relationships, but also acknowledge that they rest on many assumptions, and are thus indicative rather than definitive. After discussion of these autotrophic expressions, we also briefly describe the scale of heterotrophic effects.

Controls on the $^{13}C$ composition of phytoplankton are complex, and have been explored in hundreds of papers since an early survey of the variability in marine carbon isotopic compositions (Craig, 1953), with occasional significant advances and reviews, e .g. (Farquhar et al., 1982;Goericke et al., 1994;Laws et al., 1995;Laws et al., 2002;Rau et al., 1996;Schulz et al., 2007;Tortell et al., 2008). In brief, there are two main causes for $^{13}C$ variations of any given phytoplankton cell. Firstly, the cell $^{13}C$ content depends on the chemical form of DIC that is assimilated, because the less abundant aqueous molecular $CO_2$ form contains much less $^{13}C$ than the bicarbonate anion form which makes up more than 90% of the total DIC. At the temperatures pertaining during the KEOPS study, this equilibrium fractionation lowers the $^{13}C$ content of aqueous molecular $CO_2$ by ~11‰ (Rau et al., 1997):

$$^{13}C\text{-}CO_2 = {}^{13}C\text{-DIC} + 23.644 - 9701.5/T_{kelvin} \quad (1)$$

Secondly, the cell $^{13}C$-POC content depends on the extent to which the enzymatic kinetic discrimination against $^{13}C$ during photosynthetic carbon fixation (of 20-30 ‰, varying with

367 the specific metabolic pathways) is expressed. It is only fully expressed when inorganic
368 carbon flow into and out of the cell (supply) is faster than fixation (demand).
369 Both these effects often lead to higher $^{13}C$ contents in faster growing cells, because faster
370 growth favours use of the more abundant bicarbonate form of DIC and also leads to less
371 expression of the kinetic fractionation.
372 Thus the association of higher $^{13}C$ contents with faster growing cells is very strongly
373 justified for any particular phytoplankton species, from both metabolic understanding and the
374 plethora of batch and chemostat experimental studies. Despite this understanding, inferring
375 growth rates for communities of phytoplankton from field measurements of $^{13}C$-POC is
376 fraught with difficulties. The magnitudes of these two main isotopic effects vary strongly
377 among different phytoplankton (and with their conditions of growth including temperature,
378 nutrient and trace metal availability, light levels, specific enzymatic pathways, etc.
379 (Burkhardt et al., 1999b;Burkhardt et al., 1999c;Fontugne et al., 1991;Schulz et al., 2007)),
380 and there is no universal quantitative relationship between growth rate and phytoplankton $^{13}C$
381 content. In particular, cell size is a key variable in the control of $^{13}C$ contents (Popp et al.,
382 1999;Rau et al., 1996;Rau et al., 1997;Rau et al., 1990). This effect is so important that the
383 global range of surface water bulk $^{13}C$-POC values can be observed across different size
384 fractions within a single Southern Ocean sample (Trull and Armand, 2001). Good
385 correlations between growth rates and $^{13}C$ contents when cell size is expressed in terms of the
386 surface/volume ratio suggest this results from the balance of supply versus demand (Popp et
387 al., 1998b), of either or both aqueous $CO_2$ and bicarbonate forms (Burkhardt et al.,
388 1999a;Keller and Morel, 1999;Schulz et al., 2007), and with further modulation by other
389 environmental controls such as the availability of light and other nutrients (Burkhardt et al.,
390 1999c;Gervais and Riebesell, 2001;Schulz et al., 2004).

391 This complexity means that our observed $^{13}$C-POC variations, even within a given size
392 fraction, could arise by multiple mechanisms. Higher $^{13}$C contents could reflect faster growth
393 rates (via either greater use of bicarbonate or an increase of fixation of all DIC chemical
394 forms relative to supply), or might instead reflect changes in species with inherently different
395 uptake and assimilation metabolisms, or changes in metabolism driven by other controls such
396 as light or iron availability. Our chemometric methods cannot distinguish among these
397 possible causes, and thus our expression of the $^{13}$C-POC variations in terms of growth rate
398 variations can only be viewed as an indicative exercise. To pursue this, we chose a model fit
399 to chemostat data (Popp et al., 1998b):

400 $$^{13}\text{C-POC} = (^{13}C_{source} - \varepsilon_f) + k \text{ demand-rate/supply-rate} \quad (2)$$

401 in which the first term expresses the lowest possible $^{13}$C contents of the cell as growth rate
402 approaches zero, and the second term describes the linear (constant k) dependence of isotopic
403 composition on the relative rates of $CO_2$ supply into the cell and it's cellular fixation. Popp et
404 al. (1998) assumed the chemical form was aqueous molecular $CO_2$, but further evaluation
405 showed that the data could also be fit by a model allowing either or both $CO_2$ and bicarbonate
406 uptake (Keller and Morel, 1999). Both models assume that the supply rate depends linearly
407 on its external concentration modulated by the surface area of the cell, and thus while the
408 fitting constants we use here are from Popp et al (1998), the scaling to the surface/volume
409 ratio (S/V) of the cell is independent of the chemical form of uptake):

410 $$^{13}\text{C-POC} = (^{13}\text{C-}CO_2 - 25) + 182\ \mu/([CO_2]\ S/V) \quad (3)$$

411 Rewriting this equation for growth rate, μ, and our measured $^{13}$C-DIC and $^{13}$C-POC values
412 yields an indicative path to possible growth rates for our size fractions:

413 $$\mu = S/V\ [CO_2]\ [^{13}\text{C-POC} - (^{13}\text{C-}CO_2 - 25)]/182 \quad (4)$$

414 with $^{13}C$-$CO_2$ calculated using Eq. (1), [$CO_2$] obtained from underway $pCO_2$ observations
415 (Lo Monaco et al., 2014) and Henry's Law (Weiss, 1974). In this expression, growth rate μ
416 is in $d^{-1}$, S/V in $\mu m^{-1}$, and [$CO_2$] in $\mu mol\ kg^{-1}$.
417 This expression provides growth rates that we compare to other estimates. Of course,
418 comparison of these rates is very sensitive to *S/V* estimates, as well as to all the other possible
419 sources of variations in $^{13}C$ contents summarized above. For example, a 30% increase in the
420 mean size of cells, such as could occur within a given size fraction, would yield a 69%
421 increase in the model growth rate (for spherical cells). For this reason, our growth rate
422 estimates must be viewed with great caution, not only in terms of their absolute magnitudes,
423 but also in terms of their relative magnitudes across the different stations.
424 In comparison to these fractionation effects accompanying primary production, trophic
425 $^{13}C$ enrichment is thought to be relatively small within a given class of compounds for carbon
426 (~ 1‰ per trophic level; (Michener and Schell, 1994)). However, accumulation of lipids,
427 which are $^{13}C$ depleted owing to their multi-step synthesis pathways, causes many
428 zooplankton to have lower $^{13}C$ contents than their diet (Michener and Schell, 1994;Syvaranta
429 and Rautio, 2010). This is a probable contributor to the $^{13}C$-POC values of the two largest
430 size fractions, as discussed in the results section.
431 Finally, because our focus is on extracting information about growth conditions for the
432 communities at the time of sampling, we remove the influence of source inorganic carbon
433 isotopic composition spatial variations on the 13C-POC variations, by examining their offset
434 relative to the source: $^{13}C\text{-}POC_{rs} = {}^{13}C\text{-}POC - {}^{13}C\text{-}DIC$.
435
436 **2.5.2 Isotopic chemometric principles – $^{15}N$**
437 Phytoplankton $^{15}N$-PN variations result primarily from the relative use of reduced
438 nitrogen (mainly ammonium) which has low $^{15}N$ contents vs. the more abundant nitrate pool

439 which has higher $^{15}N$ contents, and secondarily from variations in the isotopic fractionation
440 accompanying nitrate assimilation (Goericke et al., 1994;Karsh et al., 2003;2014;Trull et al.,
441 2008). As with the carbon isotopes, we discuss the $^{15}N$-PN variations relative to co-located
442 $^{15}N$-$NO_3$ source values ($^{15}N$-$PN_{rs}$ = $^{15}N$-PN - $^{15}N$-$NO_3$), to separate source composition
443 effects (that have accumulated from the history of nitrogen metabolism in a given parcel of
444 water) from the fractionation associated with current PN production. This source
445 composition effect was larger for nitrogen than for carbon, because variation in $^{15}N$-$NO_3$
446 values was larger (6.1 to 8.0‰), and $^{15}N$-PN variations were smaller (6‰).
447 By estimating expected values for $^{15}N$-$PN_{rs}$ formation from nitrate and from
448 ammonium, estimates of new vs. recycled production (i.e. *f* ratios) can be obtained for each
449 size fraction by mass balance. The observed range of fractionation factors for nitrate
450 assimilation during KEOPS2, namely $\varepsilon_{na}$ of -4 to -4.5 ‰, as estimated from $^{15}N$-$NO_3$
451 variations in the water column (Dehairs et al., 2014), provides an upper limit for growth on
452 nitrate of $^{15}N$-$PN_{rs}$ (-4‰). For ammonium, the simplest approximation is to use a value just
453 below the lowest observed $^{15}N$-$PN_{rs}$, i.e. to assume that these cells grew on ammonium alone
454 (Trull et al., 2008). Using these end members ($^{15}N$-$PN_{Nrs}$ = -4 ‰ for growth on nitrate; $^{15}N$-
455 $PN_{Ars}$ = -8 ‰ for growth on ammonium), yields *f* ratio estimates for each size-fraction, from:

456 $$f = (^{15}N\text{-}PN_{rs} - {}^{15}N\text{-}PN_{Ars})/(\,{}^{15}N\text{-}PN_{Nrs} - {}^{15}N\text{-}PN_{Ars}) \quad (5)$$

457 In comparison to carbon, trophic enrichment of $^{15}N$ is relatively large (~3‰ vs ~1‰;
458 (Michener and Schell, 1994;Wada and Hattori, 1978), which provides a cautionary note on
459 the interpretation of the *f* ratio estimates. The largest zoo-plankton containing size fractions
460 (210-300 µm, 300-1000 µm) have higher $^{15}N$-$PN_{rs}$ values than are achievable by primary
461 production and derive from this process.
462

463 **3 Results**

### 3.1 Total biomass variations

POC biomass concentrations in surface waters varied from ~ 3 to 25 μM (Table 2), reported as the tota sum of fractions as filtered from as much as 2600 L of underway supply water, and are in agreement with our 1 L single filter bulk filtrations (Appendix A). Although there were some differences in POC results across the multiple sample methodologies of the entire KEOPS2 program e.g. from underway supply, Niskin bottles, and in-situ pumps (Dehairs et al., 2014;Lasbleiz et al., 2014;Tremblay, 2014), these remain to be fully assessed and here we focus on our own internally consistent results.

There were significant variations of POC concentrations within the Groups as well as among them (Fig. 3). The upstream Fe-poor HNLC reference station R2 and the early sampled furthest south and coldest Group 3 plateau station A3-1 had the lowest values. The recirculation initial survey stations in Group 1 had somewhat higher values (5-10 μM; with a single higher value of 15 μM at TEW-4, attributable to a high heterotropic contribution to its largest size fractions), with little increase over time as represented by the Group 2 recirculation time series (again with a single outlier at E4-E). The Group 5 downstream Polar Front bloom stations had the highest biomasses, exceeding all but 1 of the Group 3 Plateau stations as well as all Group 4 coastal stations. Note that the Group 5 stations from warmer waters north of and near the Subantarctic front (TNS 1 and 2), where the upstream flow may not cross the Kerguelen shelf, stand out from the other Group 5 stations as having much lower biomass, similar to the upstream HNLC reference station (R2). This distribution of POC among the Groups provides important results: (i) waters that have not crossed the plateau have low biomass, presumably reflecting a lack of Fe fertilisation, and (ii) downstream blooms achieve higher concentrations of biomass than coastal blooms. Given that Fe concentrations were highest in the coastal waters (Table 1; section 2.2), this means that ecosystem dynamics must also contribute importantly to the control of biomass.

Distributions of POC with particle size also varied significantly (Fig. 3). All stations exhibited the highest concentrations in the smallest size fraction (1-5 μm) *when normalized to the width of this fraction interval* (Fig. 3), but these concentrations were relatively constant across the Groups. In contrast the concentrations in the three phytoplankton dominated intermediate size fractions (5, 20, 50 μm filters) varied among the groups, and drove the total POC biomass changes described above. There were significant variations within these 3 size fractions as well. Abundance decreased monotonically with size at the HNLC reference station. The Group 1, and even more so the Group 2, stations exhibited greater increases (as total biomass increased either among stations in Group 1 or with time in the Group 2 time series; note that Table 2 lists all stations in chronological order) in the 20 μm fraction than the 5 μm fraction, but still low values in the 50 μm fraction. The Group 3 plateau stations started with this slightly "humped" POC distribution (i.e. POC higher in the 20 μm fraction than in both the 5 and 50 μm fractions), but as biomass increased with time the 50 μm fraction came to dominate. Interestingly, this never occurred in the Group 4 coastal or Group 5 Polar Frontal biomass rich stations, which remained dominated by the 20 μm size fraction.

Heterotrophic biomass (as represented by the two largest size filters, 210 and 300 μm) was generally an order of magnitude lower than autotrophic biomass (as represented by the 3 intermediate fractions), and more than 2 orders of magnitude lower if the smallest fraction is also included as an autotroph fraction. Heterotrophic biomass generally increased with total biomass in all the Groups, except the Group 4 coastal waters. As mentioned earlier, station TEW-4 in Group 1 had unusually high heterotrophic biomass, which explains its outlier status of exceptionally high total POC for this Group.

**3.2 Variations in BSi concentrations and associated contributions to biomass**

513 BSi estimates were not possible for the smallest size fraction (owing to use of a quartz
514 1 μm filter). Thus total BSi is underestimated, and comparisons to total POC must be done
515 cautiously. As shown in Fig. 3 (top row), the highest BSi levels were observed in the Plateau
516 stations late in the voyage, with these exceeding those of the Group 5 Polar Frontal bloom
517 stations as well as all the other Groups. The lowest levels were in the Polar Frontal Zone and
518 Subantarctic stations (Group5, stations TNS1 and 2). More detailed evaluation is possible on
519 a size-fractionated basis. The initial survey of Group 1 low biomass waters found a wide
520 range of BSi/POC ratios that covered most of the variability seen across the entire KEOPS2
521 study (Fig. 3; bottom row). Among the other groups, the Group 3 plateau stations stands out
522 for having high BSi/POC ratios in all the autotrophic fractions (5, 20, 50 μm filters), in
523 contrast to uniformly low ratios for the Group 5 stations. The presence of non-zero BSi/POC
524 ratios in many of the largest, zooplankton dominated size fractions (210 and 300 μm filters)
525 reflects the presence of chain-forming diatoms, although their POC biomass was insignificant
526 in comparison to that of the autotrophic intermediate fractions.
527 Much of the range in BSi/POC ratios for the intermediate size fractions overlaps with
528 that expected for diatoms under iron-impoverished (BSi/POC ~0.6) to iron-replete (BSi/POC
529 ~0.15) conditions (Hoffman et al., 2007;Hutchins and Bruland, 1998;Takeda, 1998), but note
530 that this is a simplistic view of diatom BSi/POC variations in response to Fe inputs which
531 ignores variations across taxa and across life cycle stages (Leynaert et al., 2004;Marchetti and
532 Cassar, 2009;Ragueneau et al., 2006) . There was no clear correspondence across the groups
533 between BSi/POC values and Fe fertilisation levels, in that the Group 4 Fe-rich coastal waters
534 had intermediate BSi/POC ratios in comparison to the moderately Fe-rich Group 3 plateau
535 and Group 5 downstream Polar Front waters. Community variations in the ratio of diatom to
536 non-diatom taxa thus appear to overprint any dependence of diatom BSi/POC ratios on Fe
537 levels.

538

539 **3.3 $^{13}$C variations**

540 We first note that the $^{13}$C-POC$_{rs}$ values of the HNLC reference station (R-2) were the
541 lowest of all stations, and we take them as an indication of expectations for slowly growing
542 offshore polar phytoplankton (Fig. 4). In comparison, Group-1 and Group-2 stations (which
543 had indistinguishable $^{13}$C-POC$_{rs}$ values), were elevated by ~2‰ (ranging from 1 to 4‰) in
544 comparison to the R-2 HNLC reference level. These stations also displayed an increase in
545 $^{13}$C-POC$_{rs}$ values from the smallest (1-5 µm) towards larger size fractions (5-20, 20-50 µm)
546 before decreasing again in the largest autotrophic size fraction (50-210 µm) and generally
547 also in the heterotrophic dominated size fractions (210-300 and 300-1000 µm). This hump-
548 shaped pattern was also present at the Group-3 plateau stations, where $^{13}$C-POC$_{rs}$ values were
549 elevated further. The Group-4 coastal stations had the highest $^{13}$C-POC$_{rs}$ values, with values
550 as high as -20‰.

551 This pattern has been found before in Antarctic polar waters, with the initial increase
552 in $^{13}$C-POC$_{rs}$ with size attributed to the effect of decreasing surface/volume on $CO_2$ uptake
553 (Popp et al., 1998a;Popp et al., 1999), and the subsequent decrease in larger fractions
554 attributed to the presence of needle-shaped diatoms with high surface/volume (*S/V*) ratios
555 similar to small cells (Trull and Armand, 2001). Detailed *S/V* estimates for our samples are
556 not yet available to assess this explanation or the influence of the presence of chains of
557 *Fragillariopsis kerguelensis, Eucampia antarctica*, and *Chaetoceros hyalochaeta* diatoms
558 which contribute strongly to the larger autotrophic size fractions at many stations (Armand et
559 al., personal communication, 2014). The presence of lipid-rich zooplankton in the two
560 largest size fractions is another probable cause of their low $^{13}$C-POC values, based on low
561 $^{13}$C-POC values for zooplankton collected with nets during KEOPS2 (Carlotti et al., 2014).

562 To translate our observed $^{13}$C-POC variations (in the autotrophic size classes) to
563 growth rates using the relationships described in the Methods (section 2.5.1), we must make
564 some assumptions about the size and shapes of the phytoplankton in the different filter
565 fractions. This choice is difficult in the absence of detailed observations, and we took a very
566 simple approach of representing the phytoplankton as rectangular prisms with square cross-
567 sections, with the dimensions given in Table 3 for the 1, 5, 20, and 50 μm filter fractions. For
568 the two larger fractions, we assumed diatoms were predominantly present as chains (based on
569 microscopy; Armand et al., personal communication, 2014), and that the surface for $CO_2$
570 exchange was accordingly reduced (the details accompany Table 3). These assumptions are
571 of course tenuous because diatom chains vary in their morphology, and of course the
572 relationship between *S/V* and uptake is itself a large assumption, in that it presupposes that
573 both diffusive and active inorganic carbon uptake scale with cell surface area (see Methods
574 for additional discussion of the uncertainties in estimating growth rates from $^{13}$C-POC
575 contents). Nevertheless, on this basis, we obtained $^{13}$C model growth rate variations for each
576 of the autotrophic size fractions (Table 2) and total community growth rates (Fig. 5) for each
577 station by summing results for the four smallest size fractions (1, 5, 20, 50 μm). Similar
578 variations across the stations were obtained by limiting the sum to the 5, 20, and 50 μm
579 fraction results (data not shown). The $^{13}$C model growth rates decreased with size across the
580 size fractions (from the 1 to the 50 μm filter) by factors of 10 to 15, in excellent agreement
581 with allometric relationships assembled for a much broader range of phytoplankton, although
582 the high growth rates of 2 to 3 $d^{-1}$ in the smallest fraction are greater than expected for polar
583 waters (Chisholm, 1992;Cózar and Echevarría, 2005). This could reflect significant
584 contributions from detritus from larger autotrophs and bacteria in this fraction, or other errors
585 in the model (see the Methods section for discussion of the low fidelity of the $^{13}$C model
586 growth rates).

587 Our community (sum of fractions) $^{13}C$ model growth rates compare reasonably well
588 with a limited set of incubation results, calculated by integrating results from different light
589 level deck onboard incubations (Cavagna et al., 2014) over the depth of the surface mixed
590 layers as shown in Table 4 (Park et al., 2014b;Park et al., 2014a). The overall dynamic range
591 of the incubation and model growth rates was identical (0.18 $d^{-1}$). For the model this ranged
592 from 0.08 $d^{-1}$ at the coldest early-sampled low biomass station over the plateau (A3-1) to 0.27
593 $d^{-1}$ at coastal station TEW-2. The incubations ranged from a low value of 0.065 $d^{-1}$ at the
594 HNLC reference station (A3-1 was not studied) to a high of 0.24 $d^{-1}$ at the Group 5 Polar
595 Front station F-L (coastal stations were not studied). Overall correlation between the 8 pairs
596 of results from the same stations (though not sampled at identical times) was very poor
597 ($r^2<0.1$) but this was driven by strong disagreement at the single Group 5 downstream Polar
598 Front station where the incubations found their highest depth integrated growth rate (0.24 $d^{-1}$
599 at F-L) but our $^{13}C$-based estimates were much lower, and without this pair, the correlation
600 was reasonably strong ($r^2=0.67$).
601 Given the importance of *S/V* variations to the $^{13}C$ model growth rate estimates (see the
602 Methods section), variations between Groups with similar size distributions and
603 phytoplankton flora (the Group 1, 2 recirculation and Group 3 plateau stations) are probably
604 more reliably assessed than variations between Groups with more distinct flora (coastal
605 Group 4 stations and downstream Polar Front Group 5 stations). The Group 2 recirculation
606 time series showed quite constant and moderate growth rates (0.17 – 0.19 $d^{-1}$). Interestingly,
607 values during the earlier Group 1 initial survey were somewhat higher in this region (0.19 –
608 0.21 $d^{-1}$), and reached 0.23 $d^{-1}$ at the southern end of the north-south transect over the plateau
609 (TNS 9, 10). Later sampled Group 3 plateau stations (A3-2, G1, E4W, E4W2) also had high
610 $^{13}C$ model growth rates (0.19 - 0.24 $d^{-1}$).

These growth rate variations are in broad agreement with the development of blooms in these regions – in that the lowest biomass accumulation over the study period occurred in the recirculation, with higher values over the plateau. In contrast, the model suggests that the highest growth rates occurred in Group 4 coastal waters, where biomass accumulation was only moderate, and found only moderate growth rates for the Group 5 Polar Front stations where a strong bloom was already underway at the time of sampling (Fig. 2). Unfortunately, it is not currently possible to determine whether this reflects the simplicity of the model or the complexity of the ecosystem dynamics. This provides a useful cautionary note that the apparent growth rate variations have no real quantitative validity; at best they provide indicative information on the relative intensities of $CO_2$ assimilation across the Groups. Indeed, it is possible that the variations among the Groups results from other issues such as species metabolic differences, or light and trace element availability (as discussed in detail in the Methods section). Thus it is important to emphasize that the overall view of ecosystem responses developed in the Discussion section below does not depend only on these potential growth rate estimates from the $^{13}$C-POC observations, but also draws on biomass accumulation rates from the POC concentrations, their distribution across size fractions, and other indicators as discussed below.

### 3.4 $^{15}$N variations

Similarly to the carbon isotopes, we discuss the $^{15}$N-PN variations relative to co-located $^{15}$N-$NO_3$ values ($^{15}$N-$PN_{rs}$ = $^{15}$N-PN - $^{15}$N-$NO_3$), for the reasons outlined in the Methods (section 2.5.2). As shown in Fig. 4, almost all the phytoplankton dominated size fractions (5-20, 20-50, 50-210 μm) had $^{15}$N-$PN_{rs}$ values that fall between the upper bound of production from nitrate ($^{15}$N-$PN_{rs}$ = -4) and the lower bound of production from ammonium ($^{15}$N-$PN_{rs}$ = -8). There was also a tendency across all Groups towards lower $^{15}$N-$PN_{rs}$ in the

636 smaller phytoplankton fractions; consistent with greater use of ammonium by smaller
637 phytoplankton (Armstrong, 1999;Karsh et al., 2003). The largest zoo-plankton containing
638 size fractions (210-300, 300-1000 μm) had higher $^{15}N\text{-}PN_{rs}$ values, which presumably result
639 from the relatively large (~3 ‰) trophic enrichment that occurs in many marine organisms
640 (Michener and Schell, 1994;Wada and Hattori, 1978). While these general variations with
641 size held for all Groups, there were significant differences. In particular, the Group 3 plateau
642 stations had the lowest $^{15}N\text{-}PN_{rs}$values for the larger autotrophic size classes (20-50 and 50-
643 210 μm).

644 Using the end-member mixing model (Methods section 2.5.2), we obtained the estimated
645 community *f* ratios as shown in Fig. 5. The Group 3 plateau stations tended to have
646 somewhat higher values (~0.7 vs. ~0.6) than the Group 5 downstream Polar Front bloom
647 stations (TEW-7, TEW-8, and F-S); although this was not true for the highest biomass station
648 (F-L). As with the $^{13}C$ model growth rates, the Group 1 recirculation stations sampled early
649 on the TNS transit were somewhat surprising in having relatively high values, though these
650 were not observed on the later TEW transit or during the Group 2 time series. Finally, the
651 coastal stations had high *apparent f* ratios, including values that exceed 1 (pointing to
652 limitations of the model). Importantly, these high values are driven by the relatively low $^{15}N\text{-}$
653 $NO_3$ values in these coastal waters, rather than by higher $^{15}N$ contents in their PON. The low
654 $^{15}N\text{-}NO_3$ values are a surprise given the relatively low nitrate concentrations in these coastal
655 waters (Fig. 6), suggesting other processes are at work. Our observations are insufficient to
656 explain this. One possibility is delivery of low $^{15}N$ nitrate from sedimentary nitrification, but
657 this still leaves open the question of why recently formed PN does not track the overall nitrate
658 pool isotopic composition. Reliance on the *f* ratios from these coastal stations is thus not
659 advisable. In contrast, comparison of our offshore *f* ratios to incubation results (Fig. 5) shows

similar values and excellent correlation ($r^2$=0.90; provided the one very low incubation based *f* ratio at the HNLC station R2 is discounted).

**3.5 Nutrient depletion estimates**

Surface water nutrient concentrations provide an initial perspective on the efficiency of the biological pump. The surface nitrate concentrations were lower north than south of the Polar Front, but of course this may reflect longer term, basin scale, controls on nitrate. Determination of the role of local recent biological activity in nitrate depletion requires a much closer examination. Fig. 6 shows high spatial resolution maps of nitrate, temperature, and salinity obtained with the sensors operated continuously underway. Waters upstream from the plateau and south of the Polar Front were cold and saline with high nitrate concentrations, with these parameters reaching their highest values over the central plateau early in the voyage (near the Group 3 KEOPS bloom reference station A3-1), with temperature less than 2ºC, salinity greater than 33.9, and nitrate above 30 μM. At the other extreme, Group 4 coastal waters had the lowest surface nitrates (below 10 μM), in association with very fresh (salinity <33.6) and relatively warm (>3.5ºC) waters. The Group 5 waters downstream in the bloom that formed north of the Polar Front well to the east (near 74-75ºE and the Group 5 stations TEW-7, -8, F-L and F-S), also had relatively low surface nitrates (15-20 μM ) and low salinities (33.7-33.8), and were quite warm (>4 ºC). In comparison, The Group 2 recirculation feature had intermediate nitrate concentrations between the plateau, coastal, and downstream Polar Front plume conditions.

These conditions evolved over the course of the study, with decreases in surface nitrate values being particularly strong (reaching 6-8 μM from winter conditions; Table 4) in regions of rapid biomass accumulation over the central plateau (especially along the plateau edge to the north of the A3 station) and in the bloom north of the Polar Front (near stations

685 TEW-8, F-L, F-S). Low nitrate concentrations were also found in association with relatively
686 low salinities to the southeast of the recirculation region, where the ship transited without
687 station sampling. This appears to represent southward supply of waters from north of the
688 Polar Front in association with its meandering (as also suggested by the satellite chlorophyll
689 image sequences (Fig. 2 and animation in the Supplement, and by water parcel trajectories
690 estimated from drifters and satellite altimetry; d'Ovidio et al., 2014). This process also
691 appears to have driven warming and freshening in the recirculation over time. Thus nitrate
692 budgets require partitioning of temporal changes driven by both hydrology and biology.
693 To separate local biological nitrate depletion from hydrological controls, we
694 examined nitrate depletions in surface waters relative to estimates of initial winter nitrate
695 concentrations for each station, as estimated from CTD profiles. We considered integrations
696 to two different depths: (a) the frequently used choice (e.g. Arrigo et al., 1999;Sweeney et al.,
697 2000) of the depth of the remnant winter water temperature minimum ($T_{min}$-depth), and (b)
698 shallower depths based on a threshold increase in salinity of 0.05 ($S_{threshold}$-depth). This
699 second choice was motivated by the presence of significant salinity gradients above the $T_{min}$-
700 depth (examples are shown in Fig. 7), particularly in waters near and north of the Polar Front,
701 suggesting either that the most recent winter mixing was not as deep as previous years, or that
702 horizontal mixing had brought fresher waters over the top of the $T_{min}$, and thus in either case
703 that nitrate depletion between the $T_{min}$-depth and $S_{threshold}$-depth was not attributable to local
704 biological processes.
705 The two nitrate depletion metrics give differing views of the contributions to export
706 from the different community Groups (as summarized in Fig. 8). Estimates based on the $T_{min}$
707 approach were much higher than those from the $S_{threshold}$ approach, because the $T_{min}$-depth and
708 was generally deeper and had higher nitrate than the $S_{threshold}$-depth (Table 4)., The $T_{min}$
709 approach suggested that the greatest depletion occurred in the downstream plume to the north

710 of the Polar Front. In contrast, the $S_{threshold}$ approach identified the highest seasonal nitrate
711 depletion as occurring over the central plateau, with somewhat lower values in the
712 recirculation feature, followed by the Polar Frontal bloom and the reference station. These
713 methodological differences were even larger for the silicic acid depletions (Fig. 8). This
714 analysis underlines the importance of appropriate winter nitrate (and silicic acid) surface
715 nitrate concentration estimates to the assignment of export magnitudes.

716 We believe the $S_{threshold}$ approach is the most appropriate given the observed salinity
717 stratification, especially for the relatively weak subsurface thermal stratification observed in
718 the Group 5 stations near the Polar Front, where its choice makes the most significant
719 difference from estimates based on the $T_{min}$ approach. This is because the high biomass layer
720 found in these Polar Frontal sites is in this shallow salinity-defined layer, and because the Fe
721 fertilization of these waters is recent as shown by their short transit time of ~ 2 weeks since
722 crossing the plateau as determined from both altimetry and drifter releases (d'Ovidio et al.,
723 2014; Park et al., 2014). Thus attribution of nutrient depletion below the depth of the $S_{threshold}$
724 to local iron fertilized biomass production is not warranted. For all the Groups, both the $T_{min}$
725 and $S_{threshold}$ based nitrate depletions are relatively small as percentages of the initial upper
726 water column inventories (2-18%; Table 4). This reflects the early seasonal sampling, as well
727 as a significant extent of recycling via nitrification (Dehairs et al., 2014;Lasbleiz et al., 2014).
728 Fractional depletions of silicate were higher (3-53%; Table 4b), consistent with the results of
729 the autumn KEOPS expedition which revealed low nitrate removal but near complete Si
730 depletion (Mosseri et al., 2008). Finally, we note that we could not estimate export for the
731 Group 4 Kerguelen Island coastal stations because neither the $T_{min}$ nor the $S_{threshold}$ approaches
732 were compatible with their shallow water columns.

733 Our preferred $S_{threshold}$ nitrate depletion estimate can be further refined by removal of
734 the standing stock of other nitrogen forms produced by the ecosystem (ammonium, urea,

735 dissolved organic nitrogen, particulate nitrogen) to give a better estimate of N export from
736 surface waters. PN dominated these stocks, with concentrations up to 5 μM (Lasbleiz et al.,
737 2014)), in contrast to ammonium, nitrite, and surface enhancements of DON (i.e. the fresh
738 component) with concentrations below 1 μM (Blain et al., 2014;Dehairs et al., 2014).
739 Subtracting PN stocks (integrated to 200m depth (Lasbleiz et al., 2014) suggests that for
740 many stations about half of the consumed nitrate has been exported and about half remains in
741 the water column (Table 4).

742 A few stations exhibited negative N export estimates, because of higher PN stocks
743 than their nitrate depletion estimates (Table 4). This could arise from either underestimation
744 of nitrate depletions owing to entrainment of subsurface waters (an effect that can halve
745 nutrient depletion estimates under conditions of weak water column stratification and strong
746 winds; (Wang et al., 2003)), or horizontal interleaving of relatively undepleted water parcels
747 with relatively PN rich waters. Notably the largest excesses of PN stock over nitrate
748 depletions occurred at stations located close to fronts (TEW-3 and F-S).

749 Viewed at the Group level, the nitrate depletions and N export estimates (Fig. 8)
750 provide very useful insights. Firstly, given the uncertainties regarding the estimation of
751 nutrient depletions from the profiles, it could be argued that the most robust conclusion is that
752 all the Groups exhibit similar depletions, with roughly half of the N uptake exported and half
753 remaining as accumulated biomass. This is consistent with the growth estimates of roughly
754 one doubling every 3 days and the satellite biomass observations indicating slower doubling
755 approximately each week. Looking into more detail, and focusing on the salinity threshold
756 approach, suggests that the highest nitrate depletions occurred for the Group 3 plateau
757 stations, with significantly lower values in the Group 1 and Group 2 recirculation stations
758 (Fig. 8 middle panel). However, the larger standing stock of PN biomass over the plateau
759 means that the export up to the time of sampling was only slighter higher than in the Group 1

and 2 recirculation stations. This aspect is even stronger for the Si budgets, with the export of Si higher for Groups 1 and 2 than over the plateau in Group 3, emphasizing the retention of N in comparison to Si during export.

Another interesting insight is that, in comparison to the Group 3 plateau stations, nitrate depletion and export are much lower in the Group 5 Polar Frontal bloom stations. Considering the $S_{threshold}$-depths (Table 4), and the associated Si depletion and export results (Fig. 8), helps understand why the Polar Frontal bloom produced less nitrogen depletion and export than the plateau bloom. Firstly, the Polar Frontal bloom depletion is a shallow feature compared to that over the plateau (Fig. 7), secondly a much greater proportion of the assimilated nitrogen is still present as standing stock (Fig. 8 bottom panel), and thirdly, there is some suggestion that more nitrogen than silicon is retained as standing stock (as a portion of depletion; compare the Fig. 8 middle and bottom panels). Of course observation of these variations in spring does not mean that they would have persisted into summer, and it is possible that over the full season the extent of nutrient depletion was significantly different then observed during the KEOPS2 shipboard campaign, either towards homogeneity across the region or towards larger variations.

## 4. Discussion

Our overall interest is to understand community responses to iron fertilisation, with a particular focus on ecosystem control of nutrient depletion and carbon export. We expect this response to vary as a function of iron inputs, but also possibly with time since fertilisation and its persistence (as a result of cascading trophic effects), and time of year (as a result of strong seasonality of the physical and biological background). Specific probable seasonal modulators of the response to iron include insolation, stratification, and the abundance of organisms with life cycles that resonate at the seasonal scale, e.g. larger zooplankton. In the

following sections, we summarize the structure and function variations, relate them to temporal settings (as developed in the Methods section), and compare them to our estimates of nitrate (and silicic acid) depletion from surface waters as a proxy for carbon export.

### 4.1 Overview of community structure and function variations

Our size-fractionated chemometric parameters for microbial ecosystem structure and function identified significant differences among the various environments sampled by the KEOPS2 program. The upstream HNLC reference station (R2) displayed low phytoplankton abundance, relatively high BSi/POC ratios, slow growth rates (as indicated by both strong discrimination against $^{13}C$ uptake (this work) and slow growth rates measured in deckboard incubations (Cavagna et al., 2014)). Its $^{15}N$-PN values suggested that growth was predominantly on nitrate, although this result must be viewed with caution since it differs from the surprisingly low *f* ratio obtained by incubation (Cavagna et al., 2014). These characteristics are consistent with its selection as a HNLC reference, but the total integrated biomass was higher than the lowest values seen in Southern Ocean HNLC waters and mesopelagic Ba levels indicated POC remineralization, possibly indicating a low-level early production event (Jacquet et al., 2014;Lasbleiz et al., 2014) as a result of a small degree of Fe fertilisation, possibly from particulate Fe inputs from the nearby Leclaire Rise (van der Merwe et al., 2014).

The moderate iron fertilisation of the recirculation feature downstream from the plateau (stations in Groups 1 and 2) increased $^{13}C$ model growth rates (relative to the HNLC reference station R2) by ~0.02 to 0.04 $d^{-1}$ (Fig. 5) and biomass ~2-fold (increasing from ~50% to 4-fold over time; Fig. 3), particularly in the larger phytoplankton size fractions (20-50 and 50-210 μm). There was no systematic change in BSi/POC ratios, with some stations showing lower values consistent with relief of iron limitation, but others showing higher values.

Whether this resulted primarily from changes in species or the presence of empty frustules is unclear, although the analysis of depletions and standing stocks suggests loss of empty frustules (as did earlier work during KEOPS; (Mosseri et al., 2008)). This may reflect varying levels of low production (Cavagna et al., 2014) coupled closely to export, as well as the possibility that production was in part limited by variations in mixed layer depth (Lasbleiz et al., 2014). The $^{15}$N-PN observations indicated growth primarily on nitrate (as at the HNLC reference station).

Both of the more strongly iron fertilised offshore regions (the Group 3 central plateau and the Group 5 Polar Front bloom, Table 1.) exhibited increased $^{13}$C model growth rates in comparison to HNLC waters (elevated by ~0.05 $d^{-1}$), but their community structures were quite different (emphasizing caution regarding the $^{13}$C model growth rates, although the incubation results also indicated increased growth rates; (Cavagna et al., 2014)). The plateau stations exhibited most of their enhanced biomass in the largest phytoplankton size fraction (50-210 μm); whereas Polar Frontal biomass increases were dominated by the next smaller size (20-50 μm). This was also true for the very strongly Fe fertilized Group 4 coastal stations where $^{13}$C model growth rates were even more elevated (by 0.1 to 0.19 $d^{-1}$ above the HNLC reference). Use of ammonium vs. nitrate (as estimated from both natural abundance 15N values in this work and tracer 15N uptake incubations by Cavagna et al., 2014), was also different between the plateau and downstream Polar Frontal blooms, with the plateau stations using a greater proportion of nitrate.

**4.2 Links between community structure and export**

Overall, one of the most important outcomes of our results regarding export (presented in section 3.5 and Fig. 8) is that surface biomass is not a good guide to the history of export, i.e. the low biomass recirculation feature exhibited as much export as from the higher biomass

Polar Front or Plateau blooms. This same conclusion was reached on the basis of sparse sediment trap deployments at 200 m depth (Laurenceau et al., 2014) and $^{234}$Th depletions in surface waters, which identified the recirculation feature as having the highest C exports of all regions (Planchon et al., 2014).

The cause of the low export, at 200m depth, from the Polar Front bloom (Group 5 downstream stations) may in part be the shallowness of its high biomass surface layer (only ~ half that of the recirculation feature and plateau; (Lasbleiz et al., 2014;Laurenceau et al., 2014)), allowing for more remineralisation before export through the 200m depth horizon. The cause of the high export from the low biomass recirculation feature is less easy to understand – it suggests that production (also found to be moderately high in these waters compared to the other regions; (Cavagna et al., 2014)) and export have been in close balance in these waters. This is a phenomenon often found in association with small phytoplankton dominated communities, and attributed to tight coupling with small grazers (Boyd and Newton, 1999;Cullen, 1995). Our observations show that this tight coupling also persisted as very large, moderately to heavily silicified diatoms (Fig. 3) became dominant. This suggests that tight coupling may have also been achieved for the larger phytoplankton. Notably there were abundant large herbivorous zooplankton in the recirculation region (Carlotti et al., 2014), and large fecal pellets as well as diatom aggregates were important contributors to export, based on observations in polyacrylamide gel filled sediment traps (Laurenceau et al., 2014). In making these comparisons among the station Groups, it is of course important to remember that our observations of nutrient depletion and export apply only at the this early spring observation time, and the subsequent evolution of the different water parcels may lead to different outcomes when averaged over the full annual cycle.

### 4.3 Influence of fertilisation time and persistence on ecosystem responses

As developed in the Methods section, we consider four possible relative indices for the nature of the Fe fertilization and the overall ecosystem responses:

i. Intensity of Fe fertilisation (lowest to highest):

*recirculation feature* < *plateau* <≈ *Polar Front plume* << *coastal stations*

ii. Elapsed time since Fe fertilisation and its persistence (most recent to oldest):

*Polar Front plume* < *recirculation feature* ≈ *plateau* < *coastal stations*

iii. Magnitude of biomass accumulation (lowest to highest, at end of voyage):

*recirculation feature* < *coastal stations* < *plateau* <≈ *Polar Front plume*

iv. Elapsed time since initiation of biomass accumulation (most recent to oldest):

*recirculation feature* < *Polar Front plume* <≈ *plateau* << *coastal stations*

If we put aside the coastal stations, where depletion and export could not be estimated, we can ask which of these might explain why the recirculation feature achieved high export in comparison to its low to moderate biomass and low to moderate intensity of iron fertilisation. Index (ii) emerges as the most likely candidate – the recirculation feature receives low intensity ongoing iron fertilisation as a result of the recirculation of waters along the Polar Front and into it from the northeast (d'Ovidio et al., 2014), with possible augmentations from shallow Ekman transport from the nearby Kerguelen shelf (d'Ovidio et al., 2014;Sanial et al., 2014). This is a fascinating possibility, because it suggests ecosystems are modulated differently by persistent as opposed to punctual inputs of Fe.

Indices (i) and (iv) also list the recirculation as an end-member, but it seems unlikely that low Fe levels or low biomass are drivers of high export, given that many studies of export have found positive correlations with biomass, though with significant modulation by community structure, e.g. (Boyd and Newton, 1995;Boyd and Newton, 1999;Boyd and Trull, 2007;Buesseler, 1998;Buesseler et al., 2001;Buesseler et al., 2007).

884 Do any of these indices also provide insight on why the community differs between
885 the two strongly iron fertilised regions (the central plateau vs. the downstream Polar Front)?
886 For size structure, none of the time perspectives (indices ii-iv) appears to help – the plateau
887 and recirculation features with their dominance by very large diatoms (vs. the more balanced
888 size structure of the coastal and downstream Polar Front bloom) do not fall appropriately
889 along any of the time spectrums of these three 'clocks'. To the extent that the intensity of
890 iron fertilisation (index i) may have been higher in both coastal and Polar Front waters than
891 over the plateau, despite similar current Fe levels (see the Methods section for discussion),
892 this could provide an explanation, but it would imply that more Fe produces communities
893 with smaller cells and thus be counter to the results of artificial iron experiments (Boyd et al.,
894 1999;Boyd et al., 2007). This leaves us with the strong possibility that the community
895 structure differences between the plateau and Polar Front regions derive in part from other
896 factors beyond levels, timing, or persistence of iron fertilisation.
897
898 **5. Conclusions**
899 A complex mosaic of phytoplankton blooms forms in response to natural iron fertilisation
900 from the Kerguelen plateau. Community structure variations in the downstream waters
901 appear to have multiple influences, including the intensity and persistence of iron fertilisation,
902 the progress of biomass accumulation, and possibly whether they were sourced from plateau
903 vs. coastal waters. These differences developed even though phytoplankton growth rates
904 appeared to increase more directly with the level of iron availability, pointing to additional
905 influences from trophodynamics. These community effects strongly decoupled levels of
906 surface biomass from levels of particle export to the ocean interior over the timescales of
907 spring bloom development studied here.
908

909

Table 1. Station Groups

| Groups | Time in voyage | Time since bloom start | Biomass at sampling | Iron supply |
|---|---|---|---|---|
| 1 recirculation survey[1] | early | ~0-1 week | low | low to mod. |
| 2 recirc. time series | early to late | ~1-3 weeks | low, stable | moderate |
| 3 plateau | early, late | ~2-4 weeks | mod. to high | mod. to high |
| 4 coastal | early | ~4-6 weeks | mod., stable | very high |
| 5 downstream Polar Front[2] | middle, late | ~2-4 weeks | high | mod. to high |

Notes:
[1]. also includes HNLC reference stations
[2]. also includes Subantarctic stations
Fig. 1. shows map of station locations
Fig. 2. shows biomass distributions at the time of sampling
Satellite chlorophyll animation (Supplement) shows the full seasonal bloom cycle.
Timing of Fe supply is discussed in the text.

Table 2. Chemometric results for size-fractionated particles.

| Station | Volume | fraction | POC | PN | PBSi | POC/ | PBSi/ | PBSi/ | $\delta^{13}$CPOC | $\delta^{13}$CPOC-$\delta^{13}$CDIC | $\delta^{15}$NPN | $\delta^{15}$NPN-$\delta^{15}$NO3 | *f* ratio | growth rate |
|---|---|---|---|---|---|---|---|---|---|---|---|---|---|---|
| Date/location | L | µm | µM | µM | µM | PN | POC | PN | ‰$_{V\text{-}PDB}$ | ‰$_{V\text{-}PDB}$ | ‰air | ‰air | | $d^{-1}$ |
| group | | | | | | atom | atom | atom | | ***$\delta^{13}$CDIC*** | | ***$\delta^{15}$NO3*** | | ***$[CO_2]_{aq}$*** |
| A3 1 | 1181 | 300 | 0.01 | 0.00 | 0.00 | 11.15 | 0.21 | 2.30 | -25.01 | -26.24 | #N/A | #N/A | | |
| 20/10/2011 | 1181 | 210 | 0.02 | 0.00 | 0.00 | 6.46 | 0.17 | 1.13 | -26.16 | -27.39 | 3.97 | -2.12 | | |
| 50.6300 E | 184 | 50 | 0.73 | 0.13 | 0.60 | 5.62 | 0.83 | 4.65 | -23.09 | -24.32 | 1.16 | -4.93 | 0.77 | 0.07 |
| 72.0800 S | 184 | 20 | 0.65 | 0.10 | 0.50 | 6.29 | 0.76 | 4.79 | -22.09 | -23.32 | -0.28 | -6.37 | 0.41 | 0.22 |
| group3 | 184 | 5 | 0.14 | 0.02 | 0.08 | 7.91 | 0.58 | 4.57 | -24.25 | -25.49 | 0.37 | -5.72 | 0.57 | 0.58 |
| | 184 | 1 | 1.74 | 0.33 | | 5.29 | | | -27.07 | -28.31 | 2.39 | -3.70 | 1.08 | 0.89 |
| | | total | 3.29 | 0.58 | 1.19 | 5.63 | 0.77 | 4.65 | -25.07 | | 1.59 | | 0.87 | 0.08 |
| | | bulk | 3.55 | 0.64 | | 5.52 | | | | ***1.23*** | | ***6.09*** | | ***24.23*** |
| TNS 10 | 1599 | 300 | 0.02 | 0.00 | 0.01 | 6.53 | 0.32 | 2.11 | -24.35 | -25.62 | 2.64 | -3.59 | | |
| 21/10/2011 | 1599 | 210 | 0.02 | 0.00 | 0.01 | 6.17 | 0.36 | 2.25 | -25.30 | -26.57 | 2.57 | -3.66 | | |
| 50.2142 E | 271 | 50 | 0.77 | 0.14 | 0.62 | 5.70 | 0.80 | 4.56 | -22.55 | -23.81 | 0.60 | -5.63 | 0.59 | 0.21 |
| 72.1320 S | 271 | 20 | 0.42 | 0.07 | 0.33 | 5.93 | 0.78 | 4.63 | -22.38 | -23.65 | -0.18 | -6.41 | 0.40 | 0.56 |
| group3 | 271 | 5 | 0.12 | 0.02 | 0.07 | 6.94 | 0.57 | 3.99 | -24.02 | -25.28 | 0.48 | -5.75 | 0.56 | 1.04 |
| | 271 | 1 | 1.42 | 0.26 | | 5.53 | | | -26.61 | -27.88 | 2.49 | -3.74 | 1.07 | 2.27 |
| | | total | 2.77 | 0.49 | 1.03 | 5.69 | 0.76 | 4.48 | -24.70 | | 1.51 | | 0.82 | 0.23 |
| | | bulk | 3.86 | 0.74 | | 5.20 | | | | ***1.27*** | | ***6.23*** | | ***23.63*** |
| TNS 09 | 869 | 300 | 0.03 | 0.00 | 0.01 | 6.84 | 0.23 | 1.58 | -24.63 | -25.93 | 3.47 | -2.86 | | |
| 21/10/2011 | 869 | 210 | 0.09 | 0.02 | 0.03 | 5.40 | 0.30 | 1.60 | -25.77 | -27.07 | 3.11 | -3.22 | | |
| 49.7991 E | 42 | 50 | 11.60 | 1.82 | 9.84 | 6.37 | 0.85 | 5.41 | -22.57 | -23.87 | 1.25 | -5.08 | 0.73 | 0.21 |
| 72.2002 S | 42 | 20 | 1.87 | 0.27 | 1.64 | 7.02 | 0.88 | 6.16 | -22.32 | -23.62 | 1.54 | -4.79 | 0.80 | 0.56 |
| group3 | 42 | 5 | 0.81 | 0.12 | 0.45 | 7.03 | 0.55 | 3.90 | -23.15 | -24.45 | 1.00 | -5.33 | 0.67 | 1.11 |
| | 42 | 1 | 8.53 | 1.40 | | 6.11 | | | -26.52 | -27.82 | 1.20 | -5.13 | 0.72 | 2.29 |
| | | total | 22.92 | 3.62 | 11.96 | 6.33 | 0.83 | 5.38 | -24.06 | | 1.26 | | 0.73 | 0.23 |
| | | bulk | 6.97 | 1.17 | | 5.98 | | | | ***1.30*** | | ***6.33*** | | ***23.63*** |
| TNS 08 | 997 | 300 | 0.04 | 0.01 | 0.01 | 5.47 | 0.23 | 1.25 | -24.13 | -25.44 | 3.98 | -2.44 | | |
| 21/10/2011 | 997 | 210 | 0.12 | 0.02 | 0.02 | 5.03 | 0.15 | 0.73 | -25.35 | -26.66 | 3.45 | -2.97 | | |
| 49.4628 E | 216 | 50 | 1.46 | 0.23 | 1.18 | 6.37 | 0.80 | 5.12 | -23.81 | -25.12 | 1.75 | -4.67 | 0.83 | 0.19 |
| 72.2401 S | 216 | 20 | 0.60 | 0.09 | 0.51 | 6.93 | 0.85 | 5.91 | -22.27 | -23.58 | 1.90 | -4.52 | 0.87 | 0.56 |
| group1 | 216 | 5 | 0.18 | 0.03 | 0.11 | 6.82 | 0.62 | 4.21 | -23.59 | -24.90 | 0.82 | -5.60 | 0.60 | 1.07 |
| | 216 | 1 | 2.77 | 0.49 | | 5.60 | | | -26.00 | -27.31 | 0.20 | -6.22 | 0.44 | 2.42 |
| | | total | 5.18 | 0.87 | 1.83 | 5.96 | 0.76 | 4.88 | -24.83 | | 0.92 | | 0.60 | 0.21 |
| | | bulk | 6.14 | 1.09 | | 5.61 | | | | ***1.31*** | | ***6.42*** | | ***23.63*** |
| TNS 06 | 1025 | 300 | 0.03 | 0.00 | 0.00 | 6.26 | 0.06 | 0.40 | -24.77 | -26.09 | 3.77 | -2.57 | | |
| 22/10/2011 | 1025 | 210 | 0.05 | 0.01 | 0.01 | 5.02 | 0.18 | 0.89 | -24.92 | -26.25 | 3.75 | -2.59 | | |
| 48.7989 E | 110 | 50 | 1.56 | 0.27 | 0.88 | 5.86 | 0.57 | 3.32 | -23.14 | -24.46 | 2.29 | -4.05 | 0.99 | 0.19 |
| 72.3006 S | 110 | 20 | 0.93 | 0.14 | 0.58 | 6.49 | 0.63 | 4.08 | -22.63 | -23.96 | 2.15 | -4.19 | 0.95 | 0.54 |
| group1 | 110 | 5 | 0.34 | 0.05 | 0.14 | 6.93 | 0.42 | 2.91 | -24.25 | -25.57 | 1.31 | -5.03 | 0.74 | 0.99 |
| | 110 | 1 | 4.30 | 0.85 | | 5.04 | | | -26.31 | -27.63 | 0.09 | -6.25 | 0.44 | 2.28 |
| | | total | 7.20 | 1.33 | 1.62 | 5.43 | 0.56 | 3.43 | -25.04 | | 0.84 | | 0.62 | 0.21 |
| | | bulk | 4.73 | 0.79 | | 6.02 | | | | ***1.33*** | | ***6.34*** | | ***23.18*** |
| TNS 05 | 1081 | 300 | 0.03 | 0.01 | 0.01 | 5.67 | 0.20 | 1.11 | -24.28 | -25.55 | 4.06 | -2.18 | | |
| 22/10/2011 | 1081 | 210 | 0.07 | 0.02 | 0.01 | 4.80 | 0.08 | 0.39 | -25.18 | -26.45 | 4.06 | -2.18 | | |
| 48.4677 E | 151 | 50 | 1.04 | 0.19 | 0.78 | 5.50 | 0.75 | 4.14 | -24.73 | -26.01 | 2.16 | -4.08 | 0.98 | 0.17 |
| 72.2018 S | 151 | 20 | 0.61 | 0.09 | 0.51 | 6.53 | 0.84 | 5.50 | -22.95 | -24.23 | 2.06 | -4.18 | 0.95 | 0.52 |
| group1 | 151 | 5 | 0.28 | 0.04 | 0.17 | 6.72 | 0.61 | 4.11 | -23.81 | -25.08 | 1.26 | -4.98 | 0.76 | 1.03 |
| | 151 | 1 | 2.66 | 0.49 | | 5.48 | | | -26.64 | -27.92 | 0.45 | -5.79 | 0.55 | 2.20 |
| | | total | 4.68 | 0.83 | 1.48 | 5.65 | 0.73 | 4.29 | -25.54 | | 1.15 | | 0.71 | 0.19 |
| | | bulk | 4.20 | 0.75 | | 5.62 | | | | ***1.27*** | | ***6.24*** | | ***23.18*** |
| TNS 03 | 975 | 300 | 0.03 | 0.01 | 0.01 | 6.14 | 0.31 | 1.88 | -25.91 | -27.16 | 3.33 | -2.87 | | |
| 23/10/2011 | 975 | 210 | 0.02 | 0.00 | 0.01 | 7.00 | 0.54 | 3.82 | -25.41 | -26.66 | 3.29 | -2.91 | | |
| 47.8336 E | 165 | 50 | 0.91 | 0.16 | 0.66 | 5.82 | 0.73 | 4.25 | -22.98 | -24.23 | 1.74 | -4.46 | 0.89 | 0.19 |
| 71.9196 S | 165 | 20 | 0.45 | 0.07 | 0.31 | 6.79 | 0.69 | 4.67 | -22.98 | -24.23 | 1.28 | -4.92 | 0.77 | 0.51 |
| group1 | 165 | 5 | 0.17 | 0.02 | 0.06 | 8.09 | 0.38 | 3.07 | -24.07 | -25.32 | 0.75 | -5.45 | 0.64 | 0.99 |
| | 165 | 1 | 2.95 | 0.54 | | 5.51 | | | -26.96 | -28.21 | 1.17 | -5.03 | 0.74 | 2.07 |
| | | total | 4.54 | 0.79 | 1.06 | 5.76 | 0.67 | 4.20 | -25.64 | | 1.30 | | 0.77 | 0.21 |
| | | bulk | 4.04 | 0.69 | | 5.83 | | | | ***1.25*** | | ***6.20*** | | ***22.75*** |
| TNS 02 | 784 | 300 | 0.01 | #N/A | 0.00 | #N/A | 0.20 | #N/A | -26.60 | -27.93 | #N/A | #N/A | | |
| 23/10/2011 | 784 | 210 | 0.01 | 0.00 | 0.00 | 10.77 | 0.20 | 2.19 | -25.99 | -27.32 | #N/A | #N/A | | |
| 47.3318 E | 170 | 50 | 0.17 | 0.02 | 0.07 | 8.20 | 0.43 | 3.57 | -23.46 | -24.79 | 2.57 | -3.81 | 1.05 | 0.18 |
| 71.7013 S | 170 | 20 | 0.40 | 0.06 | 0.15 | 6.32 | 0.38 | 2.38 | -21.95 | -23.28 | 1.89 | -4.49 | 0.88 | 0.55 |
| group5 | 170 | 5 | 0.12 | 0.02 | 0.04 | 6.98 | 0.32 | 2.27 | -25.54 | -26.87 | 1.93 | -4.45 | 0.89 | 0.85 |
| | 170 | 1 | 2.91 | 0.53 | | 5.45 | | | -26.09 | -27.43 | 1.32 | -5.06 | 0.73 | 2.27 |
| | | total | 3.62 | 0.64 | 0.27 | 5.69 | 0.38 | 2.61 | -25.50 | | 1.43 | | 0.76 | 0.21 |
| | | bulk | 2.60 | 0.44 | | 5.92 | | | | ***1.33*** | | ***6.38*** | | ***22.75*** |
| TNS 01 | 1279 | 300 | 0.03 | 0.01 | 0.00 | 5.53 | 0.03 | 0.18 | -25.14 | -25.93 | 3.32 | -3.62 | | |
| 23/10/2011 | 1279 | 210 | 0.02 | 0.00 | 0.00 | 7.21 | 0.11 | 0.81 | -26.26 | -27.05 | 1.53 | -5.41 | | |
| 46.8333 E | 256 | 50 | 0.16 | 0.02 | 0.05 | 6.77 | 0.30 | 2.03 | -25.66 | -26.45 | 1.12 | -5.82 | 0.54 | 0.16 |
| 71.5011 S | 256 | 20 | 0.19 | 0.03 | 0.07 | 6.83 | 0.39 | 2.68 | -25.02 | -25.81 | 1.71 | -5.23 | 0.69 | 0.45 |
| group5 | 256 | 5 | 0.13 | 0.02 | 0.04 | 7.22 | 0.34 | 2.43 | -24.86 | -25.65 | 1.70 | -5.24 | 0.69 | 0.96 |
| | 256 | 1 | 2.88 | 0.52 | | 5.52 | | | -26.04 | -26.83 | -0.34 | -7.28 | 0.18 | 2.42 |

| | | | | | | | | | | | | | | |
|---|---|---|---|---|---|---|---|---|---|---|---|---|---|---|
| | | total | 3.40 | 0.60 | 0.17 | 5.69 | 0.32 | 2.19 | -25.92 | | -0.09 | | 0.23 | 0.18 |
| | | bulk | 3.70 | 0.59 | | 6.32 | | | | ***0.79*** | | ***6.94*** | | ***23.05*** |
| R 2 | 2685 | 300 | 0.00 | 0.00 | 0.00 | 10.90 | 0.26 | 2.85 | -25.76 | -27.07 | #N/A | #N/A | | |
| 26/10/2011 | 2685 | 210 | 0.01 | 0.00 | 0.00 | 9.92 | 0.37 | 3.70 | -28.86 | -30.18 | 1.56 | -4.92 | | |
| 50.3587 E | 167 | 50 | 0.45 | 0.07 | 0.23 | 6.23 | 0.50 | 3.11 | -25.66 | -26.97 | 1.73 | -4.75 | 0.81 | 0.15 |
| 66.7168 S | 167 | 20 | 0.31 | 0.04 | 0.18 | 6.94 | 0.58 | 4.06 | -24.84 | -26.16 | 2.28 | -4.20 | 0.95 | 0.44 |
| group1 | 167 | 5 | 0.16 | 0.02 | 0.06 | 8.73 | 0.38 | 3.35 | -25.64 | -26.96 | 0.90 | -5.58 | 0.60 | 0.85 |
| | 167 | 1 | 2.89 | 0.51 | #N/A | 5.71 | | | -28.14 | -29.45 | 0.84 | -5.64 | 0.59 | 1.80 |
| | | total | 3.82 | 0.64 | 0.47 | 5.94 | 0.51 | 3.46 | -27.48 | | 1.04 | | 0.64 | 0.17 |
| | | bulk | 2.37 | 0.40 | | 5.95 | | | | ***1.31*** | | ***6.48*** | | ***22.85*** |
| E 1 day | 1209 | 300 | 0.02 | 0.00 | 0.00 | 7.07 | 0.20 | 1.43 | -23.28 | -24.65 | 3.04 | -3.36 | | |
| 29/10/2011 | 1209 | 210 | 0.07 | 0.01 | 0.03 | 5.51 | 0.40 | 2.18 | -25.75 | -27.12 | 2.42 | -3.98 | | |
| 48.4664 E | 181 | 50 | 1.92 | 0.31 | 1.14 | 6.18 | 0.59 | 3.67 | -23.52 | -24.89 | 1.94 | -4.46 | 0.88 | 0.17 |
| 72.1993 S | 181 | 20 | 0.57 | 0.09 | 0.36 | 6.64 | 0.63 | 4.20 | -23.29 | -24.66 | 2.03 | -4.37 | 0.91 | 0.47 |
| group2 | 181 | 5 | 0.15 | 0.02 | 0.05 | 6.97 | 0.34 | 2.34 | -24.73 | -26.10 | 0.90 | -5.50 | 0.62 | 0.88 |
| | 181 | 1 | 3.64 | 0.62 | | 5.87 | | | -26.81 | -28.18 | -0.25 | -6.65 | 0.34 | 2.00 |
| | | total | 6.36 | 1.05 | 1.58 | 6.05 | 0.58 | 3.65 | -25.43 | | 0.64 | | 0.55 | 0.19 |
| | | bulk | 4.85 | 0.78 | | 6.19 | | | | ***1.37*** | | ***6.40*** | | ***21.88*** |
| E 1 night | 2449 | 300 | 0.48 | 0.11 | 0.03 | 4.45 | 0.06 | 0.28 | -24.26 | -25.48 | 3.24 | -3.28 | | |
| 29/10/2011 | 2449 | 210 | 0.33 | 0.06 | 0.12 | 5.26 | 0.37 | 1.94 | -24.82 | -26.03 | 2.48 | -4.04 | | |
| 48.4664 E | 310 | 50 | 3.45 | 0.57 | 1.56 | 6.10 | 0.45 | 2.76 | -23.88 | -25.10 | 1.91 | -4.61 | 0.85 | 0.17 |
| 72.1993 S | 310 | 20 | 0.40 | 0.06 | 0.18 | 6.64 | 0.44 | 2.95 | -23.55 | -24.76 | 1.96 | -4.56 | 0.86 | 0.47 |
| group2 | 310 | 5 | 0.10 | 0.01 | 0.03 | 6.85 | 0.33 | 2.25 | -24.62 | -25.83 | 0.98 | -5.54 | 0.62 | 0.90 |
| | 310 | 1 | 3.45 | 0.58 | | 5.90 | | | -26.79 | -28.00 | -0.04 | -6.56 | 0.36 | 2.04 |
| | | total | 8.21 | 1.40 | 1.92 | 5.88 | 0.40 | 2.37 | -25.16 | | 1.21 | | 0.61 | 0.19 |
| | | bulk | 5.11 | 0.79 | | 6.45 | | | | ***1.22*** | | ***6.52*** | | ***21.88*** |
| TEW 1 | 1516 | 300 | 0.03 | 0.01 | 0.00 | 5.06 | 0.08 | 0.39 | -21.37 | -22.85 | 5.05 | -1.52 | | |
| 31/10/2011 | 1516 | 210 | 0.03 | 0.01 | 0.01 | 4.88 | 0.19 | 0.91 | -20.62 | -22.10 | 3.78 | -2.79 | | |
| 49.1502 E | 59 | 50 | 2.19 | 0.39 | 1.07 | 5.62 | 0.49 | 2.75 | -19.66 | -21.14 | 3.19 | -3.38 | 1.15 | 0.23 |
| 69.8323 S | 59 | 20 | 4.02 | 0.69 | 2.11 | 5.83 | 0.52 | 3.06 | -19.36 | -20.84 | 3.04 | -3.53 | 1.12 | 0.64 |
| group4 | 59 | 5 | 1.68 | 0.29 | 0.97 | 5.90 | 0.57 | 3.39 | -20.44 | -21.92 | 2.79 | -3.78 | 1.05 | 1.25 |
| | 59 | 1 | 6.34 | 0.93 | | 6.82 | | | -22.88 | -24.36 | 2.11 | -4.46 | 0.89 | 2.96 |
| | | total | 14.29 | 2.30 | 4.15 | 6.20 | 0.52 | 3.02 | -21.10 | | 2.66 | | 1.02 | 0.26 |
| | | bulk | 9.29 | 1.57 | | 5.93 | | | | ***1.48*** | | ***6.57*** | | ***22.17*** |
| TEW 2 | 650 | 300 | 0.02 | 0.00 | 0.00 | 6.18 | 0.04 | 0.28 | -23.47 | -24.86 | #N/A | #N/A | | |
| 31/10/2011 | 650 | 210 | 0.02 | 0.00 | 0.00 | 5.88 | 0.21 | 1.24 | -23.34 | -24.74 | 3.52 | -2.89 | | |
| 48.8994 E | 161 | 50 | 0.88 | 0.14 | 0.33 | 6.21 | 0.37 | 2.31 | -19.09 | -20.48 | 2.37 | -4.04 | 0.99 | 0.24 |
| 70.6663 S | 161 | 20 | 2.16 | 0.36 | 0.63 | 6.09 | 0.29 | 1.77 | -19.18 | -20.57 | 2.20 | -4.21 | 0.95 | 0.65 |
| group4 | 161 | 5 | 0.13 | 0.02 | 0.09 | 7.25 | 0.64 | 4.67 | -22.24 | -23.63 | 2.41 | -4.00 | 1.00 | 1.11 |
| | 161 | 1 | 3.33 | 0.50 | #N/A | 6.64 | | | -24.10 | -25.49 | 1.88 | -4.53 | 0.87 | 2.68 |
| | | total | 6.53 | 1.02 | 1.05 | 6.39 | 0.33 | 2.01 | -21.76 | | 2.07 | | 0.92 | 0.27 |
| | | bulk | 8.14 | 1.33 | | 6.11 | | | | ***1.39*** | | ***6.41*** | | ***22.17*** |
| TEW 3 | 981 | 300 | 0.09 | 0.02 | 0.00 | 4.15 | 0.01 | 0.04 | -23.87 | -25.09 | 4.05 | -1.90 | | |
| 31/10/2011 | 981 | 210 | 0.01 | 0.00 | 0.00 | 5.58 | 0.17 | 0.97 | -25.01 | -26.23 | #N/A | #N/A | | |
| 48.7991 E | 93 | 50 | 0.11 | 0.02 | 0.06 | 5.82 | 0.52 | 3.05 | -24.46 | -25.67 | #N/A | #N/A | #N/A | 0.16 |
| 71.0176 S | 93 | 20 | 0.74 | 0.12 | 0.32 | 6.23 | 0.43 | 2.69 | -22.39 | -23.61 | 1.99 | -3.96 | 1.01 | 0.52 |
| group4 | 93 | 5 | 0.14 | 0.02 | 0.05 | 7.86 | 0.35 | 2.76 | -23.54 | -24.75 | 1.93 | -4.02 | 1.00 | 1.01 |
| | 93 | 1 | 8.01 | 1.27 | | 6.30 | | | -25.92 | -27.13 | 1.19 | -4.76 | 0.81 | 2.28 |
| | | total | 9.10 | 1.45 | 0.43 | 6.28 | 0.40 | 2.41 | -25.56 | | 1.29 | | 0.83 | 0.19 |
| | | bulk | 6.26 | 0.89 | | 7.04 | | | | ***1.21*** | | ***5.95*** | | ***22.17*** |
| TEW 4 | 1150 | 300 | 0.64 | 0.13 | 0.11 | 4.87 | 0.17 | 0.84 | -24.66 | -25.32 | 3.65 | -2.84 | | |
| 1/11/2011 | 1150 | 210 | 0.65 | 0.13 | 0.22 | 5.05 | 0.34 | 1.72 | -24.36 | -25.02 | 2.59 | -3.90 | | |
| 48.6331 E | 88 | 50 | 5.10 | 0.84 | 2.28 | 6.11 | 0.45 | 2.72 | -23.84 | -24.50 | 2.02 | -4.47 | 0.88 | 0.18 |
| 71.6170 S | 88 | 20 | 1.27 | 0.21 | 0.57 | 6.18 | 0.45 | 2.77 | -22.69 | -23.35 | 1.76 | -4.73 | 0.82 | 0.53 |
| group1 | 88 | 5 | 0.26 | 0.04 | 0.10 | 5.93 | 0.39 | 2.31 | -23.67 | -24.33 | 1.07 | -5.42 | 0.64 | 1.05 |
| | 88 | 1 | 7.95 | 1.45 | | 5.48 | | | -25.79 | -26.45 | 0.37 | -6.12 | 0.47 | 2.45 |
| | | total | 15.89 | 2.80 | 3.28 | 5.68 | 0.41 | 2.44 | -24.77 | | 1.23 | | 0.64 | 0.21 |
| | | bulk | 9.41 | 1.73 | | 5.43 | | | | ***0.66*** | | ***6.49*** | | ***22.17*** |
| E 2 | 1748 | 300 | 0.20 | 0.04 | 0.01 | 4.38 | 0.03 | 0.14 | -21.25 | -22.57 | 2.68 | -3.94 | | |
| 1/11/2011 | 1748 | 210 | 0.06 | 0.01 | 0.01 | 4.65 | 0.09 | 0.42 | -24.76 | -26.08 | 2.99 | -3.63 | | |
| 48.5234 E | 123 | 50 | 1.44 | 0.25 | 0.63 | 5.71 | 0.44 | 2.52 | -24.85 | -26.17 | 1.62 | -5.00 | 0.75 | 0.16 |
| 72.0771 S | 123 | 20 | 1.26 | 0.20 | 0.50 | 6.22 | 0.40 | 2.49 | -23.58 | -24.90 | 1.64 | -4.98 | 0.75 | 0.47 |
| group2 | 123 | 5 | 0.30 | 0.05 | 0.10 | 6.38 | 0.33 | 2.10 | -23.94 | -25.26 | 1.02 | -5.60 | 0.60 | 0.97 |
| | 123 | 1 | 5.60 | 1.01 | | 5.55 | | | -26.27 | -27.59 | -0.52 | -7.14 | 0.22 | 2.17 |
| | | total | 8.85 | 1.57 | 1.25 | 5.65 | 0.38 | 2.24 | -25.46 | | 0.27 | | 0.39 | 0.18 |
| | | bulk | 6.78 | 1.21 | | 5.62 | | | | ***1.32*** | | ***6.62*** | | ***22.17*** |
| TEW 5 | 1748 | 300 | 0.26 | 0.06 | 0.00 | 4.39 | 0.01 | 0.02 | -25.67 | -27.05 | 4.18 | -2.60 | | |
| 1/11/2011 | 1748 | 210 | 0.05 | 0.01 | 0.00 | 4.57 | 0.06 | 0.28 | -24.90 | -26.27 | 3.33 | -3.45 | | |
| 48.4678 E | 123 | 50 | 1.28 | 0.21 | 0.54 | 6.00 | 0.42 | 2.53 | -24.29 | -25.67 | 2.13 | -4.65 | 0.84 | 0.16 |
| 72.7997 S | 123 | 20 | 0.85 | 0.13 | 0.31 | 6.58 | 0.37 | 2.44 | -23.57 | -24.95 | 1.70 | -5.08 | 0.73 | 0.47 |
| group1 | 123 | 5 | 0.15 | 0.02 | 0.04 | 6.26 | 0.27 | 1.70 | -23.88 | -25.26 | 1.04 | -5.74 | 0.56 | 0.97 |
| | 123 | 1 | 5.32 | 0.90 | | 5.89 | | | -26.27 | -27.65 | -0.43 | -7.21 | 0.20 | 2.16 |
| | | total | 7.91 | 1.34 | 0.90 | 5.90 | 0.35 | 2.06 | -25.59 | | 0.44 | | 0.37 | 0.18 |
| | | bulk | 8.25 | 1.49 | | 5.52 | | | | ***1.38*** | | ***6.78*** | | ***22.17*** |
| TEW 6 | 986 | 300 | 0.36 | 0.09 | 0.00 | 4.17 | 0.00 | 0.01 | -23.24 | -24.63 | 3.21 | -3.61 | | |

| | | | | | | | | | | | | | | | |
|---|---|---|---|---|---|---|---|---|---|---|---|---|---|---|---|
| 1/11/2011 | 986 | 210 | 0.12 | 0.03 | 0.00 | 4.47 | 0.03 | 0.12 | -24.79 | -26.18 | 2.98 | -3.84 | | | |
| 48.4662 E | 76 | 50 | 0.74 | 0.13 | 0.21 | 5.74 | 0.29 | 1.65 | -23.59 | -24.98 | 2.31 | -4.51 | 0.87 | 0.18 | |
| 73.3998 S | 76 | 20 | 0.77 | 0.12 | 0.31 | 6.51 | 0.40 | 2.63 | -22.93 | -24.32 | 2.10 | -4.72 | 0.82 | 0.49 | |
| group1 | 76 | 5 | 0.40 | 0.07 | 0.14 | 5.72 | 0.33 | 1.91 | -23.42 | -24.81 | 1.31 | -5.51 | 0.62 | 1.00 | |
| | 76 | 1 | 6.91 | 1.33 | | 5.20 | | | -25.49 | -26.88 | 0.19 | -6.63 | 0.34 | 2.35 | |
| | | total | 9.31 | 1.76 | 0.66 | 5.29 | 0.28 | 1.54 | -24.94 | | 0.71 | | 0.43 | 0.20 | |
| | | bulk | 6.38 | 1.14 | | 5.62 | | | | ***1.39*** | | ***6.82*** | | ***22.17*** | |
| TEW 7 | 957 | 300 | 0.41 | 0.09 | 0.00 | 4.58 | 0.01 | 0.04 | -22.23 | -23.98 | 3.89 | -3.87 | | | |
| 2/11/2011 | 957 | 210 | 0.13 | 0.03 | 0.00 | 4.97 | 0.02 | 0.09 | -22.53 | -24.28 | 3.65 | -4.11 | | | |
| 48.4667 E | 35 | 50 | 6.89 | 1.19 | 1.93 | 5.81 | 0.28 | 1.63 | -20.48 | -22.23 | 2.31 | -5.45 | 0.64 | 0.20 | |
| 73.9992 S | 35 | 20 | 2.32 | 0.37 | 0.81 | 6.27 | 0.35 | 2.20 | -19.82 | -21.57 | 2.38 | -5.38 | 0.66 | 0.55 | |
| group5 | 35 | 5 | 1.71 | 0.29 | 0.31 | 5.89 | 0.18 | 1.05 | -21.38 | -23.12 | 2.34 | -5.42 | 0.64 | 1.03 | |
| | 35 | 1 | 8.43 | 1.58 | | 5.32 | | | -23.08 | -24.83 | 2.08 | -5.68 | 0.58 | 2.56 | |
| | | total | 19.90 | 3.55 | 3.06 | 5.61 | 0.27 | 1.56 | -21.63 | | 2.27 | | 0.61 | 0.22 | |
| | | bulk | 22.82 | 4.09 | | 5.58 | | | | ***1.75*** | | ***7.76*** | | ***20.04*** | |
| TEW 8 | 1509 | 300 | 0.13 | 0.03 | 0.00 | 4.90 | 0.01 | 0.05 | -22.06 | -23.80 | 3.79 | -4.21 | | | |
| 2/11/2011 | 1509 | 210 | 0.04 | 0.01 | 0.00 | 5.04 | 0.10 | 0.48 | -21.83 | -23.57 | 3.81 | -4.19 | | | |
| 48.4676 E | 56 | 50 | 6.61 | 1.07 | 1.94 | 6.16 | 0.29 | 1.81 | -20.53 | -22.27 | 2.45 | -5.55 | 0.61 | 0.17 | |
| 75.0032 S | 56 | 20 | 7.10 | 1.15 | 1.65 | 6.17 | 0.23 | 1.43 | -20.17 | -21.91 | 2.60 | -5.40 | 0.65 | 0.46 | |
| group5 | 56 | 5 | 1.95 | 0.30 | 0.39 | 6.44 | 0.20 | 1.30 | -21.14 | -22.88 | 2.46 | -5.54 | 0.61 | 0.91 | |
| | 56 | 1 | 9.02 | 1.73 | | 5.23 | | | -22.38 | -24.12 | 1.95 | -6.05 | 0.49 | 2.35 | |
| | | total | 24.86 | 4.29 | 3.99 | 5.80 | 0.25 | 1.56 | -21.16 | | 2.30 | | 0.57 | 0.19 | |
| | | bulk | 23.21 | 3.92 | | 5.92 | | | | ***1.74*** | | ***8.00*** | | ***17.43*** | |
| E 3 | 1246 | 300 | 0.07 | 0.01 | 0.00 | 4.84 | 0.04 | 0.20 | -24.53 | -25.94 | 3.47 | -2.86 | | | |
| 4/11/2011 | 1246 | 210 | 0.03 | 0.01 | 0.01 | 5.25 | 0.31 | 1.65 | -24.44 | -25.85 | 3.05 | -3.28 | | | |
| 48.6998 E | 85 | 50 | 0.69 | 0.11 | 0.43 | 6.35 | 0.62 | 3.96 | -23.64 | -25.05 | 2.51 | -3.82 | 1.04 | 0.17 | |
| 71.9670 S | 85 | 20 | 1.25 | 0.19 | 0.68 | 6.68 | 0.55 | 3.64 | -23.18 | -24.59 | 2.09 | -4.24 | 0.94 | 0.48 | |
| group2 | 85 | 5 | 0.31 | 0.04 | 0.10 | 7.59 | 0.32 | 2.41 | -23.92 | -25.33 | 1.02 | -5.31 | 0.67 | 0.95 | |
| | 85 | 1 | 6.79 | 1.24 | | 5.48 | | | -26.18 | -27.59 | -0.24 | -6.57 | 0.36 | 2.14 | |
| | | total | 9.13 | 1.60 | 1.22 | 5.72 | 0.52 | 3.43 | -25.49 | | 0.30 | | 0.48 | 0.19 | |
| | | bulk | 7.58 | 1.34 | | 5.66 | | | | ***1.41*** | | ***6.33*** | | ***21.88*** | |
| F L | 1102 | 300 | 0.13 | 0.02 | 0.01 | 5.46 | 0.06 | 0.32 | -21.96 | -23.60 | 3.38 | -3.87 | | | |
| 6/11/2011 | 1102 | 210 | 0.19 | 0.04 | 0.03 | 4.98 | 0.17 | 0.87 | -21.36 | -23.00 | 3.11 | -4.14 | | | |
| 48.5232 E | 60 | 50 | 6.93 | 1.17 | 2.14 | 5.91 | 0.31 | 1.83 | -20.85 | -22.49 | 2.35 | -4.90 | 0.78 | 0.17 | |
| 74.6673 S | 60 | 20 | 5.32 | 0.92 | 1.42 | 5.80 | 0.27 | 1.55 | -20.88 | -22.52 | 2.33 | -4.92 | 0.77 | 0.44 | |
| group5 | 60 | 5 | 2.31 | 0.39 | 0.42 | 5.88 | 0.18 | 1.07 | -21.44 | -23.08 | 2.17 | -5.08 | 0.73 | 0.90 | |
| | 60 | 1 | 7.51 | 1.41 | | 5.32 | | | -22.07 | -23.71 | 2.14 | -5.11 | 0.72 | 2.43 | |
| | | total | 22.38 | 3.95 | 4.03 | 5.66 | 0.27 | 1.58 | -21.34 | | 2.26 | | 0.75 | 0.18 | |
| | | bulk | 15.76 | 2.89 | | | | | | ***1.64*** | | ***7.25*** | | ***17.43*** | |
| F S | 571 | 300 | 0.23 | 0.05 | 0.02 | 5.03 | 0.10 | 0.52 | -22.71 | -24.42 | 3.50 | -4.29 | | | |
| 8/11/2011 | 571 | 210 | 0.45 | 0.09 | 0.13 | 5.21 | 0.28 | 1.46 | -22.34 | -24.05 | 2.98 | -4.81 | | | |
| 48.5006 E | 110 | 50 | 13.05 | 2.20 | 4.80 | 5.93 | 0.37 | 2.18 | -21.26 | -22.97 | 2.61 | -5.18 | 0.71 | 0.17 | |
| 73.9998 S | 110 | 20 | 2.24 | 0.36 | 0.62 | 6.15 | 0.28 | 1.71 | -21.32 | -23.03 | 2.34 | -5.45 | 0.64 | 0.45 | |
| group5 | 110 | 5 | 1.34 | 0.23 | 0.27 | 5.91 | 0.20 | 1.21 | -21.94 | -23.66 | 2.22 | -5.57 | 0.61 | 0.91 | |
| | 110 | 1 | 6.12 | 1.10 | | 5.57 | | | -22.51 | -24.22 | 1.76 | -6.03 | 0.49 | 2.48 | |
| | | total | 23.43 | 4.02 | 5.85 | 5.82 | 0.34 | 2.00 | -21.67 | | 2.35 | | 0.63 | 0.19 | |
| | | bulk | 15.76 | 2.89 | | 5.45 | | | | ***1.71*** | | ***7.79*** | | ***18.55*** | |
| G 1 | 1457 | 300 | 0.11 | 0.02 | 0.05 | 5.69 | 0.44 | 2.53 | -20.54 | -22.09 | 3.84 | -3.25 | | | |
| 8/11/2011 | 1457 | 210 | 0.25 | 0.04 | 0.13 | 5.78 | 0.52 | 2.99 | -21.43 | -22.99 | 2.10 | -4.99 | | | |
| 49.9004 E | 116 | 50 | 13.92 | 2.20 | 11.04 | 6.32 | 0.79 | 5.01 | -21.43 | -22.99 | 1.24 | -5.85 | 0.54 | 0.20 | |
| 71.8991 S | 116 | 20 | 0.50 | 0.08 | 0.32 | 6.58 | 0.65 | 4.25 | -20.44 | -22.00 | 0.94 | -6.15 | 0.46 | 0.57 | |
| group3 | 116 | 5 | 0.38 | 0.06 | 0.23 | 6.29 | 0.61 | 3.81 | -21.25 | -22.81 | 0.39 | -6.70 | 0.32 | 1.14 | |
| | 116 | 1 | 3.64 | 0.73 | | 5.00 | | | -22.25 | -23.80 | 1.85 | -5.24 | 0.69 | 3.01 | |
| | | total | 18.79 | 3.13 | 11.77 | 6.01 | 0.78 | 4.90 | -21.56 | | 1.38 | | 0.57 | 0.22 | |
| | | bulk | 19.40 | 3.29 | | 5.90 | | | | ***1.55*** | | ***7.09*** | | ***21.59*** | |
| G 2 | 631 | 300 | 0.03 | 0.01 | 0.00 | 5.78 | 0.06 | 0.36 | -22.64 | -24.19 | 4.41 | -2.12 | | | |
| 9/11/2011 | 631 | 210 | 0.16 | 0.03 | 0.08 | 5.52 | 0.50 | 2.77 | -18.04 | -19.60 | 3.61 | -2.92 | | | |
| 49.1331 E | 61 | 50 | 1.94 | 0.32 | 1.07 | 6.03 | 0.55 | 3.34 | -18.16 | -19.71 | 3.34 | -3.19 | 1.20 | 0.22 | |
| 70.6498 S | 61 | 20 | 3.63 | 0.61 | 1.21 | 5.93 | 0.33 | 1.98 | -18.99 | -20.54 | 2.96 | -3.57 | 1.11 | 0.56 | |
| group4 | 61 | 5 | 0.92 | 0.17 | 0.21 | 5.54 | 0.23 | 1.25 | -21.40 | -22.95 | 2.84 | -3.69 | 1.08 | 1.01 | |
| | 61 | 1 | 5.97 | 1.12 | | 5.33 | | | -20.82 | -22.37 | 3.88 | -2.65 | 1.34 | 2.99 | |
| | | total | 12.66 | 2.25 | 2.57 | 5.61 | 0.39 | 2.27 | -19.90 | | 3.47 | | 1.23 | 0.24 | |
| | | bulk | 13.10 | 2.35 | | 5.56 | | | | ***1.55*** | | ***6.53*** | | ***19.25*** | |
| E 4W | 393 | 300 | 0.07 | 0.01 | 0.02 | 6.38 | 0.33 | 2.09 | -23.73 | -25.13 | 2.81 | -3.58 | | | |
| 11/11/2011 | 393 | 210 | 0.05 | 0.01 | 0.01 | 6.36 | 0.26 | 1.65 | -24.20 | -25.60 | 3.44 | -2.95 | | | |
| 48.7667 E | 43 | 50 | 7.09 | 1.23 | 4.53 | 5.77 | 0.64 | 3.69 | -22.29 | -23.69 | 1.41 | -4.98 | 0.75 | 0.18 | |
| 71.4294 S | 43 | 20 | 1.18 | 0.18 | 0.67 | 6.55 | 0.57 | 3.70 | -22.01 | -23.41 | 1.09 | -5.30 | 0.68 | 0.50 | |
| group3 | 43 | 5 | 0.43 | 0.06 | 0.18 | 7.46 | 0.43 | 3.21 | -22.80 | -24.20 | 0.28 | -6.11 | 0.47 | 0.99 | |
| | 43 | 1 | 6.32 | 1.31 | | 4.83 | | | -23.61 | -25.01 | 1.41 | -4.98 | 0.76 | 2.63 | |
| | | total | 15.14 | 2.79 | 5.42 | 5.42 | 0.61 | 3.65 | -22.85 | | 1.38 | | 0.74 | 0.20 | |
| | | bulk | 12.58 | 2.18 | | 5.78 | | | | ***1.40*** | | ***6.39*** | | ***20.73*** | |
| E 4E | 974 | 300 | 0.14 | 0.03 | 0.02 | 4.80 | 0.12 | 0.58 | -23.17 | -24.69 | 3.13 | -3.49 | | | |
| 13/11/2011 | 974 | 210 | 0.24 | 0.05 | 0.06 | 4.71 | 0.26 | 1.23 | -23.19 | -24.71 | 3.44 | -3.18 | | | |
| 48.7141 E | 32 | 50 | 3.12 | 0.54 | 1.74 | 5.74 | 0.56 | 3.20 | -22.71 | -24.24 | 2.46 | -4.16 | 0.96 | 0.17 | |
| 72.5708 S | 32 | 20 | 1.86 | 0.29 | 1.12 | 6.39 | 0.61 | 3.87 | -22.23 | -23.75 | 1.82 | -4.80 | 0.80 | 0.48 | |

| | | | | | | | | | | | | | | |
|---|---|---|---|---|---|---|---|---|---|---|---|---|---|---|
| group2 | 32 | 5 | 0.80 | 0.13 | 0.33 | 6.29 | 0.42 | 2.62 | -23.21 | -24.73 | 0.80 | -5.82 | 0.54 | 0.94 |
| | 32 | 1 | 11.19 | 2.01 | | 5.55 | | | -23.20 | -24.72 | 1.35 | -5.27 | 0.68 | 2.48 |
| | | total | 17.35 | 3.06 | 3.28 | 5.68 | 0.53 | 3.15 | -23.01 | | 1.62 | | 0.74 | 0.19 |
| | | bulk | 9.90 | 1.70 | | 5.83 | | | | ***1.53*** | | ***6.62*** | | ***20.63*** |
| A3 2 night | 586 | 300 | 0.04 | 0.01 | 0.01 | 4.83 | 0.17 | 0.80 | -22.85 | -24.16 | 3.79 | -2.53 | | |
| 15/11/2011 | 586 | 210 | 0.05 | 0.01 | 0.01 | 4.80 | 0.18 | 0.85 | -24.43 | -25.74 | 4.02 | -2.30 | | |
| 50.6300 E | 161 | 50 | 6.42 | 1.06 | 4.65 | 6.08 | 0.72 | 4.40 | -21.86 | -23.17 | 1.06 | -5.26 | 0.69 | 0.19 |
| 72.0802 S | 161 | 20 | 0.30 | 0.05 | 0.19 | 6.03 | 0.64 | 3.89 | -22.19 | -23.50 | 0.62 | -5.70 | 0.58 | 0.51 |
| group3 | 161 | 5 | 0.09 | 0.02 | 0.08 | 5.81 | 0.92 | 5.37 | -22.34 | -23.66 | 0.62 | -5.70 | 0.57 | 1.06 |
| | 161 | 1 | 1.84 | 0.38 | | 4.87 | | | -22.14 | -23.46 | 1.55 | -4.77 | 0.81 | 3.04 |
| | | total | 8.74 | 1.52 | 4.94 | 5.76 | 0.72 | 4.33 | -21.95 | | 1.20 | | 0.71 | 0.21 |
| | | bulk | 9.60 | 1.78 | | 5.38 | | | | ***1.31*** | | ***6.32*** | | ***21.04*** |
| A3 2 day | 1081 | 300 | 0.06 | 0.01 | 0.00 | 5.26 | 0.08 | 0.43 | -22.78 | -24.12 | 4.02 | -2.47 | | |
| 16/11/2011 | 1081 | 210 | 0.12 | 0.02 | 0.04 | 5.48 | 0.34 | 1.86 | -22.30 | -23.64 | 2.81 | -3.68 | | |
| 50.6300 E | 209 | 50 | 6.36 | 0.96 | 4.66 | 6.63 | 0.73 | 4.86 | -21.83 | -23.16 | 1.54 | -4.95 | 0.76 | 0.19 |
| 72.0802 S | 209 | 20 | 0.34 | 0.05 | 0.24 | 6.47 | 0.70 | 4.53 | -20.91 | -22.24 | 0.69 | -5.80 | 0.55 | 0.55 |
| group3 | 209 | 5 | 0.14 | 0.02 | 0.09 | 6.11 | 0.64 | 3.89 | -21.67 | -23.01 | 0.05 | -6.44 | 0.39 | 1.10 |
| | 209 | 1 | 2.90 | 0.58 | | 5.03 | | | -21.95 | -23.28 | 1.45 | -5.04 | 0.74 | 3.07 |
| | | total | 9.91 | 1.64 | 5.03 | 6.03 | 0.72 | 4.72 | -21.84 | | 1.49 | | 0.74 | 0.22 |
| | | bulk | 13.06 | 2.28 | | 5.72 | | | | ***1.33*** | | ***6.49*** | | ***20.96*** |
| E 4W 2 | 1373 | 300 | 0.14 | 0.03 | 0.04 | 4.49 | 0.28 | 1.27 | -24.25 | -25.74 | 2.57 | -3.98 | | |
| 18/11/2011 | 1373 | 210 | 0.71 | 0.13 | 0.40 | 5.36 | 0.57 | 3.03 | -23.93 | -25.42 | 2.08 | -4.47 | | |
| 48.7666 E | 131 | 50 | 6.82 | 1.13 | 6.42 | 6.02 | 0.94 | 5.66 | -23.22 | -24.71 | 1.82 | -4.73 | 0.82 | 0.17 |
| 71.4798 S | 131 | 20 | 0.24 | 0.04 | 0.17 | 6.27 | 0.71 | 4.44 | -22.77 | -24.26 | 1.35 | -5.20 | 0.70 | 0.47 |
| group3 | 131 | 5 | 0.27 | 0.05 | 0.13 | 5.62 | 0.50 | 2.79 | -22.50 | -23.99 | -0.23 | -6.78 | 0.31 | 1.02 |
| | 131 | 1 | 3.97 | 0.72 | | 5.54 | | | -25.00 | -26.50 | 0.38 | -6.17 | 0.46 | 2.33 |
| | | total | 12.15 | 2.10 | 7.16 | 5.78 | 0.88 | 5.18 | -23.83 | | 1.30 | | 0.67 | 0.19 |
| | | bulk | 13.36 | 2.51 | | 5.32 | | | | ***1.49*** | | ***6.55*** | | ***20.96*** |
| E 5 | 992 | 300 | 0.29 | 0.07 | 0.01 | 4.02 | 0.05 | 0.20 | -23.96 | -25.40 | 2.97 | -3.64 | | |
| 18/11/2011 | 992 | 210 | 0.11 | 0.03 | 0.01 | 4.43 | 0.13 | 0.57 | -25.14 | -26.58 | 2.94 | -3.67 | | |
| 48.4178 E | 195 | 50 | 2.08 | 0.36 | 1.31 | 5.84 | 0.63 | 3.67 | -24.42 | -25.86 | 1.74 | -4.87 | 0.78 | 0.16 |
| 71.9973 S | 195 | 20 | 0.44 | 0.07 | 0.28 | 6.53 | 0.63 | 4.11 | -23.38 | -24.82 | 1.40 | -5.21 | 0.70 | 0.46 |
| group2 | 195 | 5 | 0.16 | 0.03 | 0.07 | 6.14 | 0.44 | 2.70 | -23.21 | -24.65 | -0.14 | -6.75 | 0.31 | 0.98 |
| | 195 | 1 | 2.60 | 0.46 | | 5.61 | | | -25.72 | -27.16 | -0.99 | -7.60 | 0.10 | 2.19 |
| | | total | 5.67 | 1.01 | 1.68 | 5.62 | 0.55 | 3.08 | -24.90 | | 0.53 | | 0.42 | 0.18 |
| | | bulk | 7.59 | 1.31 | | 5.78 | | | | ***1.44*** | | ***6.61*** | | ***21.43*** |

*Bolded column headers refer to bolded quantities shown on the bulk sample lines; bulk samples were measured on water and unfractionated particle samples collected separately*

Table 3. Phytoplankton cell dimensions used in $^{13}C$ supply versus demand model.

| Size Fraction | Prism Dimensions | | | Form |
|---|---|---|---|---|
| μm | d1 | d2 | d3 | |
| 1 - 5 | 3 | 3 | 3 | single cells |
| 5 - 20 | 7 | 7 | 15 | single cells |
| 20 - 50 | 15 | 15 | 30 | chains* |
| 50 - 210 | 40 | 40 | 80 | chains* |

*$CO_2$ exchange is assumed to be negligible on the surface of the cell contact within the chains, taken to be the long faces of the prisms.

933

934

Table 4a. Surface mixed layer N depletion and export estimates.

| Station | CTD | timestamp | | Depth | | | Nitrate | | | Nitrate depletion | | | | PN stock | N Export | N Export |
|---|---|---|---|---|---|---|---|---|---|---|---|---|---|---|---|---|
| | | | MLD[1] | $T_{min}$ | $S_{threshold}$ | surface | $T_{min}$ | $S_{threshold}$ | $T_{min}$ | $S_{threshold}$ | $T_{min}$[2] | $S_{threshold}$[2] | | 200m | $S_{threshold}$ | fraction[3] |
| | cast | mm-dd hh-mm | m | m | m | μM | μM | μM | mmol.m$^{-2}$ | mmol.m$^{-2}$ | % | % | | mmol.m$^{-2}$ | mmol.m$^{-2}$ | % |
| A3-1 | 4 | 10-20 05:32 | 161 | 175 | 175 | 29.1 | 31.1 | 31.1 | 268 | 268 | 5 | 5 | | 138 | 130 | 49 |
| TNS10 | 6 | 10-21 07:28 | 163 | 183 | 179 | 28.9 | 31.1 | 31.0 | 298 | 270 | 5 | 5 | | 193 | 77 | 28 |
| TNS09 | 7 | 10-21 13:40 | 137 | 147 | 150 | 27.9 | 30.3 | 30.7 | 243 | 324 | 5 | 7 | | 205 | 119 | 37 |
| TNS08 | 8 | 10-21 18:48 | 139 | 192 | 201 | 27.9 | 30.8 | 31.2 | 362 | 470 | 6 | 7 | | 179 | 291 | 62 |
| TNS06 | 10 | 10-22 11:18 | 67 | 280[4] | 149 | 26.5 | 33.5 | 29.8 | 1034 | 317 | 11 | 7 | | 219 | 99 | 31 |
| TNS05 | 11 | 10-22 16:56 | 114 | 174[4] | 155 | 26.5 | 30.1 | 29.5 | 438 | 345 | 8 | 8 | | 164 | 181 | 52 |
| TNS03 | 13 | 10-23 06:41 | 111 | 191[4] | 164 | 26.9 | 31.0 | 29.9 | 494 | 326 | 8 | 7 | | 144 | 183 | 56 |
| TNS02 | 14 | 10-23 12:06 | 65 | 364[4] | 150 | 19.5 | 34.0 | 28.8 | 1711 | 279 | 14 | 6 | | 101 | 179 | 64 |
| TNS01 | 15 | 10-23 17:13 | 45 | 328[4] | 144 | 23.6 | 31.2 | 25.5 | 1506 | 196 | 15 | 5 | | 135 | 61 | 31 |
| R2 | 17 | 10-25 22:59 | 111 | 184[4] | 168 | 25.7 | 28.0 | 27.3 | 346 | 232 | 7 | 5 | | 78 | 154 | 66 |
| R2 | 18 | 10-26 01:48 | 123 | 193 | 167 | 26.0 | 28.3 | 27.3 | 430 | 239 | 8 | 5 | | 78 | 161 | 67 |
| E-1 | 27 | 10-29 22:46 | 84 | 200 | 173 | 25.7 | 29.0 | 28.6 | 492 | 421 | 8 | 9 | | 208 | 213 | 51 |
| E-1 | 30 | 10-30 09:15 | 63 | 183 | 151 | 26.0 | 29.0 | 30.8 | 293 | 493 | 6 | 11 | | 208 | 285 | 58 |
| TEW3 | 38 | 10-31 18:41 | 62 | 165[4] | 138 | 27.2 | 29.1 | 28.1 | 225 | 89 | 5 | 2 | | 145 | -56 | -63 |
| TEW4 | 42 | 11-01 05:19 | 95 | 208 | 185 | 25.0 | 30.1 | 29.2 | 631 | 463 | 10 | 9 | | 250 | 213 | 46 |
| TEW5 | 44 | 11-01 19:00 | 60 | 173 | 174 | 26.1 | 30.2 | 29.8 | 434 | 354 | 8 | 7 | | 201 | 153 | 43 |
| TEW6 | 45 | 11-02 03:59 | 22 | 164 | 142 | 26.0 | 30.9 | 30.1 | 493 | 371 | 10 | 9 | | 175 | 197 | 53 |
| TEW7 | 46 | 11-02 09:34 | 17 | 423[4] | 91 | 26.0 | 35.0 | 27.0 | 2103 | 391 | 14 | 16 | | 309 | 82 | 21 |
| TEW8 | 47 | 11-02 18:47 | 22 | 293[4] | 75 | 19.5 | 32.7 | 27.2 | 1282 | 303 | 13 | 15 | | 252 | 51 | 17 |
| E-2 | 43 | 11-01 12:00 | 42 | 210[4] | 157 | 18.9 | 32.7 | 29.3 | 857 | 221 | 12 | 5 | | 185 | 36 | 16 |
| E-3 | 50 | 11-03 11:57 | 41 | 203 | 177 | 25.4 | 30.1 | 29.5 | 467 | 371 | 8 | 7 | | 194 | 177 | 48 |
| E-3 | 51 | 11-04 01:29 | 32 | 200 | 166 | 25.8 | 30.0 | 28.7 | 486 | 253 | 8 | 5 | | 194 | 59 | 23 |
| E-3 | 55 | 11-04 17:22 | 37 | 184 | 161 | 26.0 | 29.5 | 28.6 | 520 | 361 | 10 | 8 | | 194 | 166 | 46 |
| F-L | 63 | 11-06 21:49 | 21 | 182 | 79 | 26.0 | 30.5 | 26.4 | 686 | 368 | 12 | 18 | | 215 | 153 | 42 |
| F-S | 69 | 11-08 06:13 | 31 | 267 | 54 | 18.9 | 35.2 | 24.7 | 1598 | 140 | 17 | 11 | | 354 | -214 | -153 |
| G-1 | 70 | 11-09 00:30 | 37 | 118 | 127 | 19.9 | 29.8 | 30.3 | 380 | 447 | 11 | 12 | | nd | - | - |
| E-4W | 79 | 11-11 08:25 | 67 | 158 | 147 | 23.0 | 30.2 | 30.1 | 548 | 527 | 11 | 12 | | 288 | 239 | 45 |
| E-4W | 81 | 11-11 21:07 | 67 | 152 | 158 | 22.1 | 30.1 | 30.0 | 544 | 532 | 12 | 11 | | 288 | 243 | 46 |
| E-4W | 87 | 11-12 09:30 | 66 | 164 | 164 | 22.1 | 30.4 | 30.3 | 652 | 645 | 13 | 13 | | 288 | 357 | 55 |
| E-4E | 94 | 11-13 22:02 | 77 | 158 | 108 | 22.1 | 28.8 | 27.7 | 382 | 236 | 8 | 8 | | 253 | -17 | -7 |
| E-4E | 95 | 11-14 01:30 | 80 | 159 | 112 | 24.1 | 28.9 | 27.4 | 439 | 227 | 10 | 7 | | 253 | -26 | -11 |
| A3-2 | 99 | 11-15 23:20 | 143 | 179 | 179 | 24.1 | 30.6 | 30.7 | 652 | 670 | 12 | 12 | | 436 | 234 | 35 |
| A3-2 | 108 | 11-17 01:08 | 123 | 182 | 177 | 25.8 | 30.9 | 30.8 | 593 | 576 | 11 | 11 | | 436 | 140 | 24 |
| E_4W-2 | 111 | 11-18 07:20 | 26 | 168 | 133 | 24.7 | 29.3 | 28.0 | 592 | 400 | 12 | 11 | | 354 | 46 | 11 |
| E-5 | 113 | 11-18 19:21 | 71 | 215 | 122 | 26.5 | 30.4 | 27.9 | 689 | 207 | 11 | 6 | | 210 | -3 | -1 |
| E-5 | 114 | 11-18 22:07 | 36 | 228 | 126 | 26.5 | 30.8 | 28.0 | 756 | 206 | 11 | 6 | | 210 | -4 | -2 |
| E-5 | 115 | 11-19 01:30 | 41 | 222[4] | 123 | 26.5 | 30.7 | 27.9 | 686 | 222 | 10 | 6 | | 210 | 12 | 6 |

[1] Mixed layer depth where the potential density = potential density at 10m+0.02kg.m$^{-3}$. Park et al. (2014b)
[2] % depletion of the winter mixed layer inventory.
[3] Fraction=export/depletion, calculated for the $S_{threshold}$ depletion estimate.
[4] No clear Tmin.
Surface data are from both the CTD Niskin bottles and underway systems. $T_{min}$ nitrate was estimated from nearest Niskin.
nd = no data

935
936

Table 4a. Surface mixed layer N depletion and export estimates.

| Station | CTD | timestamp | | Depth | | | Nitrate | | | Nitrate depletion | | | | PN stock | N Export | N Export |
|---|---|---|---|---|---|---|---|---|---|---|---|---|---|---|---|---|
| | | | MLD[1] | $T_{min}$ | $S_{threshold}$ | surface | $T_{min}$ | $S_{threshold}$ | $T_{min}$ | $S_{threshold}$ | $T_{min}$[2] | $S_{threshold}$[2] | | 200m | $S_{threshold}$ | fraction[3] |
| | cast | mm-dd hh-mm | m | m | m | μM | μM | μM | mmol.m$^{-2}$ | mmol.m$^{-2}$ | % | % | | mmol.m$^{-2}$ | mmol.m$^{-2}$ | % |
| A3-1 | 4 | 10-20 05:32 | 161 | 175 | 175 | 29.1 | 31.1 | 31.1 | 268 | 268 | 5 | 5 | | 138 | 130 | 49 |
| TNS10 | 6 | 10-21 07:28 | 163 | 183 | 179 | 28.9 | 31.1 | 31.0 | 298 | 270 | 5 | 5 | | 193 | 77 | 28 |
| TNS09 | 7 | 10-21 13:40 | 137 | 147 | 150 | 27.9 | 30.3 | 30.7 | 243 | 324 | 5 | 7 | | 205 | 119 | 37 |
| TNS08 | 8 | 10-21 18:48 | 139 | 192 | 201 | 27.9 | 30.8 | 31.2 | 362 | 470 | 6 | 7 | | 179 | 291 | 62 |
| TNS06 | 10 | 10-22 11:18 | 67 | 280[4] | 149 | 26.5 | 33.5 | 29.8 | 1034 | 317 | 11 | 7 | | 219 | 99 | 31 |
| TNS05 | 11 | 10-22 16:56 | 114 | 174[4] | 155 | 26.5 | 30.1 | 29.5 | 438 | 345 | 8 | 8 | | 164 | 181 | 52 |
| TNS03 | 13 | 10-23 06:41 | 111 | 191[4] | 164 | 26.9 | 31.0 | 29.9 | 494 | 326 | 8 | 7 | | 144 | 183 | 56 |
| TNS02 | 14 | 10-23 12:06 | 65 | 364[4] | 150 | 19.5 | 34.0 | 28.8 | 1711 | 279 | 14 | 6 | | 101 | 179 | 64 |
| TNS01 | 15 | 10-23 17:13 | 45 | 328[4] | 144 | 23.6 | 31.2 | 25.5 | 1506 | 196 | 15 | 5 | | 135 | 61 | 31 |
| R2 | 17 | 10-25 22:59 | 111 | 184[4] | 168 | 25.7 | 28.0 | 27.3 | 346 | 232 | 7 | 5 | | 78 | 154 | 66 |
| R2 | 18 | 10-26 01:48 | 123 | 193 | 167 | 26.0 | 28.3 | 27.3 | 430 | 239 | 8 | 5 | | 78 | 161 | 67 |
| E-1 | 27 | 10-29 22:46 | 84 | 200 | 173 | 25.7 | 29.0 | 28.6 | 492 | 421 | 8 | 9 | | 208 | 213 | 51 |
| E-1 | 30 | 10-30 09:15 | 63 | 183 | 151 | 26.0 | 29.0 | 30.8 | 293 | 493 | 6 | 11 | | 208 | 285 | 58 |
| TEW3 | 38 | 10-31 18:41 | 62 | 165[4] | 138 | 27.2 | 29.1 | 28.1 | 225 | 89 | 5 | 2 | | 145 | -56 | -63 |
| TEW4 | 42 | 11-01 05:19 | 95 | 208 | 185 | 25.0 | 30.1 | 29.2 | 631 | 463 | 10 | 9 | | 250 | 213 | 46 |
| TEW5 | 44 | 11-01 19:00 | 60 | 173 | 174 | 26.1 | 30.2 | 29.8 | 434 | 354 | 8 | 7 | | 201 | 153 | 43 |
| TEW6 | 45 | 11-02 03:59 | 22 | 164 | 142 | 26.0 | 30.9 | 30.1 | 493 | 371 | 10 | 9 | | 175 | 197 | 53 |
| TEW7 | 46 | 11-02 09:34 | 17 | 423[4] | 91 | 26.0 | 35.0 | 27.0 | 2103 | 391 | 14 | 16 | | 309 | 82 | 21 |
| TEW8 | 47 | 11-02 18:47 | 22 | 293[4] | 75 | 19.5 | 32.7 | 27.2 | 1282 | 303 | 13 | 15 | | 252 | 51 | 17 |
| E-2 | 43 | 11-01 12:00 | 42 | 210[4] | 157 | 18.9 | 32.7 | 29.3 | 857 | 221 | 12 | 5 | | 185 | 36 | 16 |
| E-3 | 50 | 11-03 11:57 | 41 | 203 | 177 | 25.4 | 30.1 | 29.5 | 467 | 371 | 8 | 7 | | 194 | 177 | 48 |
| E-3 | 51 | 11-04 01:29 | 32 | 200 | 166 | 25.8 | 30.0 | 28.7 | 486 | 253 | 8 | 5 | | 194 | 59 | 23 |
| E-3 | 55 | 11-04 17:22 | 37 | 184 | 161 | 26.0 | 29.5 | 28.6 | 520 | 361 | 10 | 8 | | 194 | 166 | 46 |
| F-L | 63 | 11-06 21:49 | 21 | 182 | 79 | 26.0 | 30.5 | 26.4 | 686 | 368 | 12 | 18 | | 215 | 153 | 42 |
| F-S | 69 | 11-08 06:13 | 31 | 267 | 54 | 18.9 | 35.2 | 24.7 | 1598 | 140 | 17 | 11 | | 354 | -214 | -153 |
| G-1 | 70 | 11-09 00:30 | 37 | 118 | 127 | 19.9 | 29.8 | 30.3 | 380 | 447 | 11 | 12 | | nd | - | - |
| E-4W | 79 | 11-11 08:25 | 67 | 158 | 147 | 23.0 | 30.2 | 30.1 | 548 | 527 | 11 | 12 | | 288 | 239 | 45 |
| E-4W | 81 | 11-11 21:07 | 67 | 152 | 158 | 22.1 | 30.1 | 30.0 | 544 | 532 | 12 | 11 | | 288 | 243 | 46 |
| E-4W | 87 | 11-12 09:30 | 66 | 164 | 164 | 22.1 | 30.4 | 30.3 | 652 | 645 | 13 | 13 | | 288 | 357 | 55 |
| E-4E | 94 | 11-13 22:02 | 77 | 158 | 108 | 22.1 | 28.8 | 27.7 | 382 | 236 | 8 | 8 | | 253 | -17 | -7 |
| E-4E | 95 | 11-14 01:30 | 80 | 159 | 112 | 24.1 | 28.9 | 27.4 | 439 | 227 | 10 | 7 | | 253 | -26 | -11 |
| A3-2 | 99 | 11-15 23:20 | 143 | 179 | 179 | 24.1 | 30.6 | 30.7 | 652 | 670 | 12 | 12 | | 436 | 234 | 35 |
| A3-2 | 108 | 11-17 01:08 | 123 | 182 | 177 | 25.8 | 30.9 | 30.8 | 593 | 576 | 11 | 11 | | 436 | 140 | 24 |
| E_4W-2 | 111 | 11-18 07:20 | 26 | 168 | 133 | 24.7 | 29.3 | 28.0 | 592 | 400 | 12 | 11 | | 354 | 46 | 11 |
| E-5 | 113 | 11-18 19:21 | 71 | 215 | 122 | 26.5 | 30.4 | 27.9 | 689 | 207 | 11 | 6 | | 210 | -3 | -1 |
| E-5 | 114 | 11-18 22:07 | 36 | 228 | 126 | 26.5 | 30.8 | 28.0 | 756 | 206 | 11 | 6 | | 210 | -4 | -2 |
| E-5 | 115 | 11-19 01:30 | 41 | 222[4] | 123 | 26.5 | 30.7 | 27.9 | 686 | 222 | 10 | 6 | | 210 | 12 | 6 |

[1] Mixed layer depth where the potential density = potential density at 10m+0.02kg.m$^{-3}$. Park et al. (2014b)
[2] % depletion of the winter mixed layer inventory.
[3] Fraction=export/depletion, calculated for the $S_{threshold}$ depletion estimate.
[4] No clear Tmin.
Surface data are from both the CTD Niskin bottles and underway systems. $T_{min}$ nitrate was estimated from nearest Niskin.
nd = no data

937
938

**Figure Captions**

Figure 1. Map of KEOPS-2 station locations. The Kerguelen and Heard islands mark the northern and southern end of the central plateau (bathymetry in meters). The Polar Front jet that passes through the mid-depth channel south of Kerguelen Island is shown as a bold line. Full ocean depth flows of the Antarctic Circumpolar Current pass to the north of Kerguelen Island in association with the Subantarctic Front and to the south of Heard Island in the Fawn Trough. This latter flow follows the eastern slope of the plateau northwards to bring cold waters into a bathymetrically trapped quasi-stationary recirculation feature (d'Ovidio et al., 2014;Park et al., 2014a). Waters over the central plateau are also carried into this region. During the initial survey, the TNS transect was sampled first (south to north) and then the TEW transect (west to east). The E stations were designed to provide a Lagrangian temporal sequence in the recirculation region (including some to the east and west of its centre), with interspersed visits to the HNLC reference station (R2); the region of high biomass near and north of the Polar Front (F-L and F-S), and the central plateau bloom station (A3) previously studied in autumn 2005 by the KEOPS project. Two additional stations (G1, G2) carried out for high volume geochemical tracer studies and provided additional plateau and coastal samples, respectively. The stations are colour coded into 5 Groups as shown on the map (QGIS) and detailed in Table 1.

Figure 2. Temporal development of the Kerguelen bloom. Successive images of surface chlorophyll distributions (NASA MODIS-Aqua; SSALTO/DUACS 1 km daily product) show the bloom development. Image date 28 October: most stations of the initial survey downstream of Kerguelen Island (TNS 1-10, TEW 1-6), the HNLC reference station (R2, upstream) and the first visit to the KEOSP1 plateau reference station (A3-1 at the southern end of the TNS transect) were sampled before any significant biomass accumulation had

964 occurred. Image date 06 November: The developing downstream Polar Front bloom (TEW 7,
965 TEW 8, F-L, F-S) was sampled early in its development, and the recirculation visited a
966 second time (E2). Image date 11 November: the now well developed central plateau bloom
967 was sampled (G1; E4-W) along with also blooming coastal waters (G2). Two more visits to
968 the still low biomass recirculation were also completed (E3 and E4-E). Image date 18
969 November: the plateau bloom was re-sampled as it began to fade (A3-2 and E4-W2), along
970 with the final recirculation station (E5). Bathymetry is shown by contours at 1000, 2000, and
971 3000 m depths. A full annual animation of the phytoplankton bloom evolution is available in
972 the Supplement.
973
974 Figure 3. Surface water total and size-fractionated POC and BSi concentrations.
975 Top row: total POC and BSi concentrations for the identified station Groups (see Table 1);
976 individual stations in each group are in chronological order from left to right. Middle row:
977 POC size distribution spectra, i.e. concentrations normalised by dividing by the width of the
978 size fraction (i.e. division by 4 for the 1-5 μm fraction); dotted lines provide visual guides
979 and reveal little variation among groups for the smallest particles, and largest variations in the
980 intermediate size fractions. Bottom row: BSi/POC ratios; grey band indicates approximate
981 range of values for extant diatoms, with higher values possibly indicative of higher iron stress.
982
983 Figure 4. Isotopic variations in the size-fractionated particles.
984 Top row: $^{13}$C-POC values relative to $^{13}$C-DIC values; dotted line shows the lowest values for
985 the intermediate, autotrophic, size fractions samples as observed at upstream Fe poor
986 reference station (R2). Bottom row: $^{15}$N-PON values relative to co-located $^{15}N\text{-}NO_3^-$ values;
987 grey band indicates values expected for phytoplankton that grow exclusively on nitrate.
988

Figure 5. Isotopic chemometric estimates of growth rates and f-ratios

Top row: Growth rates based on the supply vs. demand $^{13}C$ isotopic fractionation model (summed across the 4 smallest particle size fractions). Estimates from a limited set of $^{13}C$ tracer uptake incubations are shown as darker bars (measured at varying light levels and integrated to the mixed layer depth light level; (Cavagna et al., 2014)). Bottom row: *f* ratios, i.e. the fraction of total nitrogen nutrition provided by nitrate, based on the $^{15}N$ ammonium and $^{15}N$ nitrate end-member mixing model (summed across 4 smallest particle size fractions). Estimates from a limited set of $^{15}N$ tracer uptake incubations are shown as darker bars (Cavagna et al., 2014).

Figure 6. High resolution distributions of surface water properties from continuous sensor measurements.

Top to bottom: ship trajectory as revealed by dates of sampling; nitrate concentrations (from ISUS ultra-violet spectrometry), temperature, and salinity. Stations at the ends of the trajectories are indicated to aid in co-location with the lower resolution station sampling map (Fig. 1).

Figure 7. Example profiles of temperature, salinity, nitrate concentrations, and nitrate isotopic compositions. Top row: Group 3 central plateau station A3-2. Middle row: Group 5 downstream Polar Front station F-L. Bottom row: Group 5 Subantarctic station TNS-1. Depths of the remnant winter water $T_{min}$ mixed layer depth ($T_{min}$-depth; solid line) and salinity stratification mixed layer depth ($S_{threshold}$-depth; dotted lines) are shown. These depths define our two approaches for the calculation of depth integrated nitrate and silicate depletions (Table 4; Fig. 8).

Figure 8. Nitrogen and silicon depletion and export estimates

Top row: nitrate (light bars) and silicate (dark bars) depletions from the $T_{min}$ winter concentration method. Middle row: nitrate (light bars) and silicate (dark bars) depletions from the $S_{threshold}$ winter concentration method. Bottom row: N (light bars) and Si (dark bars) export, as estimated from the $S_{threshold}$ depletion method, after accounting for the PN and BSi standing stocks integrated to 200m (Table 4; (Lasbleiz et al., 2014)). Group 4 coastal stations are not shown because CTD casts could not define winter values. Negative export values are not plotted (see Table 4 and text). Groups 1, 2, 3 and 4 are coloured as in Fig. 1 and are ranked from left to right with temporal order within each group.

## Appendix A: Chemical and isotopic analyses

### A1 Particle collection

The ship supply collected water from ~7m depth via a 10 cm diameter plastic hose extended through a vertical stainless-steel stand-pipe protruding ~1 m below the ship's forward hull. A sealed rotary propeller pump drew the supply through a 1000 μm nylon cylindrical pre-filter and distributed it via a manifold at more than 50 L $min^{-1}$, with most water returned over the side. This pre-filter was cleaned before each sample, and then a manifold valve was opened to supply a smaller flow of 8-10 L $min^{-1}$ through our small volume bulk particle and large volume sequential filtration systems. The large volume size fractionation system passes the water through a 47 mm diameter 1000 μm screen (to remove any large particles that managed to pass through the pump pre-filter at higher flow rates), followed by 142 mm diameter Nitex nylon screens (300, 210, 50, 20, and 5 μm mesh sizes) and a final 142 mm diameter QMA quartz fibre filter (1 μm nominal pore size, Sartorius). The small volume bulk enclosed sample system rapidly fills a precisely known ~1 L volume and low pressure filters it through a QMA quartz filter (muffled and pre-loaded under clean conditions into in-line filter holders). Quartz filters were used in preference to glass to minimize $^{234}$Th backgrounds and to give better combustion characteristics during elemental and isotopic analysis. The flow path allowed a larger flow rate through the larger meshes (Table 2). The very minor amounts of material on the 1000 μm screen were not analysed. Particles on the other nylon screens were immediately resuspended (1 μm filtered seawater from the sampling location) and refiltered onto 25 mm diameter, 1.2 micron pore size silver membrane filters (Sterlitech) and, along with the QMA filter (Sartorius T293), were dried at 60ºC. Following drying, the particles were examined under stereo-microscopy onboard the ship at magnification up to 50x, and then analysed non-destructively onboard for $^{234}$Th

activities (Planchon et al., 2014). All other analyses were carried out in the Hobart laboratories.

**A2 Particle analyses**

Biogenic silica (BSi), Particulate organic carbon (POC), and particulate nitrogen (PN), $\delta^{13}$C-POC, and $\delta^{15}$N-PN analyses were carried out in Hobart. For BSi, a single 5mm diameter punch of the silver filters was analysed using an approach used previously for Southern Ocean samples (Queguiner, 2001). The biogenic silica was dissolved by adding 4mL of 0.2M NaOH and incubating at 95°C for 90 minutes. Samples were then rapidly cooled to 4°C and 1mL of 1M HCl was added. Thereafter samples were centrifuged at 1880 x *g* for 10 minutes and the supernatant was transferred to a new tube and diluted with artificial seawater (36 g $L^{-1}$ NaCl). Biogenic silica concentrations were determined by spectrophotometry using an Alpkem model 3590 segmented flow analyser and following USGS Method I-2700-85 with these modifications: ammonium molybdate solution contained 10g $L^{-1}$ $(NH_4)_6Mo_7O_{24}$, 800µl of 10% sodium dodecyl sulphate detergent replaced Levor IV solution, acetone was omitted from the ascorbic acid solution, and artificial seawater was used as the carrier solution. Biogenic silica standard concentrations were 0 µM, 28 µM, 56 µM, 84 µM,112 µM and 140 µM. Standard curves across all runs had an average slope of 48 438 ± 454 (1 s.d. *n*=4). The mean concentration of repeated check standards (140 µM) was 139.85± 0.31 µM (n=68). The average blank value was 0.009 ± 0.006 µmoles $punch^{-1}$ (1 s.d. *n*=5), equating to 0.08% of the mean of 50 µm fraction samples (highest concentrations) and 1.22% of the mean of 300 µm fractions (lowest concentrations).

For the POC and PN analyses, 3 x 5mm punched sub-samples of the 25 mm diameter silver membrane filters were placed in acid-resistant silver capsules (Sercon SC0037), treated with two 10 µL aliquots of 2N HCl (and 2 x 20 µL for the bulkier QMA filter sub-samples, 5

1074 x 5mm punches) to remove carbonates (King et al., 1998), and dried at 60 ºC. A first set of
1075 sub-samples was analysed for POC and PN concentrations by combustion of the encapsulated
1076 samples in a Thermo-Finnigan Flash 1112 elemental analyser with reference to
1077 sulphanilamide standards in the Central Sciences Laboratory of the University of Tasmania.
1078 Precision of the analyses was ~1 %, but the overall precision was limited to 5-10 % by the
1079 sub-sampling of the filters that often had patchy or uneven coverage. Based on the POC and
1080 PN results, a third set of sub-samples was punched for isotopic analyses with the number of
1081 punches adjusted to ensure similar voltages within the dynamic range of the spectrometer.
1082 $\delta^{13}$C-POC and $\delta^{15}$N-PN on the silver filters were analysed separately using a Fisons
1083 NA1500 Elemental Analyser coupled via a Con-flow IV interface to a Finnigan Delta $V^{PLUS}$
1084 isotope ratio mass spectrometer at CSIRO Marine and Atmospheric Research with separate
1085 oxidation and reduction columns installed. For the QMA filters, a Flash 2000 EA1112 HT
1086 Thermoscientific was fitted with a single combined oxidation/reduction column with dead
1087 spaces minimised for improved precision at <20µg N. During all $^{15}$N analyses, $CO_2$ was
1088 removed using a sodium hydroxide scrubber (self-indicating Ascarite 2, Thomas Scientific)
1089 to avoid $CO^+$ interference at m/z 29 and 28 (Brooks et al., 2003). The $\delta^{15}$N and $\delta^{13}$C isotopic
1090 compositions are expressed in delta notation vs. atmospheric $N_2$ and the VPDB standard,
1091 respectively. Standardization was by reference to $CO_2$ and $N_2$ working gases injected before
1092 and after each sample, with normalization to solid reference materials inserted (along with
1093 blank cups) after each 6 samples. For $\delta^{13}$C, the solid standards were NBS-22 oil (RM8539, -
1094 29.73 ‰) and NBS-19 (limestone, RM8544, +1.95 ‰), and casein (Protein Standard OAS
1095 B2155 batch 114859, Elemental Microanalysis, $\delta^{13}$C +5.94 and $\delta^{15}$N -26.98). For $\delta^{15}$N, the
1096 solid standards were IAEA-N1 (ammonium sulphate, RM8547, +0.43‰) and IAEA-N3
1097 (potassium nitrate, RM8549, +4.72 ‰) and casein (as above). Based on replicate analyses of

these standards the estimated precisions were typically 0.1‰ or 1 standard deviation for both $\delta^{13}C$ (n=15) and $\delta^{15}N$ (n=20).

Sample replicates generally had comparable precisions to the reference materials, but filters with patchy coverage had lower precision (0.3‰ in the worst cases, presumably reflecting isotopic heterogeneity within the size fractions). In addition, a small correction of <+0.4‰ was made to the QMA filter results after indirect estimation of the blank $\delta^{13}C$ to be-29.6 (Avak and Fry, 1999), at ~10% of the sample signal strength. Procedural blanks were measured by passing 1 litre of seawater through the onboard pumping system and subsequent processing in parallel to the samples, and yielded negligible amounts of POC and PN (<1% of typical samples), and with ratios close to those of the samples, and no correction was applied.

**A3 Dissolved component analyses**

Underway nitrate concentrations were mapped using an ultra-violet nitrate sensor (ISUS V3, Satlantic), calibrated 3 times during the voyage against sea water nitrate standards (~15, 20, 25, 30 μM) , with additional comparisons to nitrate samples collected from the underway supply at every station sampled for particle analyses, yielding precision of ~1.5 μM. Nitrate concentrations for these samples and the CTD-Niskin bottles were measured onboard using a segmented flow spectrometric autoanalyser, with precision of ~0.1 μM. The N and O isotopic compositions of dissolved nitrate were measured via its bacterial conversion to nitrate to nitrous oxide followed by isotope ratio mass spectrometry at the Vrije Universitait Bruxelles, with precision of approximately 0.2‰ for $^{15}N\text{-}NO_3$ and of 0.4‰ for $^{18}O\text{-}NO_3$ (further analytical details are provided in Dehairs et al., 2014).

Samples for measurement of the carbon isotopic composition of dissolved inorganic carbon were collected in 10mL Exetainer vials, with airtight septa, by filling the tubes from

QMA filtered (~0.8 μm ) underway supply and preserving them by addition of 20μL of saturated mercuric chloride. 1mL aliquots were withdrawn and injected into acid washed, helium flushed Exetainer tubes. 100μL of ortho-phosphoric acid (99%, Fluka) was injected and the headspace equilibrated at 25$^{o}$C for 18 hours (modification of Assayag et al., 2006). Solid NBS19 $CaCO_3$ (200 to 230ug, $\delta^{13}C$=+1.98, *n*=10 standard deviation 0.02), and bulk quality assurance sediment trap material (1200μg, 12.9%CaCO3, $\delta^{13}C$=+2.9), was weighed into smooth wall tin capsules (5x5.5mm SC1190, Sercon) and lowered into the Exetainer tubes, purged, then 1mL of DIC free sea water added before proceeding as for the samples. Blank, standard and sample headspaces (one standard after each 5 samples) were sampled using a Finnigan GasBench2 (Thermoscientific) fitted with a 100μL sample loop. The headspace gases from the Gas Bench were analysed (continuous flow) by the DeltaV$^{Plus}$ isotope ratio mass spectrometer and Isodat 3 software at CSIRO Marine and Atmospheric Research.

**The Supplement related to this article is available online at doi:10.5194/bgd-11-13841-2014 supplement.**

File: Animation_keops2bloom2011_2012.mp4

The animation shows a full annual cycle of phytoplankton bloom development over and downstream of the Kerguelen plateau from daily 8km resolution NASA MODIS Aqua chlorophyll images. The images were provided by SSALTO/DUACS at CLS with support from the Centre Nationale des Etudes Spatiales, Toulouse, France.

*Acknowledgements.* The Institute Polaire Paul-Emile Victor, the captain and crew of the *Marion Dufresne*, the Australian Commonwealth Cooperative Research Centre Program, and CSIRO Marine and Atmospheric Research (CMAR) provided logistic and financial support. Special thanks to Pierre Sangiardi (IPEV) for implementing the underway seawater supply for our high volume particle sampling and underway sensor mapping; Louise Oriole (Laboratoire d'Océanographie Microbienne, Banyuls sur mer, France) for shipboard nutrient analyses; Abraham Passmore (ACE CRC) for BSi analyses; Peter Jansen (IMOS) for the logging system for the underway ISUS ultra-violet nitrate sensor; Ben Weeding (IMOS) for advancing ISUS calibration; Thomas Rodemann for CHN analyses in the University of Tasmania Central Sciences Laboratory; VUB for nitrate isotope analyses, Clair Lo Monoco and Nicolas Metzl (LOCEAN, UPMC-CNRS) for access to $pCO_2$ results; and Andy Bowie (ACE CRC/UTAS), Pier van der Merwe (ACE CRC), and Fabien Queroue (UTAS/UBO) for access to iron results. This work was supported by the French Research program of INSU-CNRS LEFE−CYBER (Les enveloppes fluides et l'environnement –Cycles biogéochimiques, environnement et ressources), the French ANR (Agence Nationale de la Recherche, SIMI-6 program, ANR-10-BLAN-0614), and the French CNES (Centre National d'Etudes Spatiales).

## References


Anderson, L., and Sarmiento, J.: Redfield ratios of remineralization determined by nutrient data analysis, Global Biogeochemical Cycles, 8, 65– 80, 1994.

Armstrong, R. A.: An optimization-based model of iron-light-ammonium colimitation of nitrate uptake and phytoplankton growth, Limnology and Oceanography, 44, 1436-1446, 1999.

Arrigo, K. R., Robinson, D. H., Worthen, D. L., Dunbar, R. B., DiTullio, G. R., VanWoert, M., and Lizotte, M. P.: Phytoplankton community structure and the drawdown of nutrients and $CO_2$ in the Southern Ocean, Science, 283, 365-367, 1999.

Assmy, P., Smetacek, V., Montresor, M., Klaas, C., Henjes, J., Strass, V. H., Arrieta, J. M., Bathmann, U., Berg, G. M., and Breitbarth, E.: Thick-shelled, grazer-protected diatoms decouple ocean carbon and silicon cycles in the iron-limited Antarctic Circumpolar Current, Proceedings of the National Academy of Sciences, 110, 20633-20638, 2013.

Avak, H., and Fry, B.: EA-IRMS: Precise and accurate measurement of d15N on <10ug N, Finnigan MAT Application flash report G29, 1-4, 1999.

Blain, S., Queguiner, B., and Trull, T.: The natural iron fertilization experiment KEOPS (KErguelen Ocean and Plateau compared Study): An overview, Deep-Sea Research Part Ii-Topical Studies in Oceanography, 55, 559-565, 10.1016/j.dsr2.2008.01.002, 2008.

Blain, S., Capparos, J., Guéneuguès, A., Obernosterer, I., and Oriol, L.: Distributions and stoichiometry of dissolved nitrogen and phosphorus in the iron fertilized region near Kerguelen (Southern Ocean), Biogeosciences Discuss., 11, 9949-9977, 10.5194/bgd-11-9949-2014, 2014.

Bowie, A., van der Merwe, P., Trull, T., Queroue, F., Fourquez, M., Planchon, F., Sarthou, G., and Blain, S.: Iron budgets for three distinct biogeochemical sites around the Kerguelen plateau (Southern Ocean) during the natural fertilization experiment KEOPS-2, Biogeosciences Discuss., 11, submitted, 2014.

Boyd, P., Watson, A., Law, C. S., Abraham, E., Trull, T., and Murdoch, R.: SOIREE - A Southern Ocean iron release experiment elevates phytoplankton stocks in Polar waters., EOS Trans. AGU Ocean Sciences Meet. Suppl., 80, OS30, 1999.

Boyd, P. W., and Newton, P.: Evidence of the potential influence of planktonic community structure on the interannual variability of particulate carbon flux., Deep-Sea Research I, 42, 619-639, 1995.

Boyd, P. W., and Newton, P.: Does planktonic community structure determine downward particulate organic carbon flux in different oceanic provinces?, Deep-Sea Research I, 46, 63-91, 1999.

Boyd, P. W., Jickells, T., C. S. Law, Blain, S., Boyle, E. A., Buesseler, K. O., Coale, K. H., Cullen, J. J., Baar, H. J. W. d., Follows, M., Harvey, M., Lancelot, C., Levasseur, M., Owens, N. P. J., Pollard, R., Rivkin, R. B., Sarmiento, J., Schoemann, V., Smetacek, V., Takeda, S., Tsuda, A., Turner, S., and Watson, A. J.: Mesoscale Iron Enrichment Experiments 1993-2005: Synthesis and Future Directions, Science, 315, 612 - 617, DOI: 610.1126/science.1131669, 2007.

Boyd, P. W., and Trull, T. W.: Understanding the export of marine biogenic particles: is there consensus?, Progress in Oceanography, 4, 276-312, doi:210.1016/j.pocean.2006.1010.1007, 2007.

Brooks, P. D., Geilmann, H., Werner, R. A., and Brand, W. A.: Improved precision of coupled 13C and 15N measurements from single samples using an elemental analyser, Rapid Communications in Mass Spectroscopy, 17, 1924-1926, 2003.

Buesseler, K. O.: The decoupling of production and particulate export in the surface ocean, Global Biogeochemical Cycles, 12, 297-310, 1998.

Buesseler, K. O., Ball, L., Andrews, J. E., Cochran, J. K., Hirschberg, D. J., Bacon, M. P., Fleer, A., and Brzezinski, M.: Upper ocean export of particulate organic carbon and biogenic silica in the Southern Ocean along 170$^{o}$W, Deep-Sea Research II, 48, 4275–4297, 2001.

Buesseler, K. O., Lamborg, C. H., Boyd, P. W., Lam, P. J., Trull, T. W., Bidigare, R. R., Bishop, J. K. B., Casciotti, K. L., Dehairs, F., Elskens, M., Honda, M., Karl, D. M., Siegel, D., Silver, M., Steinberg, D., Valdes, J., Van Mooy, B., and Wilson, S. E.: Revisiting carbon flux through the Ocean's twilight zone, Science, 316, 567 - 570, DOI: 510.1126/science.1137959, 2007.

Burkhardt, S., Riebesell, U., and Zondervan, I.: Effects of growth rate, CO2 concentration, and cell size on the stable carbon isotope fractionation in marine phytoplankton, Geochimica et Cosmochimica Acta, 63, 3729-3741, 1999a.

Burkhardt, S., Riebesell, U., and Zondervan, I.: Effects of growth rate, $CO_2$ concentration, and cell size on the stable carbon isotope fractionation in marine phytoplankton, Geochimica Cosmochimica Acta, 63, 3729-3741, 1999b.

Burkhardt, S., Riebesell, U., and Zondervan, I.: Stable carbon isotope fractionation by marine phytoplankton in response to daylength, growth rate, and CO2 availability, Marine ecology-progress series, 184, 31-41, 1999c.

Carlotti, F., Jouandet, M.-P., Nowaczyk, A., Harmelin-Vivien, M., Lefèvre, D., Guillou, G., Zhu, Y., and Zhou, M.: Mesozooplankton structure and functioning during the onset of the Kerguelen Bloom during Keops2 survey., Biogeosciences Discuss., 11, submitted, 2014.

Cavagna, A.-J., Fripiat, F., Elskens, M., Dehairs, F., Mangion, P., Chirurgien, I., Closset, I., Lasbleiz, M., Flores-Leive, L., Cardinal, D., Leblanc, K., Fernandez, C., Lefevre, D., Oriol, L., and Queguiner, B.: Biological productivity regime in the surface water around the Kerguelen Island area, Southern Ocean. , Biogeosciences Discuss., 11, submitted, 2014.

Chisholm, S. W.: Phytoplankton size, in: Primary productivity and biogeochemical cycles in the sea, edited by: Falkowski, P., and Woodhead, A., Environmental Science Research, Springer, 213-237, 1992.

Christaki, U., Lefèvre, D., Georges, C., Colombet, J., Catala, P., Courties, C., Sime-Ngando, T., Blain, S., and Obernosterer, I.: Microbial food web dynamics during spring phytoplankton blooms in the naturally iron-fertilized Kerguelen area (Southern Ocean), Biogeosciences Discuss., 11, 6985-7028, 10.5194/bgd-11-6985-2014, 2014.

Cózar, A., and Echevarría, F.: Size structure of the planktonic community in microcosms with different levels of turbulence, Scientia Marina, 69, 187-197, 2005.

Craig, H.: The geochemistry of the stable carbon isotopes, Geochimica et Cosmochimica Acta, 3, 53-92, 1953.

Cullen, J. J.: Status of the iron hypothesis after the Open-Ocean Enrichment Experiment, Limnology and Oceanography, 40, 1336-1343, 1995.

d'Ovidio, F., Della Penna, A., Trull, T. W., Nencioli, I., Pujol, I., Rio, M. H., Park, Y.-H., Cotte, C., Zhou, M., and Blain, S.: The biogeochemical structuring role of horizontal stirring: Lagrangian perspectives on iron delivery downstream of the Kerguelen plateau, Biogeosciences Discussions, 11, submitted, 2014.

de Baar, H. J. W., de Jong, J. T. M., Bakker, D. C. E., Loscher, B. M., Veth, C., Bathmann, U., and Smetacek, V.: Importance of iron for phytoplankton blooms and carbon dioxide drawdown in the Southern Ocean, Nature, 373, 412-415, 1995.

Dehairs, F., Fripiat, F., Cavagna, A. J., Trull, T. W., Fernandez, C., Davies, D., Roukaerts, A., Fonseca Batista, D., Planchon, F., and Elskens, M.: Nitrogen cycling in the Southern Ocean Kerguelen Plateau area: evidence for significant surface nitrification from nitrate isotopic compositions, Biogeosciences Discuss., 11, 13905-13955, 10.5194/bgd-11-13905-2014, 2014.

Farquhar, G. D., O'Leary, M. H., and Berry, J. A.: On the relationship between carbon isotope discrimination and the intracellular carbon dioxide concentration in leaves, Australian Journal of Plant Physiology, 9, 121-137, 1982.

Fontugne, M., Descolas-Gros, C., and de Billy, G.: The dynamics of $CO_2$ fixation in the Southern Ocean as indicated by carboxylase activities and organic carbon isotope ratios, Marine Chemistry, 35, 371-380, 1991.

Georges, C., Monchy, S., Genitsaris, S., and Christaki, U.: Protist community composition during early phytoplankton blooms in the naturally iron-fertilized Kerguelen area (Southern Ocean), Biogeosciences Discuss., 11, 11179-11215, 10.5194/bgd-11-11179-2014, 2014.

Gervais, F., and Riebesell, U.: Effect of phosphorus limitation on elemental composition and stable carbon isotope fractionatiaon in a marine diatoms growing under different CO2 concentrations., Limnology and Oceanography, 46, 497-504, 2001.

Goericke, R., Montoya, J. P., and Fry, B.: Physiology of isotopic fractionation in algae and cyanobacteria, in: Stable Isotopes in Ecology and Environmental Science, edited by: Lajtha, K., and Michener, R. H., Blackwell Scientific Publications, Oxford, 1870-1221, 1994.

Hoffman, L. J., Peeken, I., and Lochte, K.: Effects of iron on the elemental stoichiometry during EIFEX and in the diatoms *Fragilariopsis kerguelensis and Chaetoceros dichaeta*, Biogeosciences, 4, 569-579, 2007.

Hutchins, D. A., and Bruland, K. W.: Iron limited diatom growth and Si:N uptake ratios in a coastal upwelling regime, Nature, 393, 561-564, 1998.

Jacquet, S. H. M., Dehairs, F., Cavagna, A. J., Planchon, F., Monin, L., André, L., Closset, I., and Cardinal, D.: Early season mesopelagic carbon remineralization and transfer efficiency in the naturally iron-fertilized Kerguelen area, Biogeosciences Discuss., 11, 9035-9069, 10.5194/bgd-11-9035-2014, 2014.

Karsh, K. L., Trull, T. W., Lourey, A. J., and Sigman, D. M.: Relationship of nitrogen isotope fractionation to phytoplankton size and iron availability during the Southern Ocean Iron RElease Experiment (SOIREE), Limnology and Oceanography, 48, 1058-1068, 2003.

Karsh, K. L., Trull, T. W., Sigman, D. M., Thompson, P. A., and Granger, J.: The contributions of nitrate uptake and efflux to isotope fractionation during algal nitrate assimilation, Geochimica et Cosmochimica Acta, 132, 391-412, http://dx.doi.org/10.1016/j.gca.2013.09.030, 2014.

Keller, K., and Morel, F. M. M.: A model of carbon isotopic fractionation and active carbon uptake in phytoplankton, Marine Ecology-Progress Series, 182, 295-298, 1999.

King, P., Kennedy, H., Newton, P., Jickells, T., Brand, T., Calvert, S., Cauwet, G., Etcheber, H., Head, B., Khripounoff, A., Manighetti, B., and Miquel, J. C.: Analysis of total and organic carbon and total nitrogen in settling oceanic particles and marine sediment: an interlaboratory comparison, Marine Chemistry, 60, 203-216, 1998.

Lasbleiz, M., Leblanc, K., Blain, S., Ras, J., Cornet-Barthaux, V., Hélias Nunige, S., and Quéguiner, B.: Pigments, elemental composition (C, N, P, Si) and stoichiometry of particulate matter, in the naturally iron fertilized region of Kerguelen in the Southern Ocean, Biogeosciences Discuss., 11, 8259-8324, 10.5194/bgd-11-8259-2014, 2014.

Laurenceau, E. C., Trull, T. W., Davies, D. M., Bray, S. G., Doran, J., Planchon, F., Carlotti, F., Jouandet, M. P., Cavagna, A. J., Waite, A. M., and Blain, S.: The relative importance of phytoplankton aggregates and zooplankton fecal pellets to carbon export: insights from free-drifting sediment trap deployments in naturally iron-fertilised waters near the Kerguelen plateau, Biogeosciences Discuss., 11, 13623-13673, 10.5194/bgd-11-13623-2014, 2014.

Laws, E. A., Popp, B. N., Bidigare, R. R., Kennicutt, M. C., and Macko, S. A.: Dependence of phytoplankton carbon isotopic composition on growth rate and $[CO_2]_{aq}$: Theoretical considerations and experimental results, Geochimica et Cosmochimica Acta, 59, 1131-1138, 1995.

Laws, E. A., Popp, B. N., Cassar, N., and Tanimoto, J.: 13C discrimination patterns in oceanic phytoplankton: likely influence of CO2 concentrating mechanisms, and implications for palaeoreconstructions, Functional Plant Biology, 29, 323-333, 2002.

Leynaert, A., Bucciarelli, E., Claquin, P., Dugdale, R. C., Martin-Jézéquel, V., Pondaven, P., and Ragueneau, O.: Effect of iron deficiency on diatom cell size and silicic acid uptake kinetics, Limnology and Oceanography, 49, 1134-1143, 2004.

Lo Monaco, C., Metzl, N., D'Ovidio, F., Llort, J., and Ridame, C.: Rapid establishment of the CO2 sink associated with Kerguelen's bloom observed during the KEOPS2/OISO20 cruise, Biogeosciences Discuss., 11, in preparation, 2014.

Maldonado, M. T., Boyd, P. W., Abraham, E., Bowie, A., Croot, P., Strzepek, R., Waite, A., LaRoche, J., Frew, R., and Price, N.: Iron uptake and physiological response of phytoplankton during a mesoscale Southern Ocean Iron enrichment, Limnology and oceanography, 46, 1802-1808, 2001.

Marchetti, A., and Cassar, N.: Diatom elemental and morphological changes in response to iron limitation: a brief review with potential paleocenaographic applications, Geobiology, 7, 419-431, 2009.

Michener, R. H., and Schell, D. M.: Stable isotope ratios as tracers in marine aquatic food webs, in: Stable isotopes in ecology and environmental science, edited by: Lajtha, K., and Michener, R. H., Blackwell Scientific Publications, Oxford, 138-157, 1994.

Morel, F. M. M., Reuter, J. G., and Price, N. M.: Iron nutrition of phytoplankton and its possible importance in the ecology of ocean regions with high nutrient and low biomass, Oceanography, 4, 56-61, 1991.

Mosseri, J., Quéguiner, B., Armand, L., and Cornet-Barthaux, V.: Impact of iron on silicon utilization by diatoms in the Southern Ocean: a case study of the Si/N cycle decoupling in a naturally iron-enriched area, Deep Sea Research II, 55, 801-819, 2008.

Park, Y.-H., Roquet, F., Fuda, J.-L., and Durand, I.: Large scale circulation over and around the Kerguelen Plateau, Deep Sea Research II, 55, 566-581, 2008.

Park, Y.-H., Durand, I., Kestenare, E., Rougier, G., Zhou, M., d'Ovidio, F., Cotté, C., and Lee, J.-H.: Polar Front around the Kerguelen Islands: An up-to-date determination and associated circulation of surface/subsurface waters, Journal of Geophysical Research: Oceans, 2169-9291, DOI: 10.1002/2014JC010061, 2014a.

Park, Y. H., Lee, J. H., Durand, I., and Hong, C. S.: Validation of the Thorpe scale-derived vertical diffusivities against microstructure measurements in the Kerguelen region, Biogeosciences Discuss., 11, 12137-12157, 10.5194/bgd-11-12137-2014, 2014b.

Planchon, F., Ballas, D., Cavagna, A.-J., Bowie, A., Davies, D., Trull, T., Laurenceau, E., van der Merwe, P., and Dehairs, F.: Carbon export in the naturally iron-fertilized Kerguelen area of the Southern Ocean based on the 234Th approach, Biogeosciences Discuss., 11, submitted, 2014.

Pollard, R., Sanders, R., Lucas, M., and Statham, P.: The Crozet Natural Iron Bloom and Export Experiment (CROZEX), Deep-Sea Research II, Volume 54, Issue 18-20, p. , 54, 1905-1914, 2007.

Popp, B. N., Kenig, F., Wakeham, S. G., Laws, E. A., and Bidigare, R. R.: Does growth rate affect ketone unsaturation and intracellular carbon isotopic variability in *Emiliania huxleyi*?, Paleoceanography, 13, 35-41, 1998a.

Popp, B. N., Laws, E. A., Bidigare, R. R., Dore, J. E., Hanson, K. L., and Wakeham, S. G.: Effect of phytoplankton cell geometry on carbon isotopic fractionation, Geochimica et Cosmochimica Acta, 62, 69-77, 1998b.

Popp, B. N., Trull, T., Kenig, F., Wakeham, S. G., Rust, T. M., Tilbrook, B., Griffiths, F. B., Wright, S. W., Marchant, H. J., Bidigare, R. R., and Laws, E. A.: Controls on the carbon isotopic composition of Southern Ocean phytoplankton, Global Biogeochemical Cycles, 13, 827-843, 1999.

Queguiner, B.: Biogenic silica production in the Australian sector of the Subantarctic Zone of the Southern Ocean in late summer 1998, Journal of Geophysical Research, 106, 31627-31636, 2001.

Queguiner, B.: Iron fertilization and the structure of planktonic communities in high nutrient regions of the Southern Ocean, Deep Sea Research II, 90, 43-54, 2013.

Quéroué, F., Sarthou, G., Planquette, H. F., Bucciarelli, E., Chever, F., van der Merwe, P., Lannuzel, D., Townsend, A., Cheize, M., Blain, S., d'Ovidio, F., and Bowie, A. R.: High variability of dissolved iron concentrations in the vicinity of Kerguelen Island (Southern Ocean), Biogeosciences Discuss., 11, submitted, 2014.

Ragueneau, O., Schultes, S., Bidle, K., Claquin, P., and Moriceau, B.: Si and C interactions in the world ocean: Importance of ecological processes and implications for the role of diatoms in the biological pump, Global Biogeochemical Cycles, 20, GB4S02, 2006.

Rau, G. H., Teyssie, J.-L., Rassoulzadegan, F., and Fowler, S. W.: 13C/12C and 15N/14N variations among size fractionated marine particles: implications for their origin and trophic relationships., Marine Ecology Progress Series, 59, 33-38, 1990.

Rau, G. H., Riebesell, U., and Wolf-Gladrow, D.: A model of photosynthetic $^{13}C$ fractionation by marine phytoplankton based on diffusive molecular $CO_2$ uptake, Marine Ecology Progress Series, 133, 275-285, 1996.

Rau, G. H., Riebesell, U., and Wolf-Gladrow, D.: $CO_{2aq}$-dependent photosynthetic $^{13}C$ fractionation in the ocean: A model versus measurements, Global Biogeochemical Cycles, 11, 267-278, 1997.

Redfield, A. C., Ketchum, B. H., and Richards, F. H.: The influence of organisms on the composition of seawater, in: *The Sea*, edited by: Hill, M. N., Inter-Science, New York, 26-77, 1963.

Sanial, V., van Beek, P., Lansard, B., Souhaut, M., Kestenare, E., d'Ovidio, F., Zhou, M., and Blain, S.: Use of Ra isotopes to deduce rapid transfer of sediment-derived inputs off Kerguelen, Biogeosciences Discuss., 11, 14023-14061, 10.5194/bgd-11-14023-2014, 2014.

Savoye, N., Trull, T. W., Jacquet, S. H. M., Navez, J., and Dehairs, F.: Th-234-based export fluxes during a natural iron fertilization experiment in the Southern Ocean (KEOPS), Deep-Sea Research Part Ii-Topical Studies in Oceanography, 55, 841-855, 10.1016/j.dsr2.2007.12.036, 2008.

Schulz, K. G., Zondervan, I., Gerringa, L. J. A., Timmermans, K. R., Veldhuis, M. J. W., and Riebesell, U.: Effect of trace metal availability on coccolithophorid calcification, Nature, 430, 673-676, 2004.

Schulz, K. G., Rost, B., Burkhardt, S., Riebesell, U., Thoms, S., and Wolf-Gladrow, D.: The effect of iron availability on the regulation of inorganic carbon acquisition in the coccolithophore *Emiliania huxleyi* and the significance of cellular compartmentation for stable carbon isotope fractionation, Geochimica et Cosmochimica Acta, 71, 5301-5312, 2007.

Smetacek, V.: Role of sinking in diatom life-history cycles: ecological, evolutionary and geological significance, Marine Biology, 84, 239-251, 1985.

Smetack, V.: Diatoms and the silicate factor, Nature, 391, 224-225, 1998.

Sokolov, S., and Rintoul, S. R.: Circumpolar structure and distribution of the Antarctic Circumpolar Current fronts: 1. Mean circumpolar paths, Journal of geophysical research, 114, C11018, 2009.
Sweeney, C., Hansell, D. A., Carlson, C. A., Codispoti, L. A., Gordon, L. I., Marra, J., Millero, F. J., Smith, W. O., and Takahashi, T.: Biogeochemical regimes, net community production and carbon export in the Ross Sea, Antarctica, Deep-Sea Research II, 47, 3369-3394, 2000.
Syvaranta, J., and Rautio, M.: Zooplankton, lipids and stable isotopes: importance of seasonal, latitudinal, and taxonomic differences, Canadian Journal of Fisheries and Aquatic Sciences, 67, 1721-1729, 2010.
Takeda, S.: Influence of iron availability on nutrient consumption ratio of diatoms in oceanic waters, Nature, 393, 774-777, 1998.
Tortell, P. D., Payne, C., Gueguen, C., Li, Y., Strzepek, R., Boyd, P., and Rost, B.: Uptake and assimilation of inorganic carbon by Southern Ocean phytoplankton, Limnology and Oceanography, 53 (4) 1278., 53, 1266-1278, 2008.
Tremblay, 2014.
Trull, T. W., and Armand, L.: Insights into Southern Ocean carbon export from the delta C-13 of particles and dissolved inorganic carbon during the SOIREE iron release experiment, Deep-Sea Research Part Ii-Topical Studies in Oceanography, 48, 2655-2680, 10.1016/s0967-0645(01)00013-3, 2001.
Trull, T. W., Davies, D., and Casciotti, K.: Insights into nutrient assimilation and export in naturally iron-fertilized waters of the Southern Ocean from nitrogen, carbon and oxygen isotopes, Deep-Sea Research Part Ii-Topical Studies in Oceanography, 55, 820-840, 10.1016/j.dsr2.2007.12.035, 2008.
van der Merwe, P., Bowie, A. R., Quéroué, F., Armand, L., Blain, S., Chever, F., Davies, D., Dehairs, F., Planchon, F., Sarthou, G., Townsend, A. T., and Trull, T.: Sourcing the iron in the naturally-fertilised bloom around the Kerguelen Plateau: particulate trace metal dynamics, Biogeosciences Discuss., 11, 13389-13432, 10.5194/bgd-11-13389-2014, 2014.
Wada, E., and Hattori, A.: Nitrogen isotope effects in the assimilation of inorganic nitrogenous compounds by marine diatoms., Geomicrobiology Journal, 1, 85-101, 1978.
Wang, X., Matear, R. J., and Trull, T. W.: Nutrient utilization ratios in the Polar Frontal Zone in the Australian sector of the Southern Ocean: a model, Global Biogeochemical Cycles, 17, 1009, doi:1010.1029/2002GB001938, 2003.
Weiss, R. F.: Carbon dioxide in water and seawater: the solubility of a non-ideal gas, Marine Chemistry, 2, 203-215, 1974.

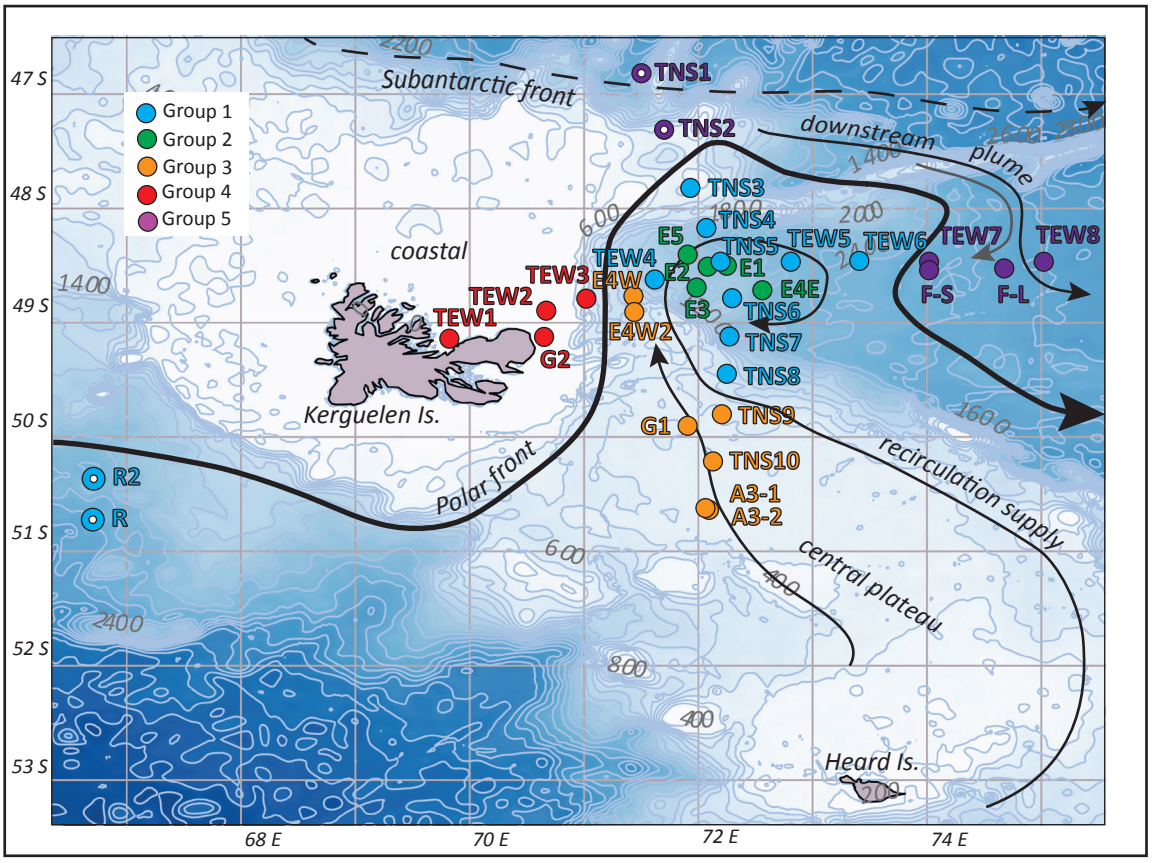
Group 1
Group 2
Group 3
Group 4
Group 5
Subantarctic front
Polar front
coastal
downstream plume
recirculation supply
central plateau
Kerguelen Is.
Heard Is.
TNS1
TNS2
TNS3
TNS4
TNS5
TNS6
TNS7
TNS8
TNS9
TNS10
A3-1
A3-2
R2
R
TEW1
TEW2
TEW3
TEW4
TEW5
TEW6
TEW7
TEW8
E1
E2
E3
E4E
E4W
E4W2
E5
G1
G2
F-S
F-L
2200
1400
600
2000
1800
2600
1600
2400
800
400
200
47 S
48 S
49 S
50 S
51 S
52 S
53 S
68 E
70 E
72 E
74 E

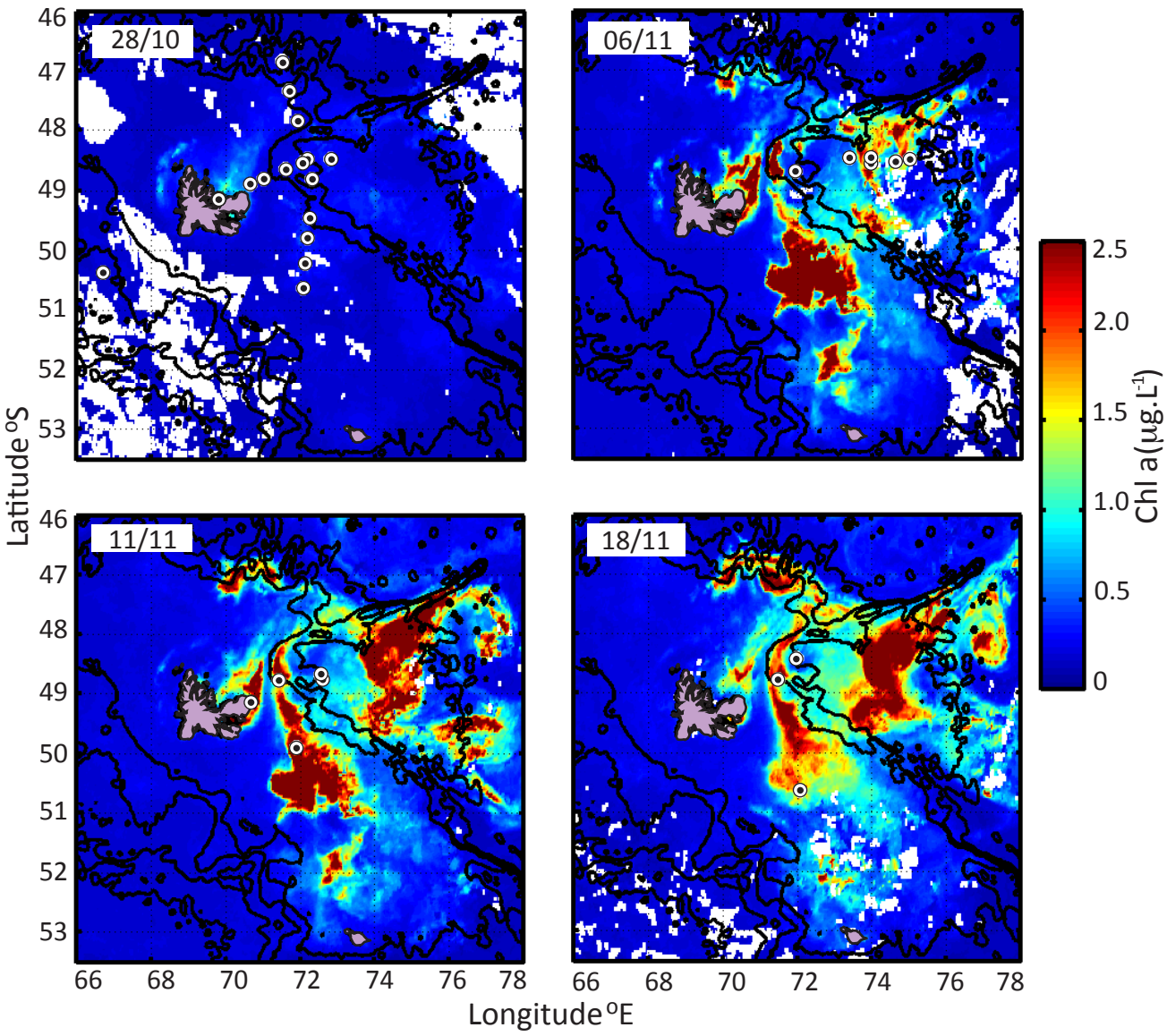
28/10
06/11
11/11
18/11
Latitude °S
Longitude °E
46
47
48
49
50
51
52
53
66
68
70
72
74
76
78
2.5
2.0
1.5
1.0
0.5
0
Chl a(µg.L-1)

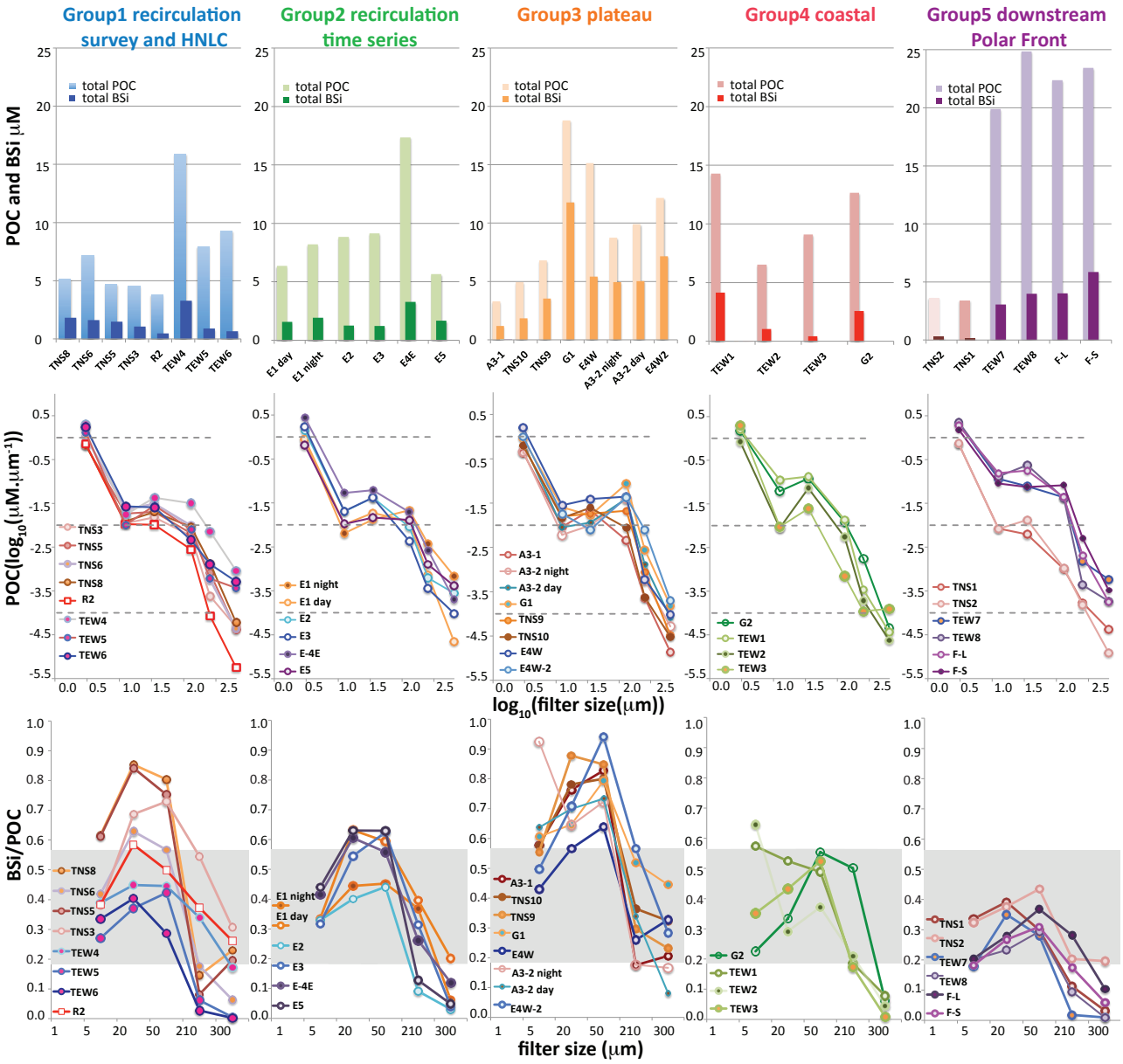
Group1 recirculation survey and HNLC
Group2 recirculation time series
Group3 plateau
Group4 coastal
Group5 downstream Polar Front
POC and BSi µM
total POC
total BSi
TNS8 TNS6 TNS5 TNS3 R2 TEW4 TEW5 TEW6
E1 day E1 night E2 E3 E4E E5
A3-1 TNS10 TNS9 G1 E4W A3-2 night A3-2 day E4W2
TEW1 TEW2 TEW3 G2
TNS2 TNS1 TEW7 TEW8 F-L F-S
POC(log10(µM.µm-1))
TNS3 TNS5 TNS6 TNS8 R2 TEW4 TEW5 TEW6
E1 night E1 day E2 E3 E-4E E5
A3-1 A3-2 night A3-2 day G1 TNS9 TNS10 E4W E4W-2
G2 TEW1 TEW2 TEW3
TNS1 TNS2 TEW7 TEW8 F-L F-S
log10(filter size(µm))
BSi/POC
TNS8 TNS6 TNS5 TNS3 TEW4 TEW5 TEW6 R2
E1 night E1 day E2 E3 E-4E E5
A3-1 TNS10 TNS9 G1 E4W A3-2 night A3-2 day E4W-2
G2 TEW1 TEW2 TEW3
TNS1 TNS2 TEW7 TEW8 F-L F-S
filter size (µm)

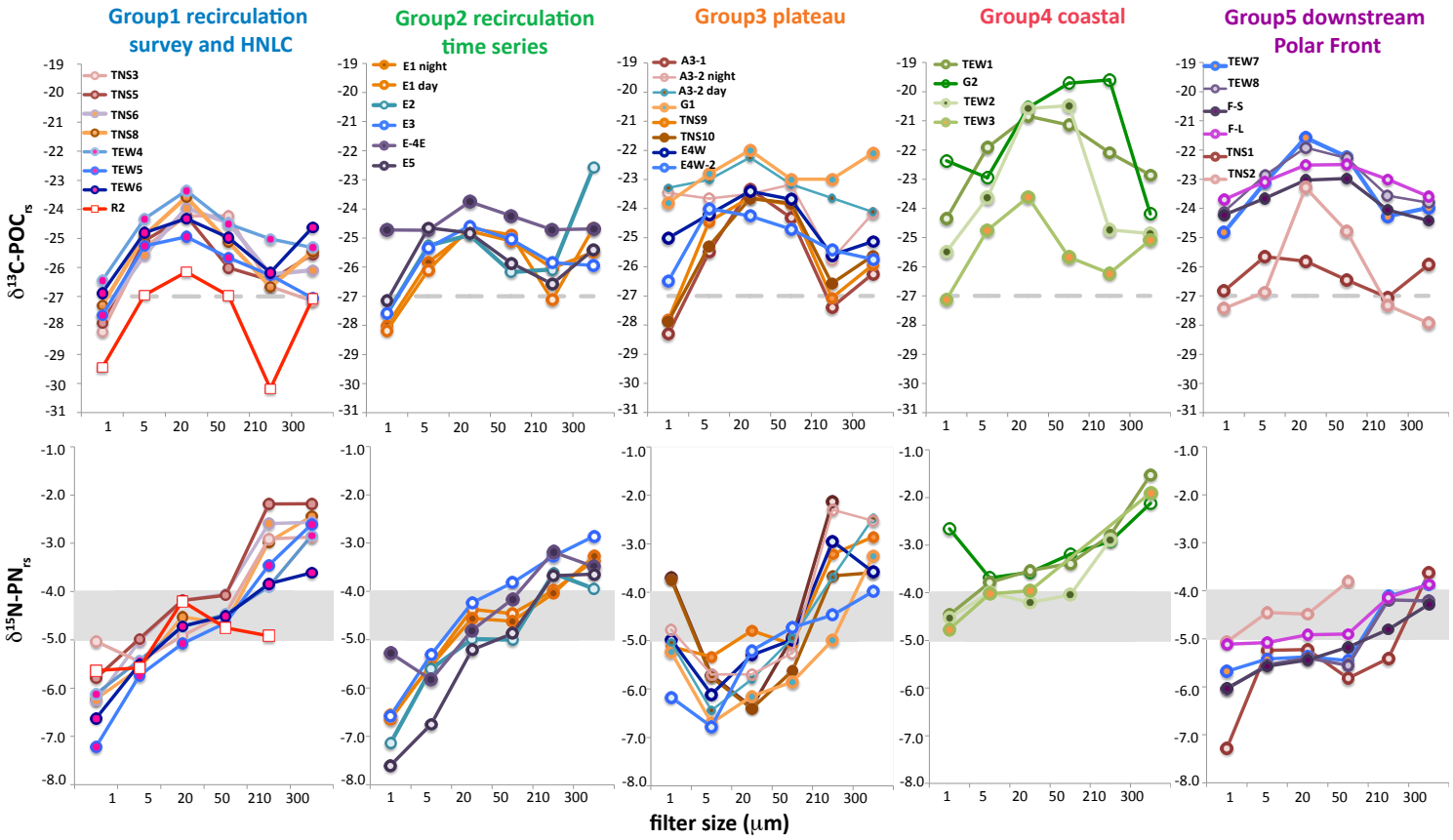
Group1 recirculation survey and HNLC
Group2 recirculation time series
Group3 plateau
Group4 coastal
Group5 downstream Polar Front
TNS3
TNS5
TNS6
TNS8
TEW4
TEW5
TEW6
R2
E1 night
E1 day
E2
E3
E-4E
E5
A3-1
A3-2 night
A3-2 day
G1
TNS9
TNS10
E4W
E4W-2
TEW1
G2
TEW2
TEW3
TEW7
TEW8
F-S
F-L
TNS1
TNS2
δ13C-POCrs
δ15N-PNrs
filter size (μm)

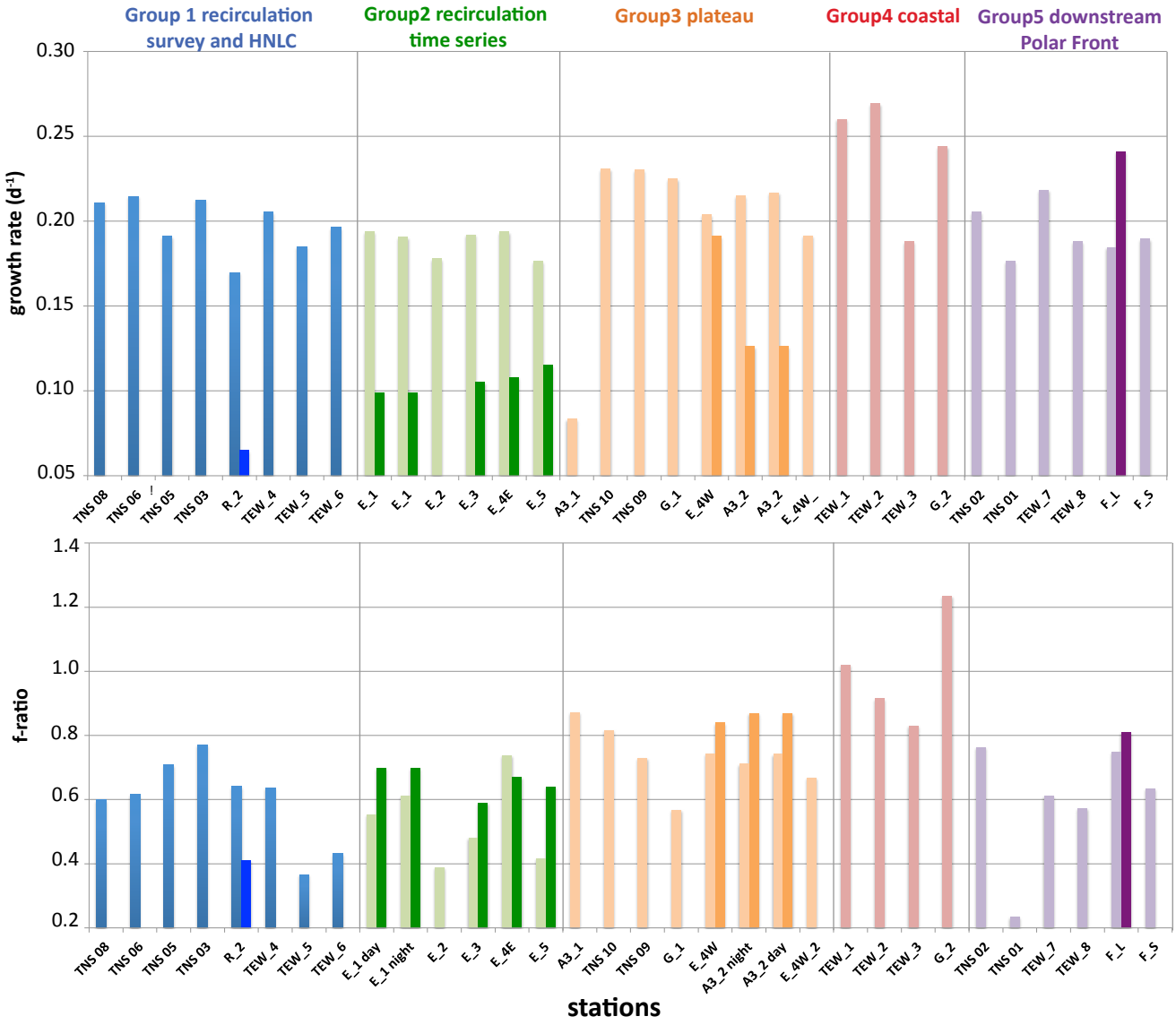
Group 1 recirculation survey and HNLC
Group2 recirculation time series
Group3 plateau
Group4 coastal
Group5 downstream Polar Front
growth rate (d-1)
0.30
0.25
0.20
0.15
0.10
0.05
TNS 08
TNS 06
TNS 05
TNS 03
R_2
TEW_4
TEW_5
TEW_6
E_1
E_1
E_2
E_3
E_4E
E_5
A3_1
TNS 10
TNS 09
G_1
E_4W
A3_2
A3_2
E_4W_
TEW_1
TEW_2
TEW_3
G_2
TNS 02
TNS 01
TEW_7
TEW_8
F_L
F_S
f-ratio
1.4
1.2
1.0
0.8
0.6
0.4
0.2
TNS 08
TNS 06
TNS 05
TNS 03
R_2
TEW_4
TEW_5
TEW_6
E_1 day
E_1 night
E_2
E_3
E_4E
E_5
A3_1
TNS 10
TNS 09
G_1
E_4W
A3_2 night
A3_2 day
E_4W_2
TEW_1
TEW_2
TEW_3
G_2
TNS 02
TNS 01
TEW_7
TEW_8
F_L
F_S
stations

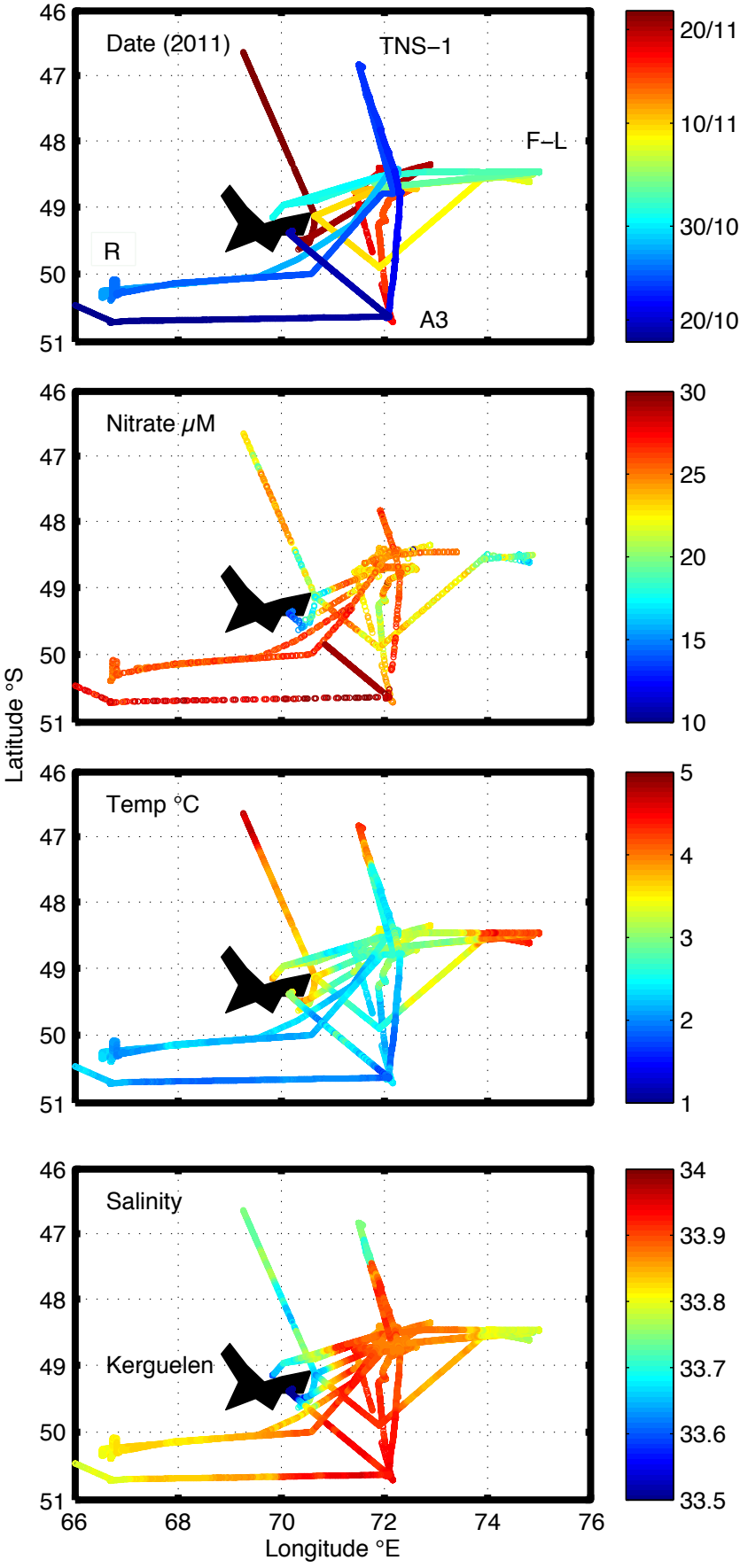
Date (2011)
TNS−1
F−L
R
A3
20/11
10/11
30/10
20/10
Nitrate μM
30
25
20
15
10
Temp °C
5
4
3
2
1
Salinity
34
33.9
33.8
33.7
33.6
33.5
Kerguelen
46
47
48
49
50
51
66
68
70
72
74
76
Latitude °S
Longitude °E

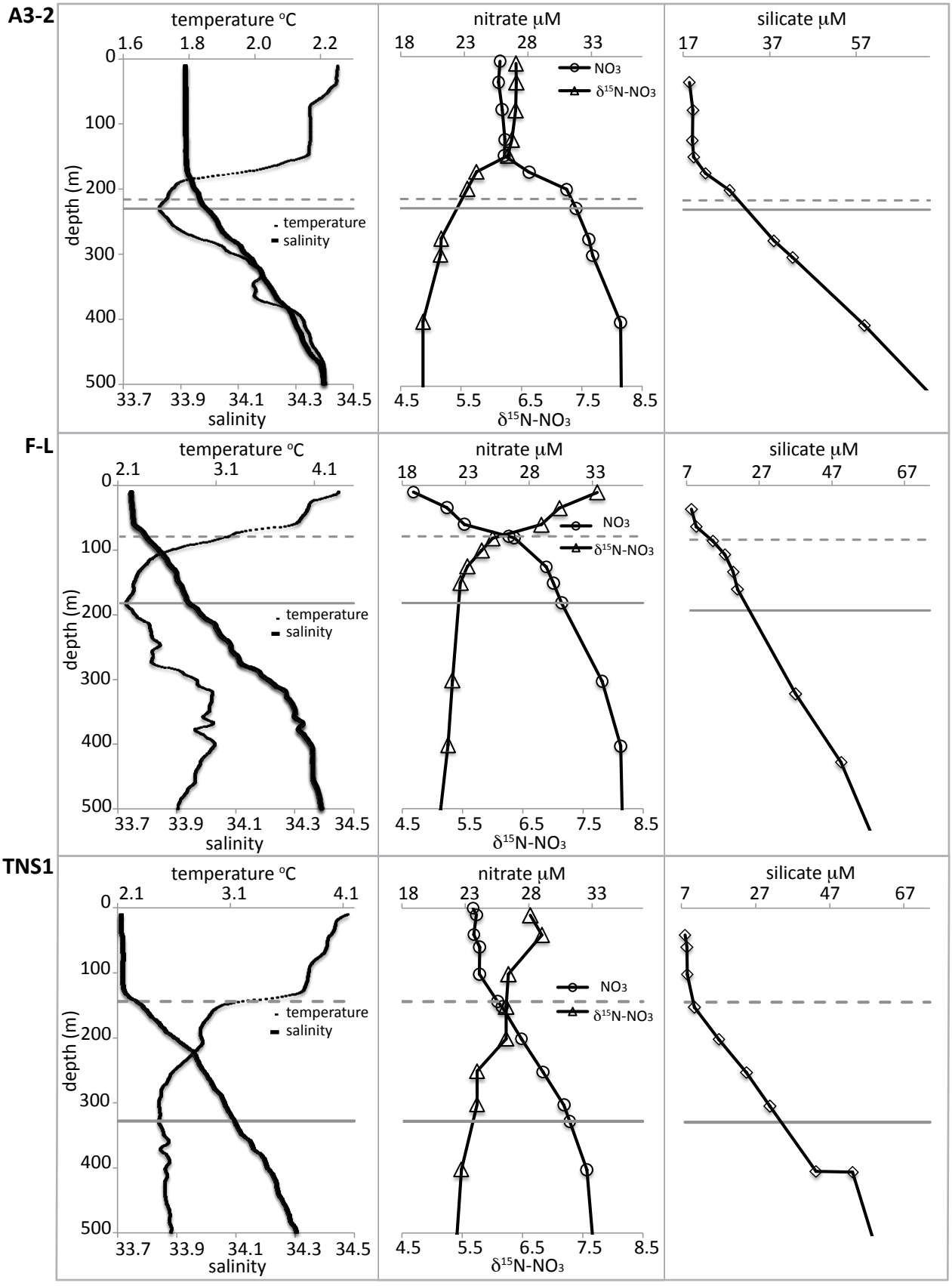
A3-2
F-L
TNS1
temperature °C
nitrate μM
silicate μM
depth (m)
salinity
δ15N-NO3
NO3
δ15N-NO3
temperature
salinity

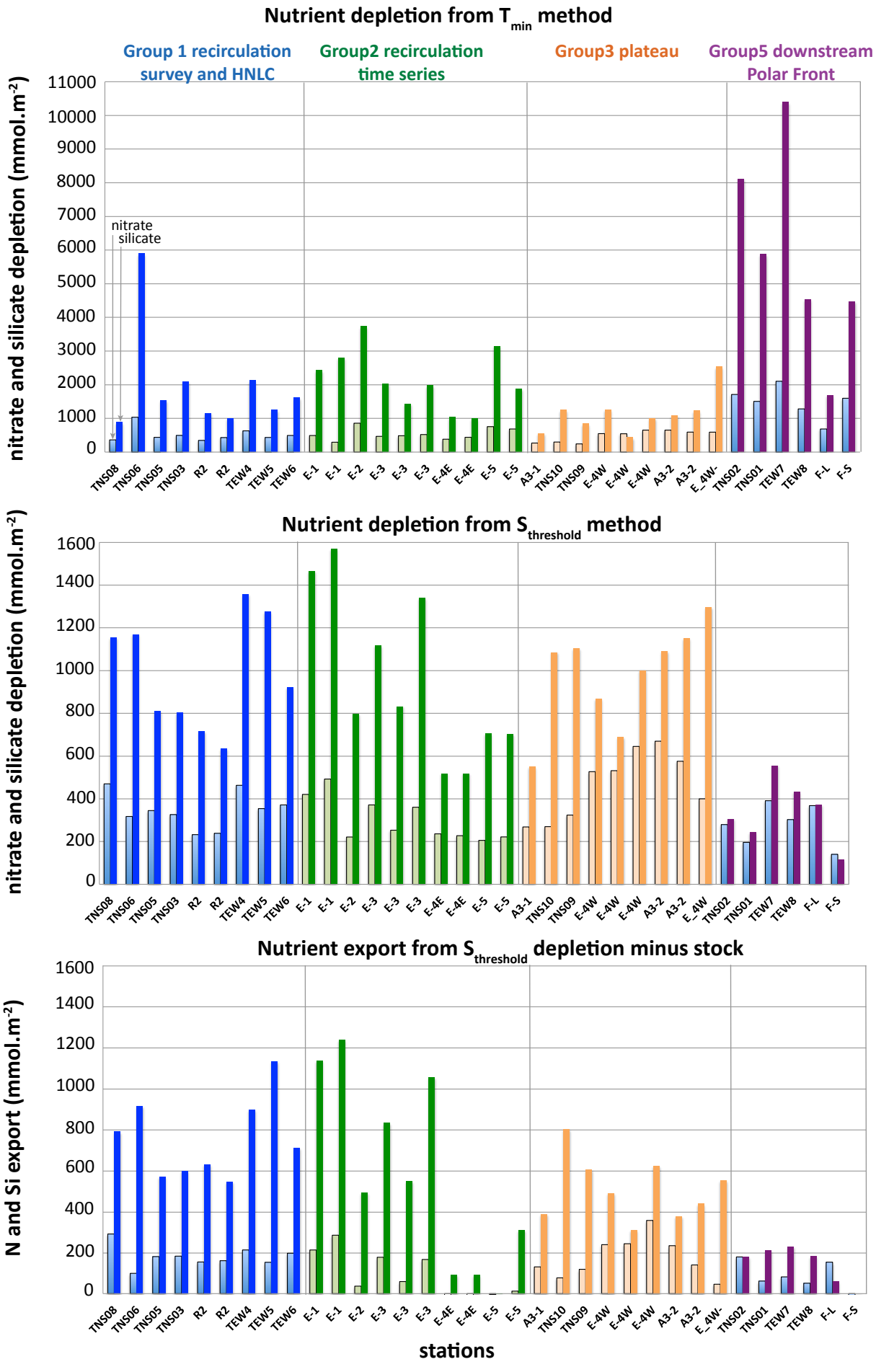
Nutrient depletion from $T_{min}$ method
Group 1 recirculation survey and HNLC
Group2 recirculation time series
Group3 plateau
Group5 downstream Polar Front
nitrate and silicate depletion (mmol.m-2)
nitrate
silicate
0
1000
2000
3000
4000
5000
6000
7000
8000
9000
10000
11000
TNS08 TNS06 TNS05 TNS03 R2 R2 TEW4 TEW5 TEW6 E-1 E-1 E-2 E-3 E-3 E-3 E-4E E-4E E-5 E-5 A3-1 TNS10 TNS09 E-4W E-4W E-4W A3-2 A3-2 E_4W- TNS02 TNS01 TEW7 TEW8 F-L F-S
Nutrient depletion from $S_{threshold}$ method
nitrate and silicate depletion (mmol.m-2)
0
200
400
600
800
1000
1200
1400
1600
TNS08 TNS06 TNS05 TNS03 R2 R2 TEW4 TEW5 TEW6 E-1 E-1 E-2 E-3 E-3 E-3 E-4E E-4E E-5 E-5 A3-1 TNS10 TNS09 E-4W E-4W E-4W A3-2 A3-2 E_4W TNS02 TNS01 TEW7 TEW8 F-L F-S
Nutrient export from $S_{threshold}$ depletion minus stock
N and Si export (mmol.m-2)
0
200
400
600
800
1000
1200
1400
1600
TNS08 TNS06 TNS05 TNS03 R2 R2 TEW4 TEW5 TEW6 E-1 E-1 E-2 E-3 E-3 E-3 E-4E E-4E E-5 E-5 A3-1 TNS10 TNS09 E-4W E-4W E-4W A3-2 A3-2 E_4W- TNS02 TNS01 TEW7 TEW8 F-L F-S
stations